SEISMIC STUDY AT EASTERN LEAD - PIONEER NORTH EASTERN TASMANIA

by

S U T R I S N O

A thesis submitted in partial fulfilment of the requirements for the degree of Master of Science

UNIVERSITY OF TASMANIA
HOBART

July, 1987

This thesis contains no material which has been accepted for the award of any other degree or diploma in any University and to the best of my knowledge and believe, contains no copy or paraphrase of material previously published or written by another person, except where due reference is made in the text of this thesis .

Sutrisno

July, 1987.

ACKNOWLEDGEMENTS

I am indebted to Dr. R.J.G. Lewis and Dr. L.E. Jones for their supervision of the project and comments on this manuscript. Thanks are due to Dr. D.E. Leaman and Mr. A.V. Brown for their discussion about the geology of the area; to Mr. Vagn Jensen, Mr. P. Cornish, Mrs. June Pongratz and other technical staff at the Geology Department, University of Tasmania for their assistance throughout this project. To Mr. M. Bendall, Mr. P. Bruce, Mr. R. Brescianini, Mrs. B. Lewis, Mr. G. Salter, their help and company during the field work are gratefully appreciated. Finally, I would like to acknowledge Prof. D.H. Green and Mrs. R. Bowden for their encouragement throughout the year.

ABSTRACT

A combination of seismic refraction and reflection methods was applied in determining the structure of deep leads at Eastern Lead, Pioneer, in North Eastern Tasmania. Four parallel traverse lines were laid across an inferred channel, and cover an area of about 1 km^2. A seismic refraction survey was carried out on all four lines and a seismic reflection survey along one of the internal lines. The purpose of the survey was to use the Generalized Reciprocal Method (GRM) of seismic refraction to determine the form of the deep lead and to compare this method with the use of shallow seismic reflection profiling.

A comparison of the seismic refraction results with bore hole data from kaolin exploration generally shows a good correlation with the boundaries of the kaolin layer but the material interpreted as basement in the boreholes is probably a boulder bed. The refraction data suggests an undulating basement with at least two channels draining to the north west.

A comparison of the reflection and refraction results is difficult. The refraction section shows a third layer with little internal structure while the reflection results show a complex structure with numerous lenses and channel fill. There seems little doubt that a superior structural interpretation is obtained from the reflection results. The reflection data also indicate that anomalies in the refraction data are due to local refraction from a lens of material and that the refractions interpreted as being due to basement are being produced from several distinct horizons. There is general agreement in the form of the structures between the two methods but the details are significantly different and no simple reconciliation is possible.

The use of automatic statics correction during reflection processing is crucial in the deep lead environment.

CONTENTS

List of Figures

CHAPTER 1

INTRODUCTION

1.1 GENERAL

The study area is located about 4 km north-east of Pioneer in North Eastern Tasmania, which is approximately 80 km north-east of Launceston or 127 km by the Tasman Highway (see Figure 1.1.). It lies between latitude $41^{\circ}02'$ and $41^{\circ}04'$ south and between longitude $147^{\circ}56'$ and $147^{\circ}58'$ east which covers an area of about 1 km^2. The area is known as the Eastern Lead and is thought to contain a tributary leading towards the primary ancient river known as the Ringarooma Lead. The Eastern Lead runs due north-west from the area where the seismic study was conducted (Figure 1.2.).

Electrical methods usually fail on the north-eastern deep leads because of the extremely low resistivity of the material in the leads. Previous geophysical work has included seismic refraction at Gladstone (Leaman, 1973-1974). The purpose of this study was to use the Generalized Reciprocal Method (GRM) of seismic refraction to examine the form of the deep lead and to compare this method with the use of shallow seismic reflection profiling which potentially has the ability to yield information about the structure of the sediments within the lead. Some drill hole control is available from work undertaken in the exploration for high quality clay deposits within the lead. The lead also contains cassiterite deposits along particular layers within the lead so that structural information from within the lead might be very useful in tin exploration.

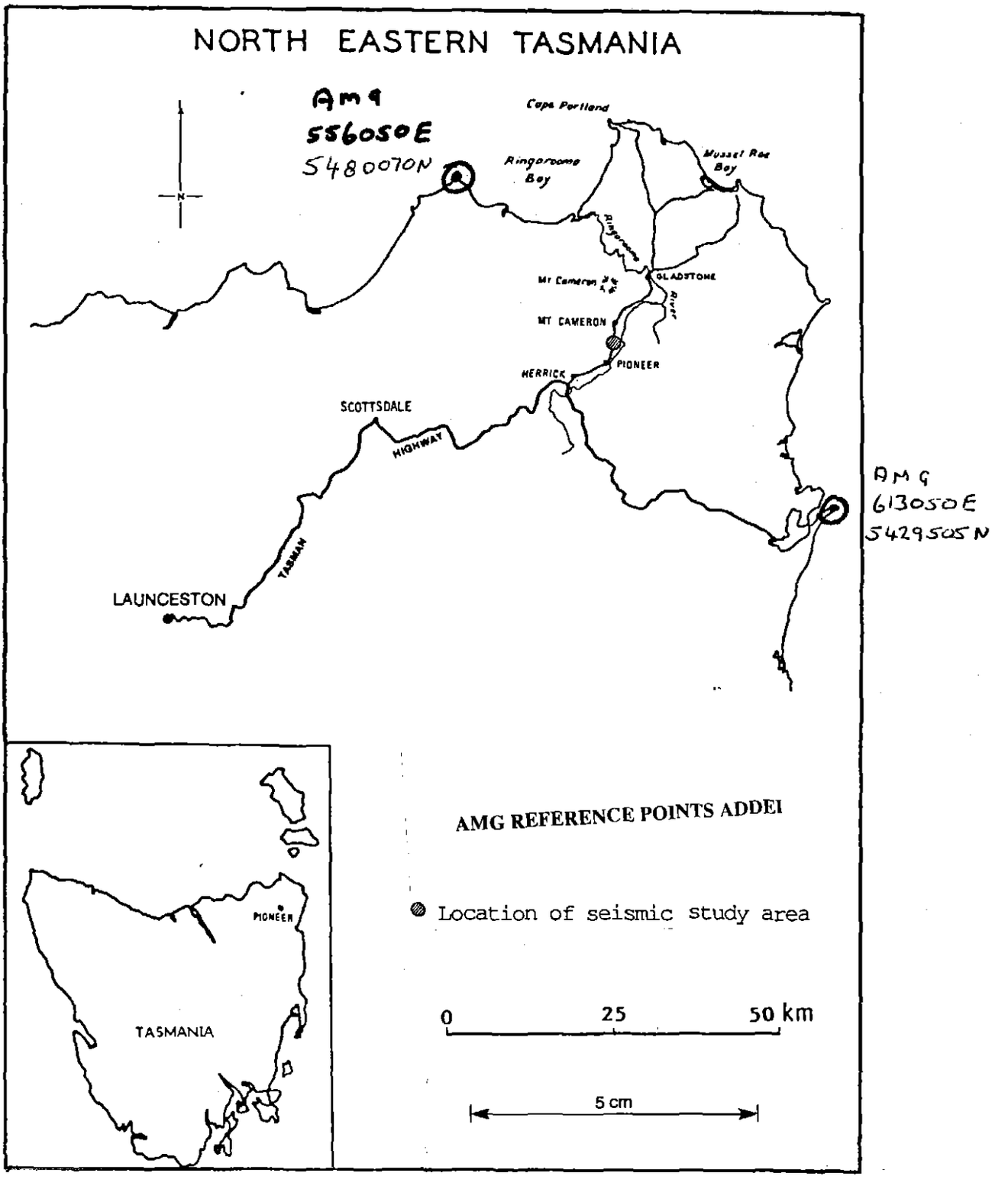

Fig.1.1. Location of seismic study near Pioneer, North Eastern Tasmania.

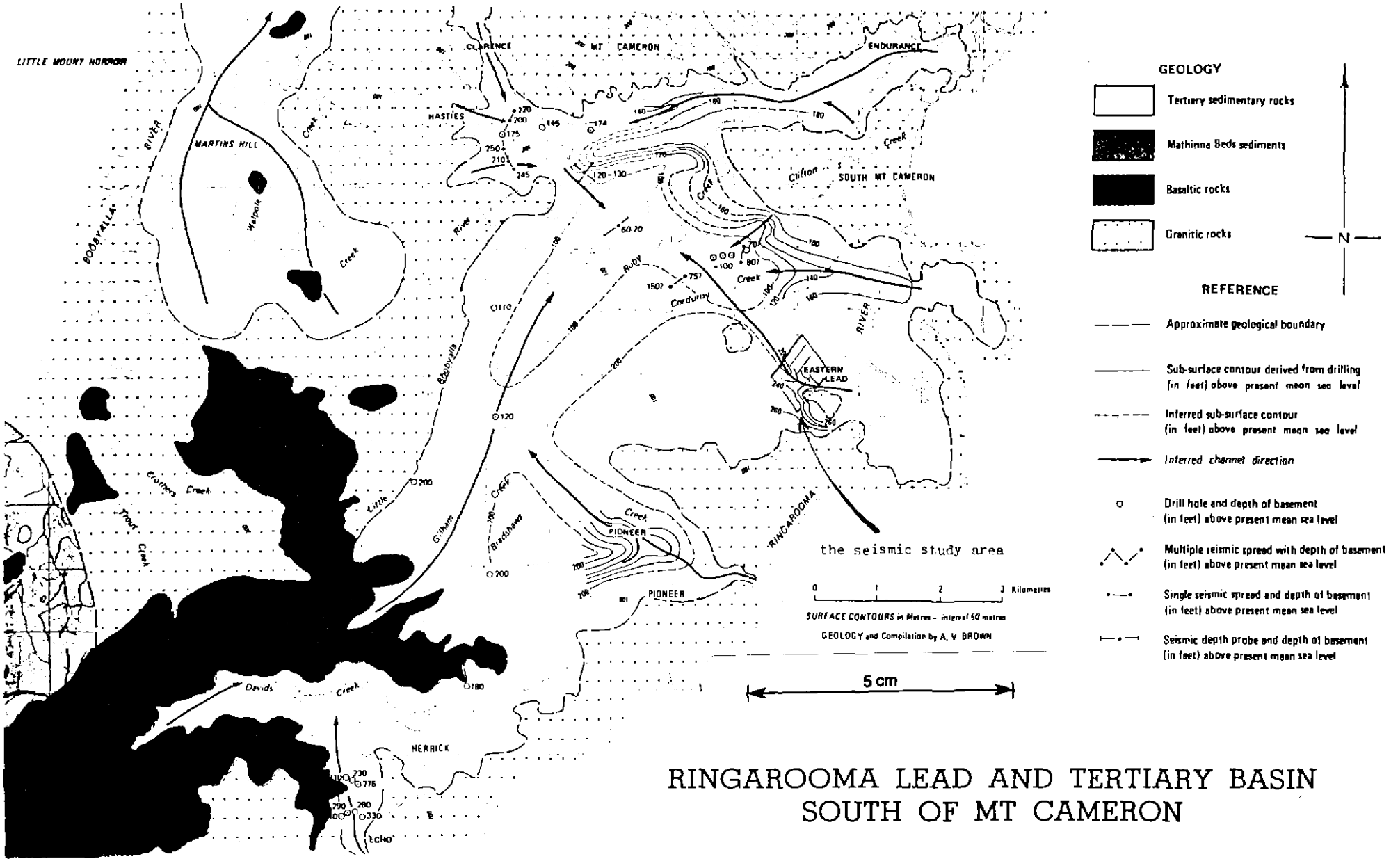

RINGAROOMA LEAD AND TERTIARY BASIN SOUTH OF MT CAMERON

Fig.1.2. Geology of the Ringarooma Lead and Tertiary Basin South of Mount Cameron (from Brown, 1982), and approximate location of the seismic study area at Eastern Lead - Pioneer.

1.2 TIN MINING HISTORY AND KAOLIN IN NORTH EASTERN TASMANIA

The discovery of tin and the establishment of the tin mining industry has played an important part in the development of North Eastern Tasmania. In the district, both primary and detrital deposits occur but the greatest production has been from detrital deposits. Tin mining locations are shown in Figure 1.3. (rear pocket) and the area has been described in detail by Nye (1925) and Jennings and Williams (1967).

The Aberfoyle and Storeys Creek mines were the major producers of primary tin ores in the district. The first discovery was in Gipps Creek in 1872 and then in Storeys Creek. The tin-bearing veins in Storeys Creek were worked from 1891 but the veins at Aberfoyle were not discovered until 1916. Tin production from the Aberfoyle mine was 11,991 tons and from the Storeys Creek mine 1,919 tons. In 1967 the ore reserves and inferred ore of the Aberfoyle mine were 377,000 tons containing 2,000 tons of metallic tin. At the same time at the Storeys Creek mine, reserves were 248,000 tons of ore containing 500 tons of metallic tin.

At the Branxholm and Blue Tier districts, ore grades are generally low. Even the Anchor mine, one of the largest in the field, averaged only 0.2 per cent SnO_2 and during 1890-1951 the tin production was 2,364 tons. Small amounts of wolfram, molybdenite and other sulphides are usually associated with the cassiterite.

Other primary tin producers were the Royal George Tin Mining Company and the Great Pyramid tin mine. From 1911 until 1922 the Royal George Tin Mining produced about 969 tons of tin oxide. Drilling intersected the orebody 113 m below the open cut, indicating an orebody about 152-244 m long

extending to a depth of 113 m carrying tin with a probable average grade of about 0.6 per cent.

At the Great Pyramid tin mine, tin was discovered in 1909 and the tin production from the mine to date is 331 tons, produced from 2,931 tons of ore giving a recovery grade of 0.88 per cent tin. Mineralization consists mainly of cassiterite, pyrite and chalcopyrite.

The major production of alluvial tin came from Tertiary deep leads and reworked material derived from the Tertiary leads of the Gladstone-Pioneer-Derby area. 30 per cent of the total tin production of Tasmania or 43,000 tons of tin was produced from deep lead deposits. At present the production is about 200 tons of tin concentrate per year. Alluvial tin was first worked in the district in 1882 and production rose rapidly following discovery of the rich alluvial deep lead systems and residual detritus deposits.

Pleistocene to Recent leads up to 15 m deep were dredged along the Ringarooma River giving an annual production of 90-100 tons of tin concentrate.

The Briseis mine was the most important of the workings and produced concentrate containing 20,787 tons of tin. The lead consists of up to 91 m of sand, gravel and clay which is covered by approximately 46 m of basalt.

The Endurance Tin Mining Company worked the Clifton lead which is up to 37 m deep, with a grade of about 0.16 kg/m^3 of 70 per cent tin, producing concentrates containing about 2,900 tons of tin up to the end of 1966.

The Pioneer Lead was worked up till 1929 and produced about 9,050 tons of cassiterite. The grade varied from 1.07 kg/m^3 in the early workings to 0.37 kg/m^3 in 1928.

Other areas of interest are possible leads in the valleys of the Mussel Roe and Anson Rivers and the Scotia-Nothern Plains lead North of Gladstone where preliminary investigations have indicated 10,058,522 m^3 of wash containing 0.16 kg/m^3 of 70 per cent tin. Currently there is exploration activity but little tin production in North Eastern Tasmania.

As shown in Figure 1.4., the southern end of the traverse line C-C' was laid out across an area where drilling was carried out by the Dorset Kaolin Division in exploring for clay. The clay is a kaolin and has possibilities for use in paper filling; a deposit nearby is currently mined for this purpose. The drilling suggested clay over an area of 33,000 m^2 with an average depth of 7 m or a total value of 231,000 m^3. The south-easterly extension of the Eastern Lead clay deposit was exposed by recent tin mining operations, and estimates of 18 m of clay over an area of greater than 40,000 m^2 (720,000 m^3) has been made (Bendall, 1983). Unfortunately there is only about 200 m of the south end of the traverse line C-C' which can be expected to give a correlation between the seismic results and the bore hole data. Further, no material from this drilling has been preserved which limits its usefulness.

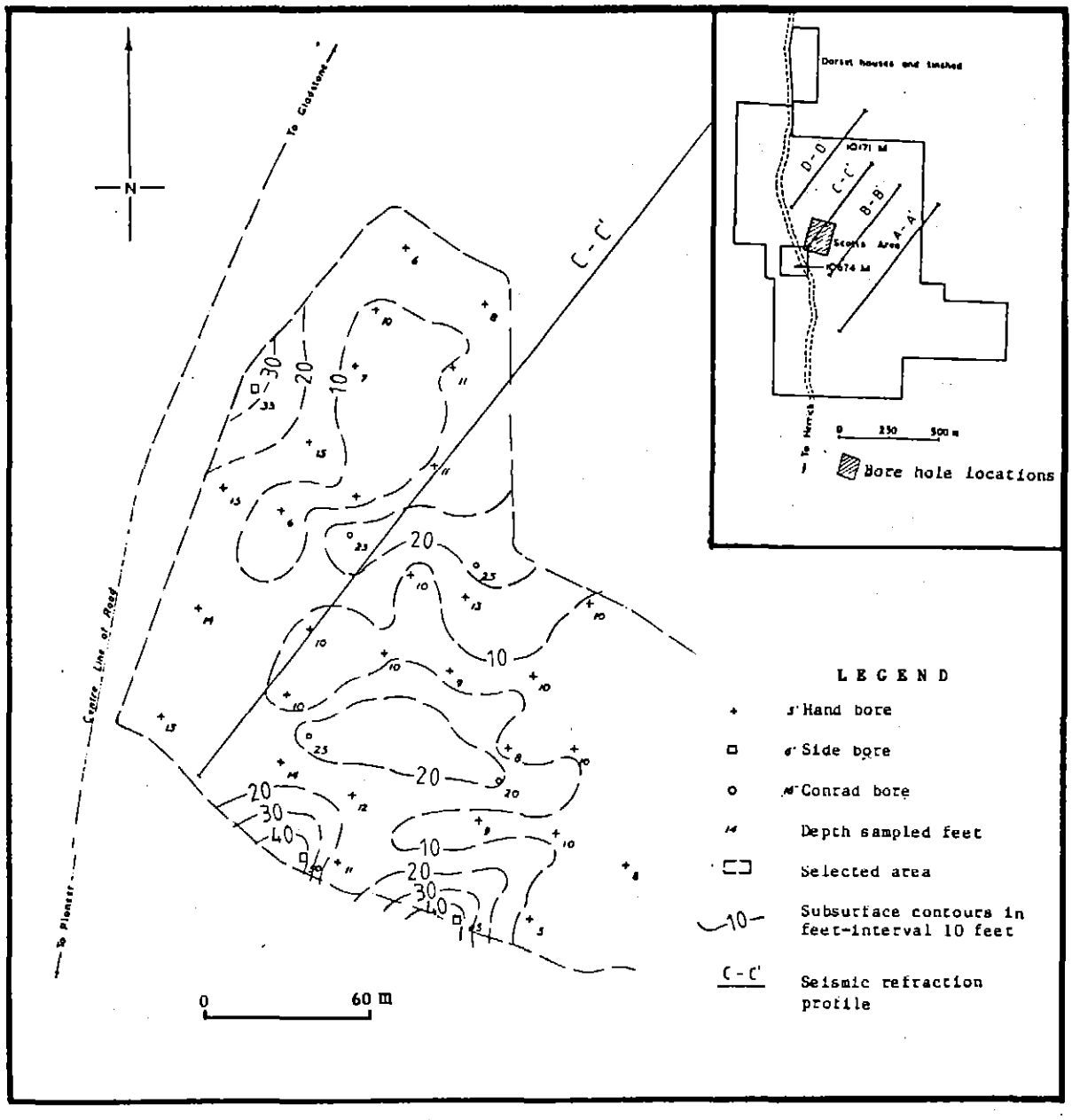

Fig.1.4. Subsurface contours of the clay deposit based on the bore hole data provided by Dorset Tin Division (R.Hare & Associates, 1961).

5 cm

1.3 PREVIOUS GEOPHYSICAL SURVEYS

During the last few decades a number of geophysical surveys have been conducted in the district. In the early 1950's , an airbone magnetic survey was conducted by Rio Tinto Australian Exploration Pty. Ltd. to locate basalt and granite. This was followed by several geophysical surveys to locate the presence of deep lead channels. Approximate locations of the surveys are illustrated in Figure 1.5.

In 1957, a seismic refraction survey was made by the Bureau of Mineral Resources over traverses chosen by Rio Tinto Australian Exploration Pty. Ltd. in the area around the confluence of the Boobyalla and Little Boobyalla Rivers (Rowston, 1961). The results gave no reliable indications of channels and it was concluded that the traverses were too far to the north and possibly in an area where estuarine conditions prevailed during the lower Tertiary (Sedmik, 1964).

Between October 1961 and April 1962, a geophysical survey was conducted by the Bureau of Mineral Resources over an area bounded by the Boobyalla and Litle Boobyalla Rivers to locate deep-lead channels emerging from underneath the basalt-covered plateau north of Winnaleah. This geophysical fieldwork was done concurrently with surveys at Great Mussel Roe River and Great Fraser River (Sedmik, 1964). The main methods used were gravity and seismic refraction, and on a few traverses magnetic and resistivity methods were tried. The results from gravity and magnetic methods indicated a rather wide, but well-defined, channel system in the unweathered bedrock surface, which is believed to indicate the general course of the deep leads. The actual position of the leads within these channels, however, could not be determined accurately because there is no

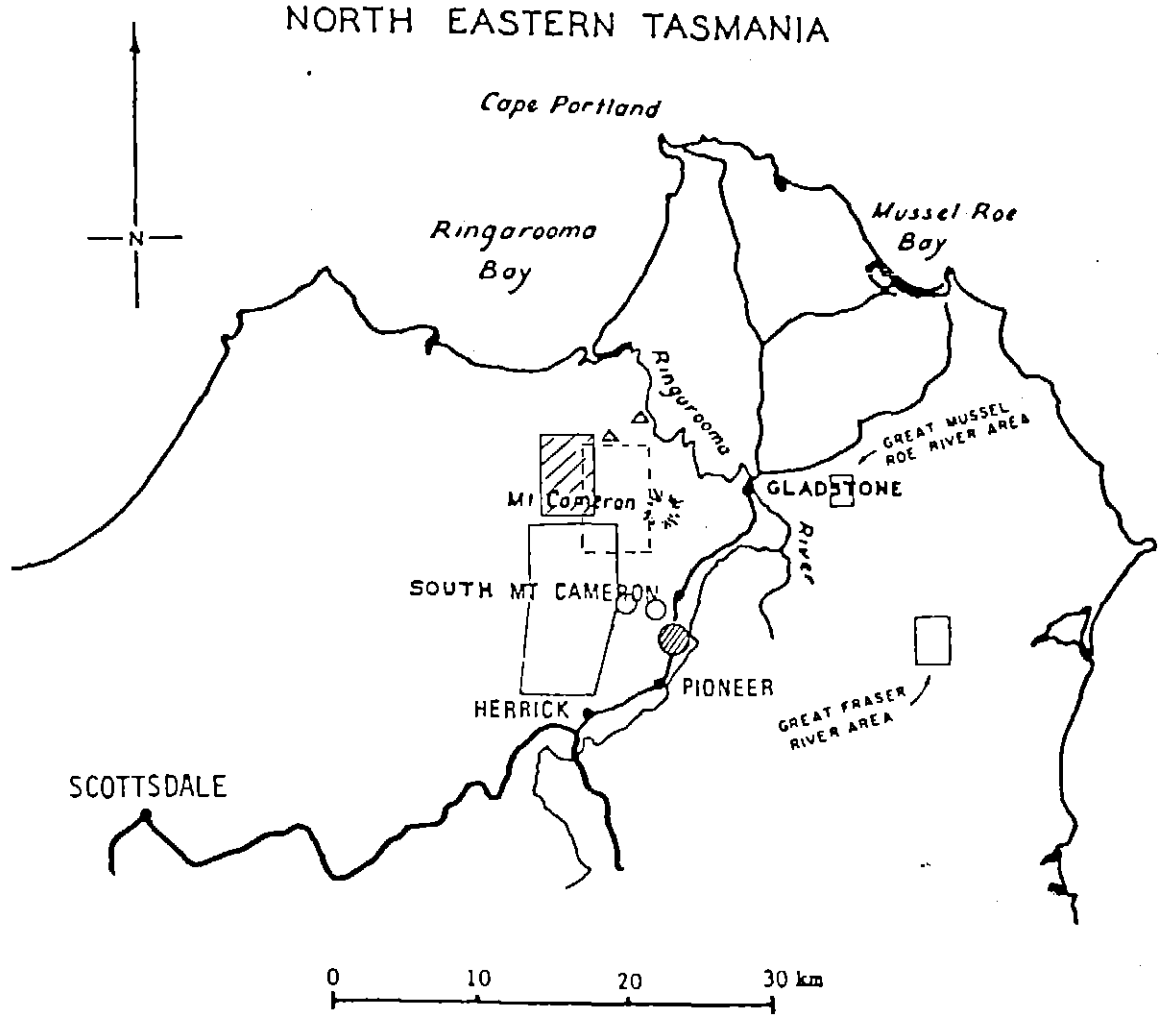

Seismic survey at the confluence of the Boobyalla and Little Boobyalla Rivers, conducted by Rowston in 1957.

Geophysical surveys at north of Winnaleah, Great Mussel Roe River, and Great Fraser River, conducted by Sednik in 1961 - 1962.

Geophysical surveys at the west of Mt. Cameron conducted by Chesnut in 1964 - 1965.

Seismic survey at Delta Mine - Gladstone, conducted by Moore and Leaman, 1971.

Seismic survey at South Mount Cameron conducted by Leaman and Moore in 1973 - 1974.

Seismic study at Eastern Lead - Pioneer (presented in this thesis).

Fig.1.5. Approximate location of previous geophysical surveys in NE Tasmania.

5 cm

clear measurable differentiation in physical properties between weathered bedrock and wet overburden. The magnetic surveys gave useful information on the location of basalt within the overburden, whereas the resistivity method gave inconclusive results and its use was discontinued.

A report on Ringarooma deep lead tin prospecting in North Eastern Tasmania by the Broken Hill Pty. Co. Ltd. has been described by Chesnut (1965). The survey area lies about ten miles north of Winnaleah. An indication of a channel in the bedrock was obtained from the geophysical surveys. Chesnut stated that the various geophysical surveys have all encountered a major problem as there is insufficient contrast between the weathered bedrock and the overlying alluvium, whether the contrast desired was in density, magnetic susceptibility or velocity of propagation. Another difficulty was found in correlating the upper surface of the unweathered bedrock defined from the seismic refraction method with any precision to the upper surface of weathered bedrock from drilling results, and it is still generally not possible to select a "break" from the seismic record which would correspond to the horizon of the top of the unwheathered bedrock even when drill hole information is available.

In the Gladstone area, geophysical surveys have been carried out by D.E.Leaman, W.R.Moore and M.J.Longman. These surveys include seismic, magnetic and gravity methods. The details and their interpretation results have been described by Leaman (1973) and Moore and Leaman (1974).

At South Mount Cameron, seismic refraction surveys were carried out by D.E.Leaman in 1973 ; and W.R.Moore in 1974 (an extension of the work carried out by D.E.Leaman in the same area). A series of spreads were used adjacent to the old Herrick-Boobyalla Road, and two other spreads were done

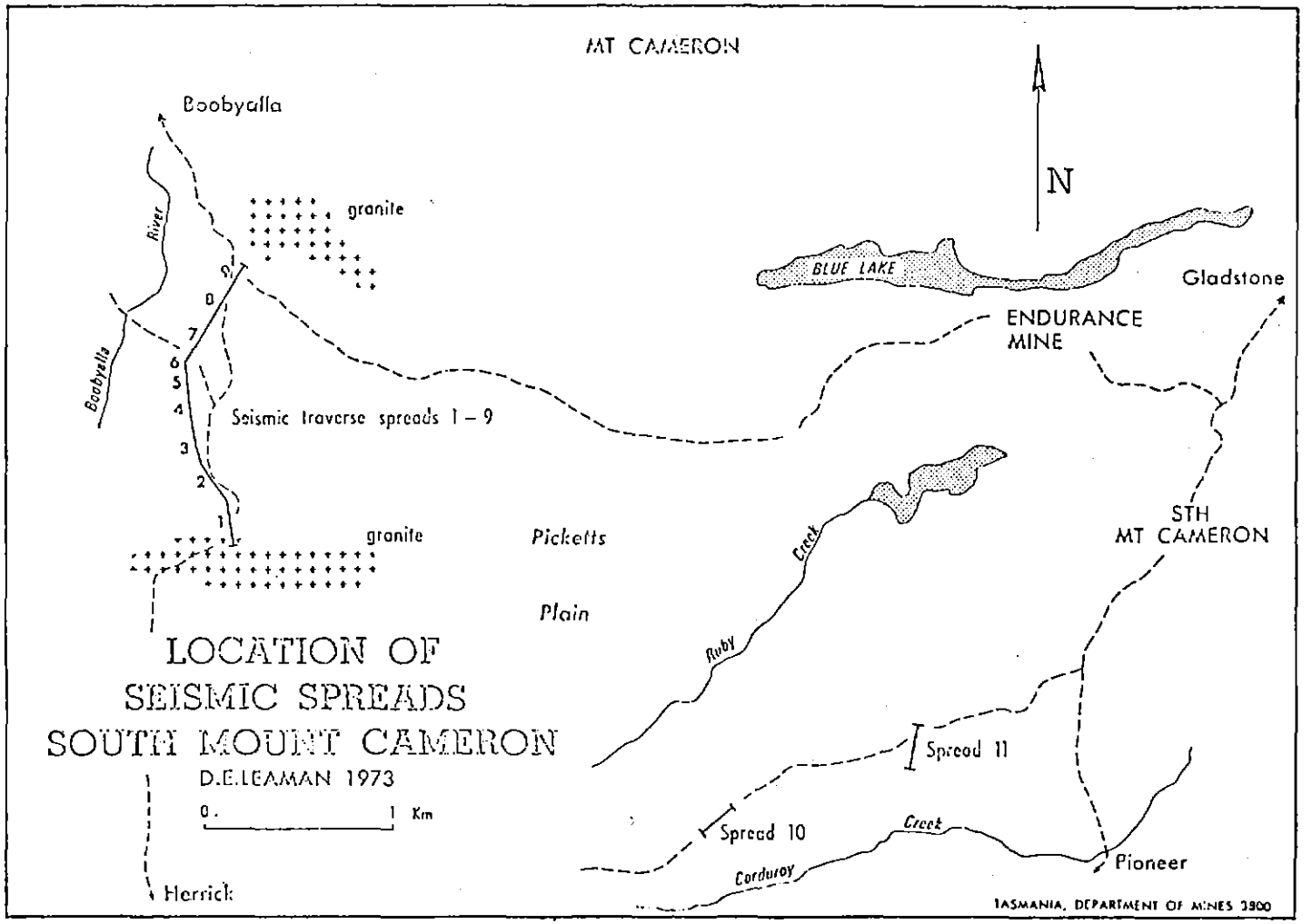

Fig.1.6. Location of seismic survey at South Mt. Cameron (From Leaman, 1973).

5 cm

on Picketts Plain between Ruby Creek and Corduroy Creek (see Figure 1.6.). The latter is believed to be the nearest area to the Eastern Lead and the geological conditions might be expected to be similar. In this area three layers were found and significant weathering of the granite appears to be absent (Leaman ,1973). The characteristics of the layers are :

-The velocity range of the first layer is 400-800 m/s with thickness variable up to 7 m , which represents soil and weathered overburden (dry or not compact) whether derived in situ from the weathering of granite or deposited as a sediment.

-The velocity range of the second layer is 1400-1800 m/s with thickness variable up to 57 m , and is considered to represent Tertiary sediment which must be both wet and well compacted. Leaman stated that the values recorded are near the maxima for Tasmanian Tertiary materials. This interpretation is supported by the presence of Tertiary sediment in the bore hole near spread 7.

-The velocity range of the third layer is 4500-6700 m/s which represents massive or fresh rock.

In spread 10 the depth of the Tertiary sediment/granite interface was found to increase from 39 m in the west to 64 m in the east. The interpretation of spread 11 is not as certain but the depth of the granite interface ranges from 53 m in the north to 49 m in the south. It has been stated that the interpreted depth may be in error by in excess of 5-10 m.

CHAPTER 2

GEOLOGY

Regionally, as shown in Figure 1.2., the geology of the study area is part of the Ringarooma lead and Tertiary basin, South of Mt. Cameron, which has been described by Brown (1982). Reports in relation to the lead are also presented by Twelvetrees (1900), Nye (1925), Jack (1960), Sedmik (1961), Chesnut (1965), Leaman (1973), Brown (1977), and many others.

The district is composed of Mathinna Beds sediment, granitic rocks, basaltic rocks and Tertiary sediments. The oldest rocks are the slates and sandstones of Mathinna series of Silurian period. During the Devonian granitic rocks were intruded over large areas within the district. The granitic rocks are part of the major batholiths of North Eastern Tasmania. During the mid-Tertiary these rocks acted as source material which filled up an active river system which is now known as the Ringarooma Lead. The lead consists of a main channel with numerous tributaries which terminated in an inland basin/lake to the south of Mt. Cameron. During the Middle -Lower Miocene, the system was covered by flows of basaltic lava originating from several sources within the district.

Based on the field mapping, drill hole, and seismic data from the Winnaleah area, the downslope direction of the channel is north-easterly from Derby towards Mt. Cameron. The channel has a very low gradient, whereas most of the tributaries which have been worked for tin, have a fairly steep initial gradient which then flattens out about 500 m before reaching the main channel. As can be seen from the map in Figure 1.2., a number of holes were drilled by the Department of Mines during 1972-1973 which established the depth to the granitic basement along a north-south

line from Herrick to the western end of Mt. Cameron. Older drilling programmes which were conducted by Austral-Malay (1935), Scott (1930) and Twelvetrees (1913) indicated the shape of the basement around Pioneer, Echo, and Clarence leads respectivelly. Some other drilling has been done in the Hasties area, Eastern Lead, and Endurance Lead. The deepest proven thickness of sediment was found on the Herrick-Boobyalla road at Winnaleah area. The thickness is 123 m which was derived from the drilling result provided by the Department of Mines.

Based on drilling and sampling results given by the Utah Development Company, alluvial tin in North Eastern Tasmania generally occurs concentrated in the basal gravels of buried Tertiary river channels or leads, although some tin also occurs scattered through thin upper Tertiary gravels and sands (Warin and Appleby, 1965). In Eastern Lead, the section consists of an upper horizon of clayey sand varying up to 5 m in thickness with basal 1.3 cm birdseye wash, overlying approximately 15 m of coarse grained clayey sand. Bore hole locations and lithological sections provided by the Utah Development Company are shown in Figure 2.1. and Figure 2.2. respectively. At the base of this section, a sub angular to sub rounded wash to 3 m in thickness lies on decomposed granite. No tin was found in this basal wash. However, the upper stanniferous horizon gave an average for 10 holes of 0.17 kg Sn/m^3 to 2 m depth. From this, 457,200 m^3 of this grade material might be expected, and should be an economic proposition for a small syndicate.

Hare (1961) showed that the kaolinised and leached granites of the South Mount Cameron area of Tasmania are suitable for mining and treatment to produce a high grade filler clay used in the paper manufacturing industry. By 1975, much of the surface at Eastern Lead had been stripped

in tin mining operations and several patches of stained saprolite were exposed. A churn drill with 12.7 cm casing was used to bore 6 holes in apparently favourable positions. Four of these passed through 18.3 m of near-white saprolite. It was concluded that in the area extending south-easterly from Scotts to the Ringarooma River, a very large volume of high-yield saprolite occurs but only small isolated patches reach or exceed 80 brightness required for paper making. In the study area the deposit is a highly weathered and leached granite, in which the feldspars have been completely kaolinised and iron almost completely removed. This resulted in a soft, white kaolinitic clay which is sometimes loaded with the quartz grains of the original granite.

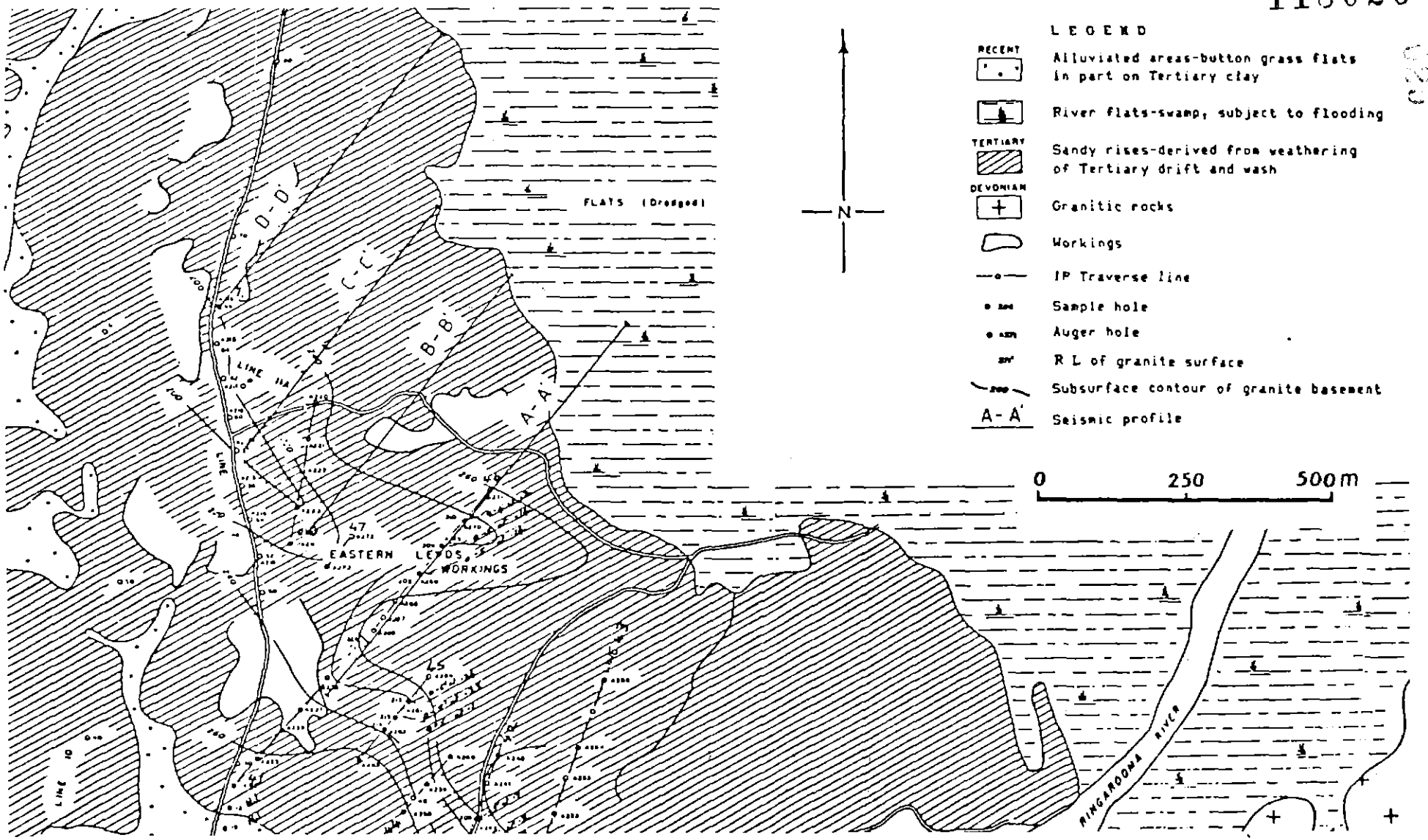

Fig.2.1. Approximate position of seismic profiles with respect to bore hole locations. This map is based on the geological map of TEST AREA 4 - EASTERN LEADS (Plate No.4) and drilling by the Utah Development Company (Appelby & McEwan, 1966).

5 cm

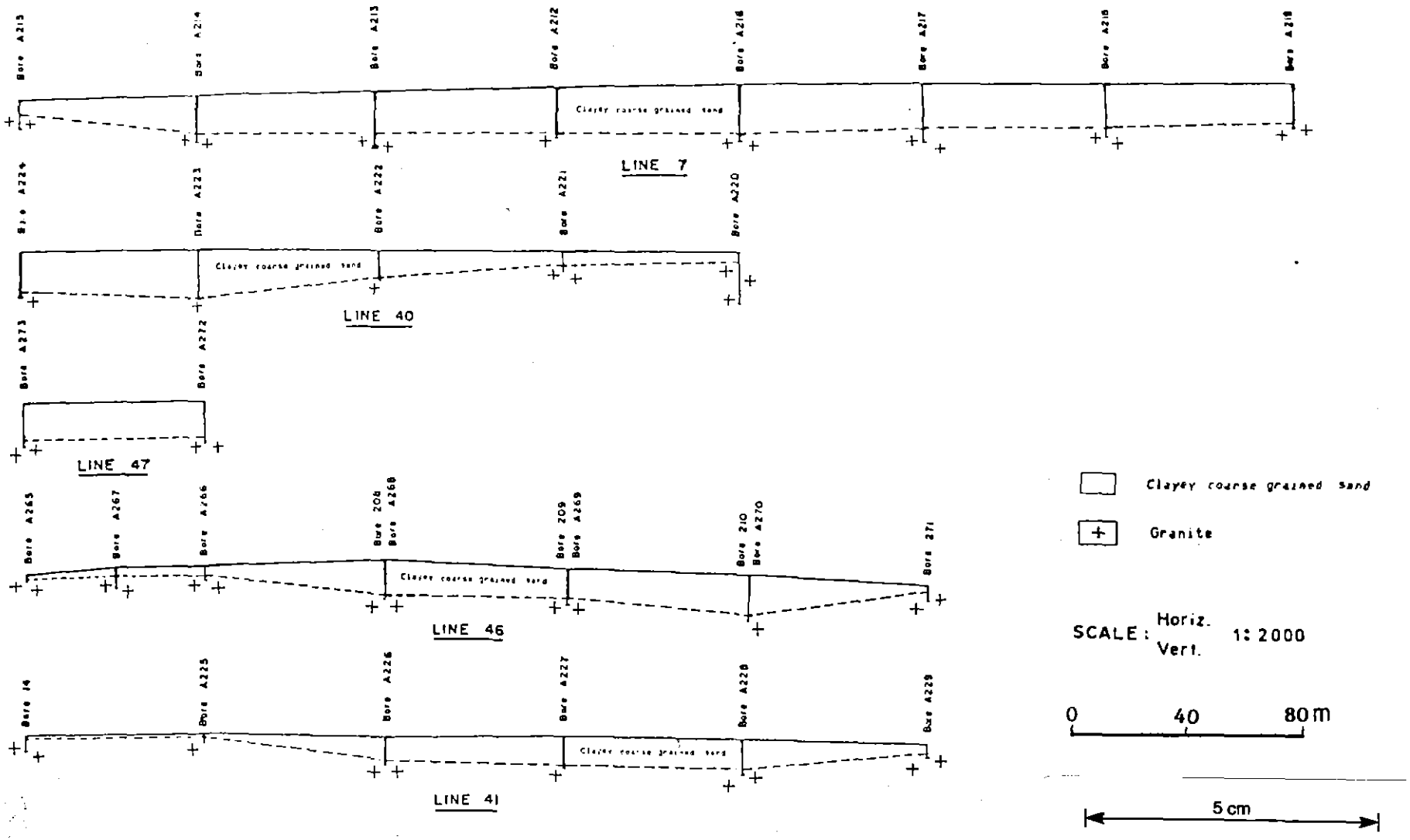

Fig.2.2. Lithological sections of TEST AREA 4 - EASTERN LEAD (Plate No.5) by the Utah Development Company (After Appleby & McEwan, 1966).

CHAPTER 3

GENERAL PRINCIPLES

3.1 ELASTIC WAVES

The seismic method is one of the geophysical techniques involving the study of the geological structure of the Earth's crust by means of studying the propagation of artificially created elastic waves. In geophysical prospecting the seismic method is based on the fact that elastic waves travel with different velocities in different geological strata. Often velocities increase with depth, a feature required for the refraction method. The seismic waves can be created by detonating a dynamite charge in a hole or above the ground, weight-dropping, electrodynamic shaking, etc. A classification of present-day seismic sources can be found in Parasnis (1979), page 189, and in the table of physical source information provided by Miller et.al. (1986), page 2069, which is suitable for shallow seismic sources. From the shot points the elastic waves propagate in all directions and penetrate into the earth and the waves are reflected and refracted at interfaces and return to the surface. The elastic waves are then picked up by detectors at certain points along a straight line on the surface, and by determining the time of arrival of the waves, the depth to the reflector or refractor and angles of dip of the strata can be determined.

In seismic prospecting methods the frequency of the wave oscillations can be low-frequency (< 25-30 HZ), medium-frequency (30-80 HZ), and high-frequency (> 80 HZ). The frequency used is usually based on the depth of the geological interest and the absorption properties of the media.

Useful waves (signal) and interfering waves (noise) are generally recorded on a seismic record. These include reflected and refracted longitudinal waves, surface waves, microseisms, sound waves, diffracted waves, and multiply reflected, reflected-refracted, and refracted-reflected waves.

3.2 SEISMIC REFRACTION

The seismic refraction method is based on the propagation of elastic waves transmitted in a medium containing velocity discontinuities. The refraction of seismic waves is shown in Figure 3.1.a. where the first medium with velocity V_1 is underlain by the second medium with velocity V_2 (where $V_2 > V_1$). According to Snell's law

$$\frac{\sin i}{\sin r} = \frac{V_1}{V_2} \qquad (3\text{-}1)$$

where i is angle of incidence and r is angle of refraction.

When the angle of incidence increases so that the angle of refraction becomes 90° (Figure 3.1.b.), the equation (3-1) becomes

$$\frac{\sin i_c}{1} = \frac{V_1}{V_2} \quad \text{or} \quad i_c = \sin^{-1}\left(\frac{V_1}{V_2}\right) \qquad (3\text{-}2)$$

where i_c is the critical angle of incidence. In this condition the ray AB is refracted and travels along the boundary between the medium. As a result of the oscillating stress at the interface, the wave travelling along

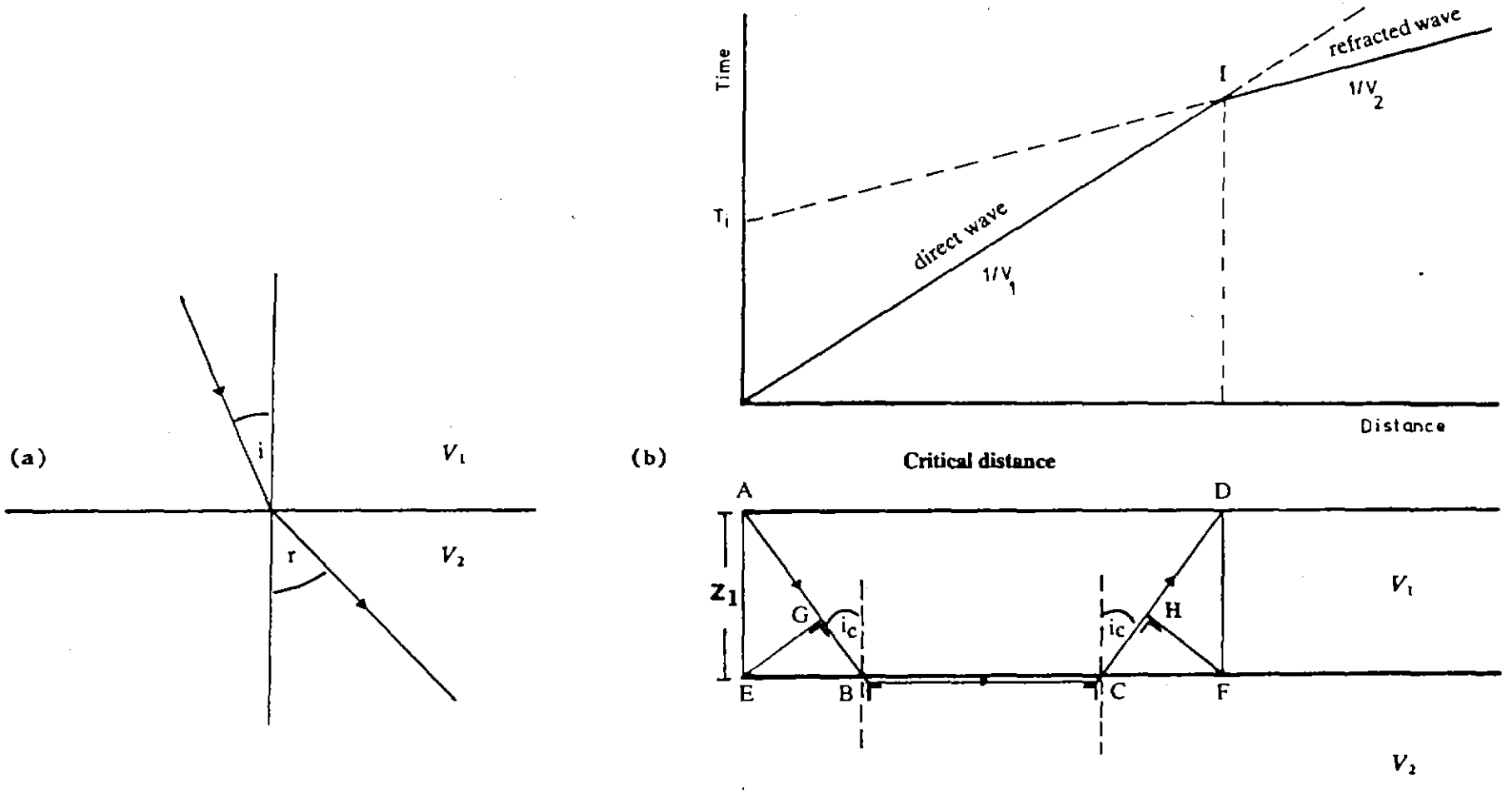

Fig.3.1. **(a)** Snell's law. **(b)** The basic idea of time-distance graphs and seismic refraction method.

the boundary generates a secondary waves CD which then emerge in the first medium at the same angle i_c to reach the surface.

Other possibilities can also be found such as downward deflection of the raypath in the second medium which occurs when the velocity of the second medium is less than the velocity of the first one ; a diffracted wave as a result of prominent velocity changes in the refractor or due to edges in the refracting interfaces or faults ; and non-critical refraction which is generated when the wavefronts are not normal to the refractor. These are discussed by Sjogren (1984), Dobrin (1976), etc.

As shown in Figure 3.1.b. , a traveltime-distance graph can be made by plotting the first arrival of the elastic waves recorded by detectors. The slopes $1/V_1$ and $1/V_2$ are the reciprocal of the velocity of the first and the second media respectively. At point D the travel time of direct and refracted waves is equal. On the traveltime-distance gräph the point is specified by point I. This point can also be regarded as an intersection between the direct wave velocity line and the refracted one. The point D is called the break point, and the distance between the impact point or shotpoint and the break point is known as the crossover distance or critical distance. Depth calculation at the impact point can be obtained by using critical distance or intercept time T_i where the intercept time is specified by the intersection between the extrapolation of the refracted wave velocity line and the time axis through the impact point. With a condition shown in Figure 3.1.b. :

- the direct arrival time $T_1 = AD / V_1$;

- the refracted arrival time $T_2 = AD / V_2 + 2 Z_1 \cos_{ic} / V_1$;

- the intercept time $T_i = 2 Z_1 \cos_{ic} / V_1$;

so that the depth Z_1 at the impact point A can be given as

$$Z_1 = T_i V_1 / 2 \cos_{ic} \qquad (3\text{-}3)$$

or in terms of velocities V_1 and V_2 as

$$Z_1 = T_i V_1 V_2 / 2 \sqrt{(V_2^2 - V_1^2)} \qquad (3\text{-}4)$$

since $\cos_{ic} = \sqrt{1 - V_1^2 / V_2^2}$

The seismic refraction method uses a concept known as delay time. According to Barry (1967), delay time is not an observable quantity but is a function of the depth to a refracting horizon and of the velocities of propagation along the refractor and through the overlying media. Since the refracted waves propagate from the impact point and finally emerge at the receiving point along the line on the surface, there will be a source delay time and a receiver delay time. From Figure 3.1.b. the delay time at the impact point A is equal to the delay time at the receiver point D because the refractor is assumed to be flat and is parallel to the ground surface. This can also be regarded as the traveltime for the slant raypath (AB or CD) minus the time required to travel the normal projection of the raypath on the refractor (EB or CF),or the shot or receiver delay time can be written as

$$T_{AB} - T_{EB} = T_{AG} = Z_1 \cos_{ic} / V_1 \qquad (3\text{-}5)$$

In these conditions, the intercept time will be equal to the sum of these two delay times.

When the depth of the interface or refractor is not constant, however, the delay times are different. Sjogren (1984) stated that one of the main problems in refraction depth determination is to partition the intercept time into one delay time at the impact point and another at the detector position. Details of depth determinations for three-layer case and multilayer cases including fieldwork and interpretation procedure in shallow refraction seismic can be found in Sjogren (1984), Barry (1967), and Gardner (1967).

3.3 THE GENERALIZED RECIPROCAL METHOD

The Generalized Reciprocal Method is part of the seismic refraction method developed by Palmer (1980), which can be regarded as a combination of the migration aspects of the delay time method (Barry, 1967) and the simplicity of computation of the reciprocal method of Hawkins (1961). In this method the reciprocal time or the traveltime from shotpoint to shotpoint is required, and the interpretation is obtained by examining the time distance curves. A forward and reverse arrival time at different geophone separations known as XY distance or XY value along a refraction profile can be determined from the characteristic features of plotted velocity function and time-depth. In this case the optimum XY value will be assumed to be associated with arrival times from approximately the same point on the refractor. A depth section can be obtained by converting the best time-depth or time section available. These solutions can be achieved

manually or by means of a computer programme. In this thesis, however, part of the seismic refraction work has been done by computer, that is the trace plotting and frequency filtering of the raw seismic refraction data.

Palmer (1980) stated that the method offers many advantages compared with the previously published methods of seismic refraction interpretation. These includes the detection of possible hidden layers and the average velocity in the overburden and also accurate depth calculations even in the presence of hidden layers and continuous changes in velocity with depth.

3.3.1 The reciprocal time correction

In the reciprocal method the seismic data is obtained using an in line arrangement of receivers or geophones and shotpoints with pairs of corresponding shotpoints bracketing the geophone spread. Theoretically the traveltime from shotpoint to shotpoint via the refractor (forward and reverse) or the reciprocal time has to be the same. In reality, however, there are discrepancies. This probably due to the position of the reciprocal geophone which is at the most distant from the shotpoint. As a result it receives only a small amount of energy because the head waves are attenuated as the inverse square of the distance (Grant and West, 1965). In addition, as the earth acts as a low-pass filter, the higher frequency of the seismic waves will be attenuated more rapidly than the lower ones (Attewel and Ramama, 1966).

Hatherly (1980) stated that the traveltime errors can be due to delays in the shot firing system or detonator ; errors in the up hole correction ; poorly picked arrival times ; and disturbance of the ground near the

shotpoints as a result of previous shots. He also suggested that the first two errors will affect every traveltime from a given shot with a constant amount of error, and the third one will only affect an individual traveltime, while the last one may either be a constant error affecting all times or just affecting an individual traveltime. Since the individual time errors have been removed the constant errors due to the reciprocal time within the spread can be corrected by using the Hatherly's formula :

$$a_i = -1/n \sum_{j=1}^{n} [\, C_{ij} \,]\ j \neq i \qquad (3\text{-}6)$$

where a_i is the reciprocal time correction

n is the number of shots inside the spread

C_{ij} is the traveltime from shotpoint i to shotpoint j minus the traveltime from shotpoint j to shotpoint i (the error in the reciprocal times)

When forward and reverse traveltimes between all shotpoints are available, the reciprocal time correction a_i then added to all of the traveltimes from the i_{th} shot. Another formula has also been described by Hatherly (1980), that is a reciprocal time correction which can be applied if the traveltime data to the shotpoints is missing.

3.3.2 The intercept time

Intercept time also plays an important role in The Generalized Reciprocal Method, because in the interpretation phase the time-depths have to be adjusted as closely as possible with half-intercept times. In the case where the interfaces are flat with no lateral changes in velocity, the

intercept times can be obtained by simply projecting the simple straight line segments of the traveltime curve corresponding to the successive layer back to the shotpoint.

With undulating interfaces or lateral velocity variations, however, inflections of traveltime curves of refraction first arrivals occur. Generally, this requires the interpreter to relate inflection points on traveltime curves either to crossover points or to lateral geologic changes, to identify the segments between crossover points with their corresponding refracting horizon, and to reconstruct the hidden remainder of the traveltime curve for each horizon from the limited first arrival data. This problem can be solved with the use of multiple shotpoints. To achieve an unambiguous identification, Ackermann et.al. (1986) used related traveltime curves. They classify such related curves as reversed, split and offset profiles. They also give examples of how to identify crossover points and possible horizons together with the identification of intercept times with the use of parallelism.

According to Palmer (1980), with undulating refractors or lateral velocity variations, the traveltime curves depart from sets of simple straight line segments. For this reason the intercept times are obtained from lines of the best fit. This, of course, will reduce the accuracy of the intercept times. Fortunately, he developed a generalized intercept time which is valid for the plane layer case and undulating refractors, and even for the traveltime data recorded in one direction. Referred to Figure 3.2., the generalized intercept time at A can be given as

$$[\, t_{CA} - (t_{CG} - t_{AG})] \qquad (3\text{-}7)$$

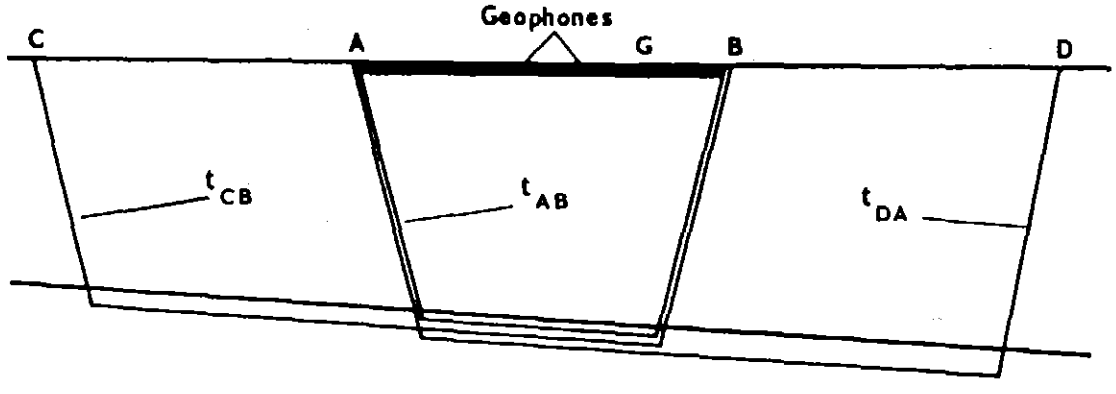

Fig.3.2. Raypaths used in the calculation of a reciprocal time from an intermediate value (From Palmer, 1980).

In this case the term (t_{CG} - t_{AG}) is the separation between the curves, and this equation displaces the traveltime curve from the shotpoint at C to coincide with the traveltime curve for the shotpoint at A.

3.3.3 The velocity analysis functions

In this thesis, the velocity analysis function is calculated through the equation (2) developed by Palmer (1980), which is defined as

$$t_v = (t_{AY} - t_{BX} + t_{AB})/2 \qquad (3\text{-}8)$$

Here, the value (t_v) is referred to G which is midway between X and Y (Figure 3.3.). This equation can also be used even when the velocities of all layers above the refractor are not known.

For the case of XY is equal to zero, the velocity analysis functions is obtained using equation (7) of Hawkins (1961) in which this value can be specified as a corrected traveltime for the slant raypath from the shotpoint S' to the geophone G (Figure 3.4.). Thus, the velocity analysis functions for XY equal to zero is given by

$$t'_{S'G} = t_{S'G} - t_G \qquad (3\text{-}9)$$

where $t_{S'G}$ is the recorded traveltime, and

t_G is the time-depth which is given as

$$t_G = (t_{S'G} + t_{S''G} - t_{S'S''}) / 2 \qquad (3\text{-}10)$$

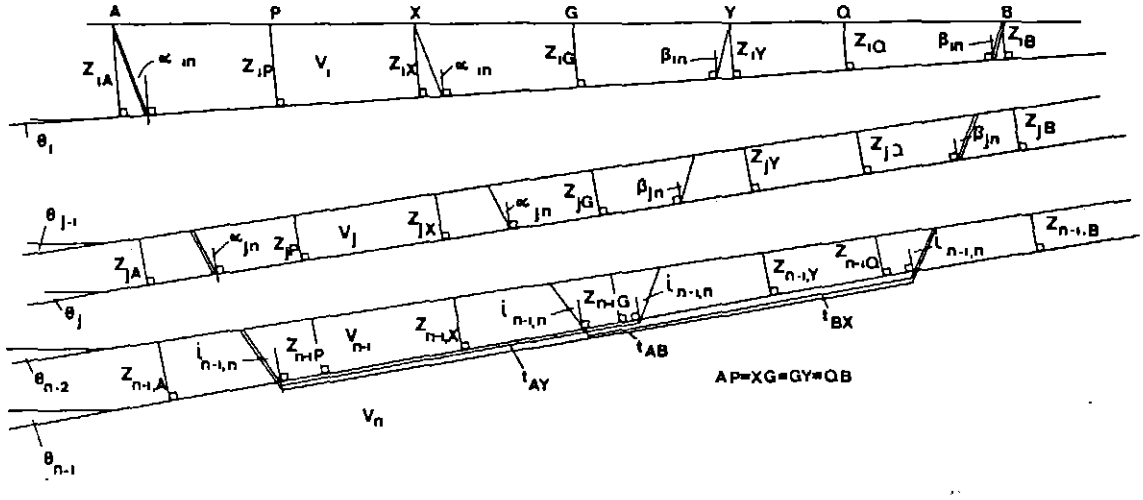

Fig.3.3. Raypaths used in the definitions of the velocity analysis and time-depth functions (From Palmer, 1980).

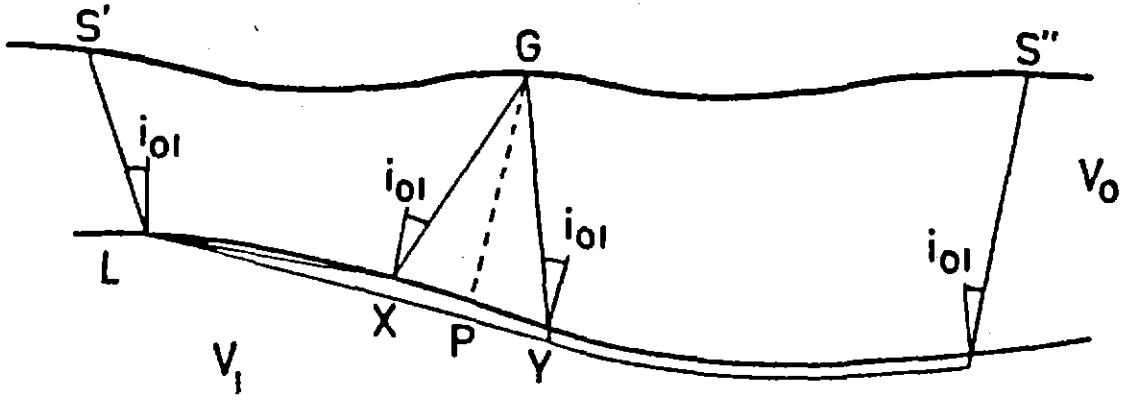

Fig.3.4. Raypaths in calculation of time-depth (From Hawkins, 1961).

In routine interpretation, the values of t_v are plotted against distance for different XY values. As the optimum XY value is obtained, a refractor velocity V'n is then given as its inverse slope. However, in this thesis only the optimum XY values are plotted for clarification.

3.3.4 The time-depth

Referred to Figure 3.3., the generalized time-depth t_G or time-depth at G is defined by the equation

$$t_G = [\, t_{AY} + t_{BX} - (t_{AB} + XY/V'n)\,]/2 \qquad (3\text{-}11)$$

where V'n is the apparent refractor velocity determined from the velocity analysis function. In this case, several special cases of the time-depth can be derived by using different XY values.

When XY is equal to zero, the time-depth t_G becomes the conventional time-depth t_G (equation 3) defined by Hawkins (1961), that is equal to

$$(\, t_{S',G} + t_{S''G} - t_{S''S'}\,) / 2 \qquad \text{(Referred back to Figure 3.4.).}$$

The time-depths near shotpoints where the ray from the shotpoint is critically refracted can be obtained using this equation (equation 15, Palmer , 1980)

$$[\, t_v \,]_{x=0} = \sum_{j=1}^{n-1} Z_{jp} (\cos \alpha jn + \cos \beta jn) / 2 Vj \qquad (3\text{-}12)$$

For the notation see Figure 3.3.

3.3.5 The optimum XY-value

Palmer (1980) stated that at the optimum XY spacing the forward and reverse rays emerge from near the same point on the refractor, so the refractor need only be plane over a very small interval. There are several methods for determination of an optimum XY value :

First, when horizontal layering occurs, the optimum XY value is specified by the following equation

$$XY = \sum_{j=1}^{n-1} 2\, Z_j G \tan i_{jn} \qquad (3\text{-}13)$$

This equation can be used for dipping layers ($< 20^{\circ}$). The notation is referred to Figure 3.3.

Second, the optimum XY value can be specified by the separation of distinctive features on the traveltime curves of forward and reverse shots.

Third, this value can be obtained from inspection of the velocity analysis and time-depth calculations for several XY values. The optimum XY values will be indicated by the simplest form of the velocity analysis curves or when the velocity analysis function most closely approximates a straight line, and the time-depths show the most detail.

When an optimum value cannot be determined, and the full presentation verifies that The Generalized Reciprocal Method parameters are a result of a featureless refractor, a zero XY-value can be used for depth calculation. An improvement in this determination can also be achieved by using more accurate traveltime data and statistical methods.

3.3.6 The depth conversion factor

The depth conversion factor for a two-layer geometry is simply a constant (denoted DCF), which, when multiplied by the time-depth t_G, results in the thickness of the first layer.

According to Hawkins (1961), the depth conversion factor is a velocity term which may be written in the form

$$\frac{V_m \quad V_n}{(V_n^2 - V_m^2)^{1/2}} \qquad (3\text{-}14)$$

where Vm and Vn are the velocities of the overburden and the refractor respectivelly. For a dipping interface, the definition of the depth conversion factor is approximate. As Palmer (1980) states that the depth conversion factor is insensitive to dip angles up to about 20 degrees, the above equation is perfectly adequate for depth calculations (Kilty et.al., 1986).

3.4 SEISMIC REFLECTION

The seismic reflection method generally determines subsurface geological structures based on measurements of the arrival time of elastic waves reflected from interfaces between geological boundaries. On land, the waves are generated by active sources of energy at the surface. For shallow seismic reflection methods, a small source of energy is needed such as a sledge hammer blow or a small detonator. If a deeper horizon is to be mapped, a large source of energy is used, generally a dynamite explosion.

From the source of energy at the shot point, three main types of elastic waves propagate through the media. These are longitudinal or compressional waves (P-waves), transverse or shear waves (S-waves), and surface waves. The P-waves are usually considered to be the useful waves in seismic exploration, so that the recorded S-waves and surface waves are categorized as noise.

In the case of nonnormal incidence, when the P-wave strikes an interface between media with prominent density and elastic constant discontinuities , wave type conversion occurs. This results in the reradiation of four different waves. These are the reflected compressional wave, the reflected shear wave, the transmitted compressional wave, and the transmitted shear wave. Snell's law of refraction gives the angles of reflection and transmission as a function of the incident angle and the shear and compressional velocities (Sengbush, 1983). This is given by

$$\frac{\sin a_1}{Vp_1} = \frac{\sin a_2}{Vp_2} = \frac{\sin b_1}{Vs_1} = \frac{\sin b_2}{Vs_2} \qquad (3\text{-}15)$$

where a_1 is the incident and reflected compressional angle, a_2 is the transmitted compressional angle, and b_1 and b_2 are the reflected and transmitted shear angles. The amplitude of the waves are designated by A_0 for incident compressional, A_1 for reflected compressional, B_1 for reflected shear, A_2 for transmitted compressional, and B_2 for transmitted shear (see Figure 3.5.). These amplitudes for various incident angles can be calculated from the Zoeppritz equations which have been described by Richter (1958).

For normal incidence or when a ray is perpendicular to the interface, the reflection coefficient R which defines the ratio of the amplitude of the reflected wave and the incident wave is given by

$$R = \frac{\rho_2 Vp_2 - \rho_1 Vp_1}{\rho_2 Vp_2 + \rho_1 Vp_1} \qquad (3\text{-}16)$$

The product of density ρ and seismic velocity Vp is known as the acoustic impedance. The greater the difference between the acoustic impedances on each side of a reflecting boundary, the greater will be the amplitude of the wave reflected from it (Gurvich, 1972). In seismic reflection, the desired reflected events are the primary reflections, that is the waves that travel down to a given reflector or reflectors and then back up to the surface, where they are recorded.

Basically, the seismic events are obtained by using a single source point and many receiver points which lie along a straight line through the source point. The maximum shot-detector distance should be of the order of or smaller than the depth to the shallowest horizon of interest, to ensure that the observed seismic waves are due to reflections and not refractions.

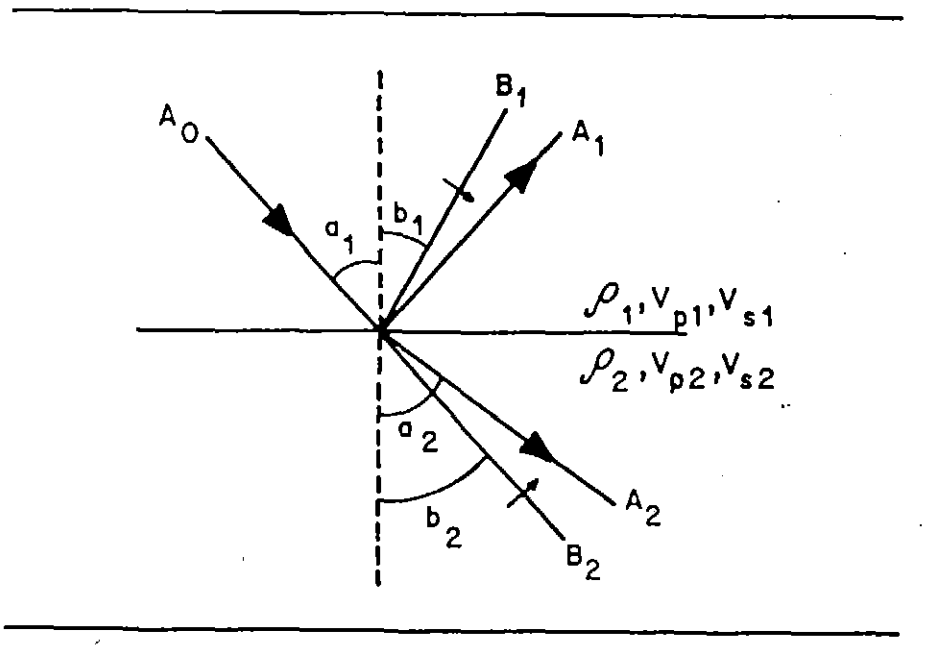

Fig.3.5. Snell's law (From Sengbush, 1983).

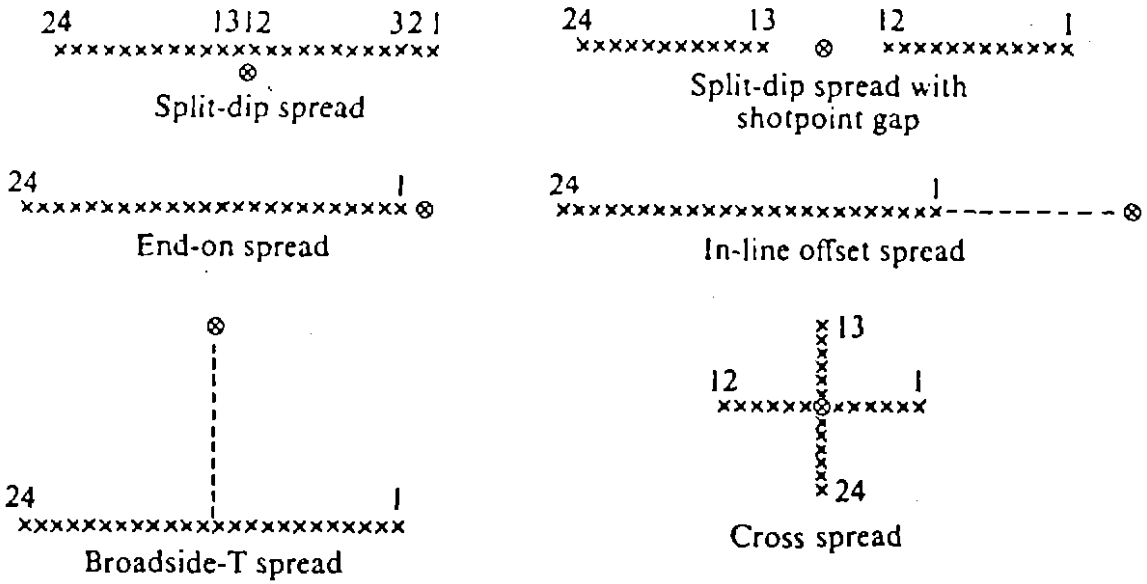

Fig.3.6. Types of reflection spreads. The symbols × and ⊗ represent geophone groups and sourcepoints, respectively (From Sheriff and Geldart, 1982).

The use of shot-detector arrangements or spread types have been described by Sheriff and Geldart (1982), and the configuration used is illustrated in Figure 3.6.

3.4.1 Geometrical considerations

In the reflection method, the subsurface geological information is obtained from the travel times of the reflected waves. In the case of a gentle dip when the direction of profiling is along the direction of dip or strike, a two-dimensional solution is generally used. For simplification, we assume that the reflections originate on plane horizontal or inclined surfaces. The primary reflected waves are the most important in this method.

Illustrated in Figure 3.7. is a simple model of a single flat interface overlain by a uniform layer with velocity V. S is the shotpoint, D is the reflection point, and R is the receiver. Since the point I is the image point of the source S, the length of the raypath SD is equal to the distance ID. From the right angled triangle SIR, it can

be seen that $$(IR)^2 = (2Z)^2 + X^2 \quad ,$$

where $$IR = SDR = VT \quad \text{and} \quad 2Z = VT_0$$

In this case T is the total traveltime for the slant raypath, whereas T_0 is the vertical two-way traveltime. Substituting VT for IR , and VT_0 for 2Z

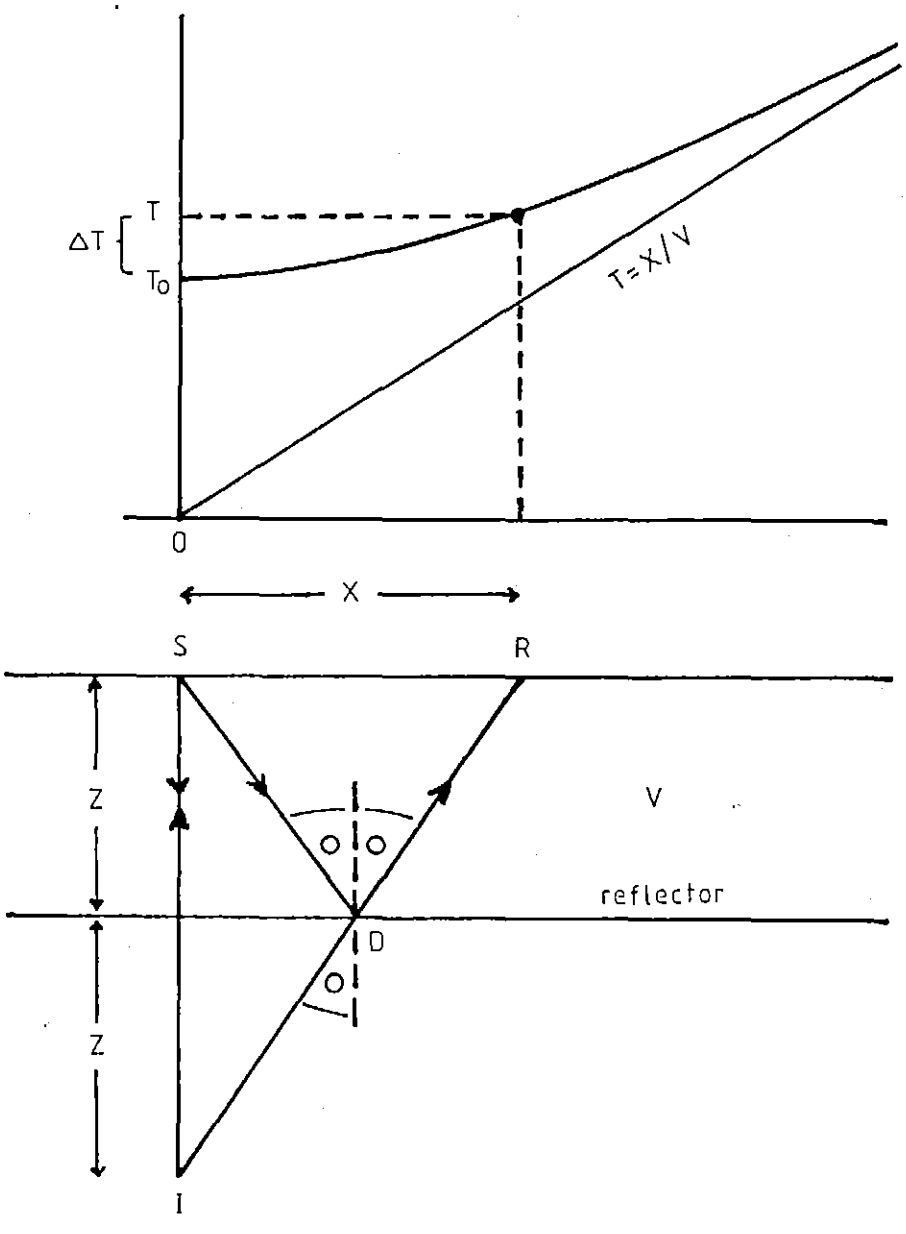

Fig.3.7. Traveltime curve for horizontal reflector.

in the above equation, we have $V^2T^2 = V^2T_0^2 + X^2$, or

$$T^2 = T_0^2 + X^2 / V^2 \qquad (3\text{-}17)$$

which is a hyperbolic equation for the reflection traveltime curve. For large offset distances the slope of the reflection traveltime curve becomes asymptotic to $T = + X/V$ (which is a linear equation of the direct traveltime curve), with the reflected rays emerging near horizontally. The difference in traveltime given by $T - T_0$ is called the normal moveout. For the model of a single horizontal interface with 2Z greater than X , the normal moveout or NMO is

$$T - T_0 \approx X^2 / 2 V^2 T_0 \qquad (3\text{-}18)$$

In the case where a single flat interface is inclined, the axis of symmetry of the hyperbolic traveltime curve is shifted from the T-axis (see Figure 3.8.). The axis of symmetry becomes the line $X = - 2 Z\sin \alpha$. On a reflection field record the vertex of the hyperbola and its asymptotes will be displaced in the updip direction with respect to the shotpoint, whereas the updip branch of the reflection hyperbola terminates at the traveltime curve of the direct wave. This give rise to different values of the arrivaltime T even if the receivers are symmetrically placed on opposite sides of the shotpoint. The simplest method of finding the dip has been described by Sheriff and Geldart (1983), that is from the difference in traveltimes for two geophones equally distant from, and on opposite sides of the shotpoint. From this, the dip α, for example, is given by

$$\sin\alpha \simeq 1/2\ V\ (\triangle T_d / \triangle X) \qquad (3\text{-}19)$$

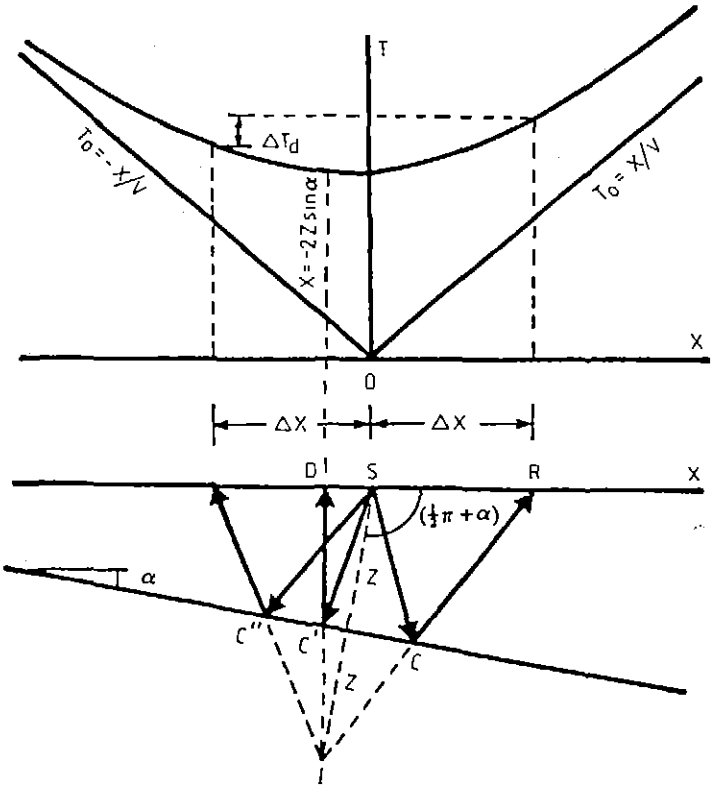

Fig.3.8. Traveltime curve for dipping reflector (After Sheriff and Geldart, 1982).

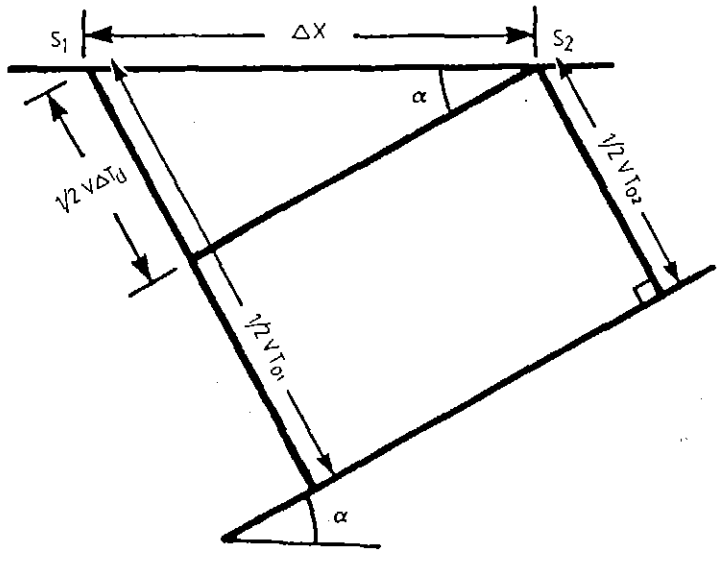

Fig.3.9. Geometry involved in dip moveout measured between shotpoints or on record sections (After Sheriff and Geldart, 1982).

where the quantity of $\Delta T_d / \Delta X$ is called the dip moveout ; ΔT_d is the difference between the traveltimes for two geophones equally distant from, and on opposite sides of the shotpoint; ΔX is the shotpoints-geophones distance; and V is the wave velocity. In addition, the dip moveout can also be measured by the time difference between T_0 at different shotpoints. As shown in Figure 3.9., in which

$$T_d = T_{01} - T_{02} \quad \text{,and} \quad \sin\alpha = 1/2\ V\ (\Delta T_d / \Delta X) \ ,$$

where ΔX is the distance between shotpoints. When measuring dip on a record section, ΔX is the distance between any two convenient points. Sheriff and Geldart (1983) also described the method of determining the dip moveout in the case of unavailability of a symmetrical spread (that is, by removing the effect of normal moveout).

3.4.2 Velocities estimation

Velocity distribution both vertically and horizontally is required in the conversion of reflection times to depths. This can be obtained by analysis of the time-distance relationships on the reflection records themselves, or by determining the velocity from well surveys. In addition it is also possible to use the velocity derived from non-reflection travel paths, such as head-wave or refraction wave velocity. The accuracy of velocity values derived from sources such as the curvature of diffractions, automatic migration methods, and the amplitude of reflections is usually poor (Sheriff and Geldart, 1983). The determination of such seismic velocities has been covered by many authors such as Dobrin (1976), Kleyn

(1983), Sengbush (1983), Robinson (1983), Sheriff and Geldart (1983), Slotnik (1959), and many others.

Dix's expanding spread technique for accurate estimation of interval velocities from surface seismic measurements has been discussed by Sengbush (1983). He mentions that the technique had a limited life because of the subsequent development of horizontal stacking, but the theoretical development is the cornerstone to an understanding of the velocity estimation. The widespread use of horizontal stacking has led to an abundance of velocity data that have proved useful for lithologic studies, in addition to their primary purpose of enhancing the stack to increase the primary-to-multiple ratio, and to improve the signal-to-noise ratio. The following velocities estimation is adopted from Dobrin (1976).

The average velocity is simply the depth Z of a reflecting surface below a datum divided by the observed one-way reflection time T from the datum to the surface, and can be written as

$$V_{average} = Z / T \qquad (3\text{-}20)$$

or if Z represents the sum of the thicknesses of layers Z_1, Z_2, $Z_3 \ldots Z_n$, the average velocity becomes

$$V_{average} = \frac{Z_1 + Z_2 + Z_3 + \ldots + Z_n}{T_1 + T_2 + T_3 + \ldots + T_n} = \frac{\sum_{1}^{n} Z_k}{\sum_{1}^{n} T_k} \qquad (3\text{-}21)$$

If two reflectors at depths Z_{i-1} and Z_i give reflections with respective one-way times of T_{i-1} and T_i , the interval velocity in the i_{th} layer is

$$V_{interval} = \frac{Z_i - Z_{i-1}}{T_i - T_{i-1}} \qquad (3\text{-}22)$$

If the velocity varies continually with depth, the instantaneous velocity at a particular depth Z becomes the derivative of Z with respect to T of the above formula, so that

$$V_{instantaneous} = dZ / dT \qquad (3\text{-}23)$$

If the section consists of respective interval velocities of V_1 , V_2 , V_3 ...., V_n and one-way interval traveltime T_1 , T_2 , T_3 ,...., T_n , the root-mean-square velocity V_{rms} is obtained from the relation

$$V_{rms}^2 = \frac{V_1^2 T_1 + V_2^2 T_2 + V_3^2 T_3 + \ldots + V_n^2 T_n}{T_1 + T_2 + T_3 + \ldots + T_n} = \frac{\sum_1^n V_k^2 T_k}{\sum_1^n T_k} \qquad (3\text{-}24)$$

This velocity can be obtained by taking the slope of the curve for T^2 versus X^2 at $X = 0$. Stacking velocity V_{st} is based on the relation

$$T^2 = T_o^2 + X^2 / V_{st}^2 \quad \text{or} \quad V_{st} = (X^2 / T^2 - T_o^2)^{1/2} \qquad (3\text{-}25)$$

where X is the variable separation of shot and receiver for a common depth point sequence of shots ; T is the traveltime at X ; and T_o is the vertical time. Dobrin (1976) suggested that it is approximately but not exactly the same as V_{rms} and is actually used in the stacking process. For a plane reflector, zero-dip case, having times T_{n-1} and T_n with respective rms velocities V_{n-1} and V_n , the interval velocity V_{int} between the reflections can be obtained from the Dix equation ,

$$V_{int} = \left(\frac{T_n V_n^2 - T_{n-1} V_{n-1}^2}{T_n - T_{n-1}} \right)^{1/2} \qquad (3\text{-}26)$$

where T_n is the total two-way time to the n_{th} reflector and V_n is the rms velocity to the n_{th} reflector. This velocity is referred to as the Dix interval velocity. Many other types of velocities determination can be found in the literature mentioned above.

Best-fit approaches are based on either finding the hyperbola which best fits coherent events assumed to be primary reflections, or finding which stacking velocity produces the "best" stacked section. This has been suggested by Sheriff and Geldart (1983). They also state that such measurements are generally sufficiently accurate for stacking but not always for the lithologic conclusions.

3.4.3 Noise attenuation

The success of seismic mapping is strongly dependent upon the quality of the seismic data. The data generally consists of signal which carries desired information and noise which tends to degrade interpretation. The seismic noise may be either coherent, or incoherent (random noise).

The coherent noise is sometimes subdivided into energy which travels horizontally and energy which reaches the spread more or less vertically. Another important distinction is whether the coherent noise is repeatable noise or not. The coherent noise characteristics (its travel direction and repeatability) form the basis of most methods of improving record quality (Sheriff and Geldart , 1982). Coherent noise includes surface

waves, reflections or reflected refractions from near-surface structures such as fault planes or buried stream channels, refractions carried by high-velocity stringers, traffic noise, multiples, etc. (Olhovich ,1964). Of these types multiples travel essentially vertically and all except traffic noise are repeatable on successive shots.

The incoherent noise which is spatially random and also repeatable is due to scattering from near-surface irregularities and inhomogeneities such as boulders, small-scale faulting, etc., whereas the non-repeatable incoherent noise may be due to wind shaking a geophone or causing the roots of trees to move generating seismic waves, falling stones ejected by the shot back to near a geophone, a person walking near a geophone, etc. (Sheriff and Geldart, 1982).

The variation of the quality of the seismic data is determined by conditions in the area and the equipment used in data acquisition, and data processing. The signal-to-noise ratio (S/N), is the ratio of the energy of the desired events with respect to all remaining noise in the same portion. In practice, this ratio is difficult to determine because of the difficulty in separating out the signal which constitutes the desired information.

A number of noise-attenuating techniques, however, can be applied in the field and also in the processing centre to provide better data which can then be interpreted in terms of the subsurface geology. These concepts have been suggested by many geophysicists such as Sheriff and Geldart (1982), Telford et.al. (1976), Sengbush (1983), Walker and Crouse (1985), Knapp and Steeples (1986), Dobrin (1976), and many others. The objective of the operations is to maximize the S/N ratio. In the field or during data acquisition, a noise spread should be done to obtain an optimum selection of

acquisition parameters such as source optimization, geophone-ground coupling, spread configuration, and the capability of the instruments. The use of properly designed and operated equipment and good field procedures, can minimize the recorded noise. In addition, multiple geophones or multiple sources (arrays) can also be used to cancel noise, because the addition of several random noises will partially cancel one another. Stacking techniques are generally used in attenuating noise by means of combining traces from different records or different places or both. These including CDP stacking, vertical stacking, uphole stacking, and several more complicated methods. In seismic data processing, other effective means of improving the S/N ratio include frequency filtering, velocity filtering, horizontal stacking, deconvolution, etc.

3.4.3.1 Common-depth-point (CDP) method

The CDP method is very well known and widely used in seismic reflection work, and was originally described by Mayne (1962). The method employs redundancy to severely attenuate unwanted interference and noise. Using the shotpoint-geophone arrangement shown in Figure 3.10. , a sampled profile representing common-depth-points is recorded with different horizontal distances between the shotpoints and geophone positions. The method involves sampling each depth point several times by moving the entire configuration laterally an appropriate increment. For a twelve-fold coverage, for example, each depth point will be mapped or recorded twelve times, once from each of twelve different offset distances. A collection of such traces for a given midpoint makes up a CDP gather which in this case is a twelve-fold gather, and is illustrated in Figure 3.11.

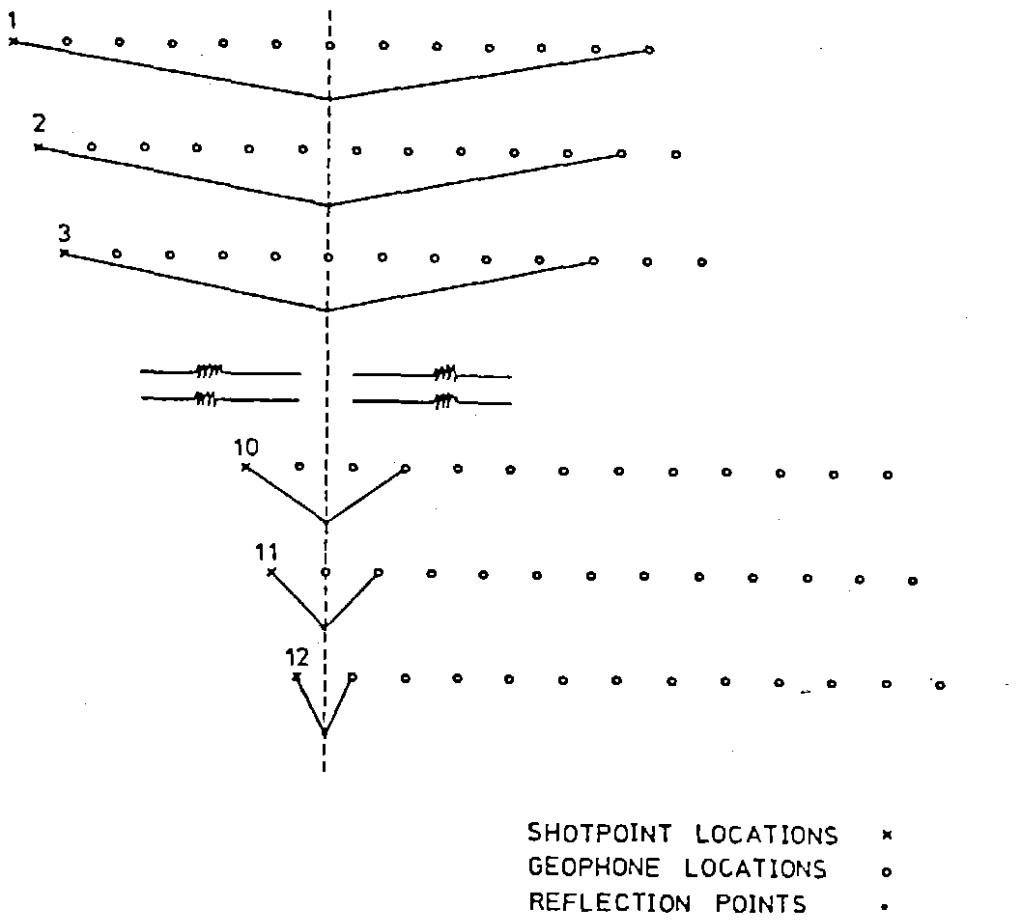

Fig.3.10. End-on spread giving 12-fold coverage. Shotpoint and spread are advanced together by half a station between successive recordings (From Brescianini, 1986).

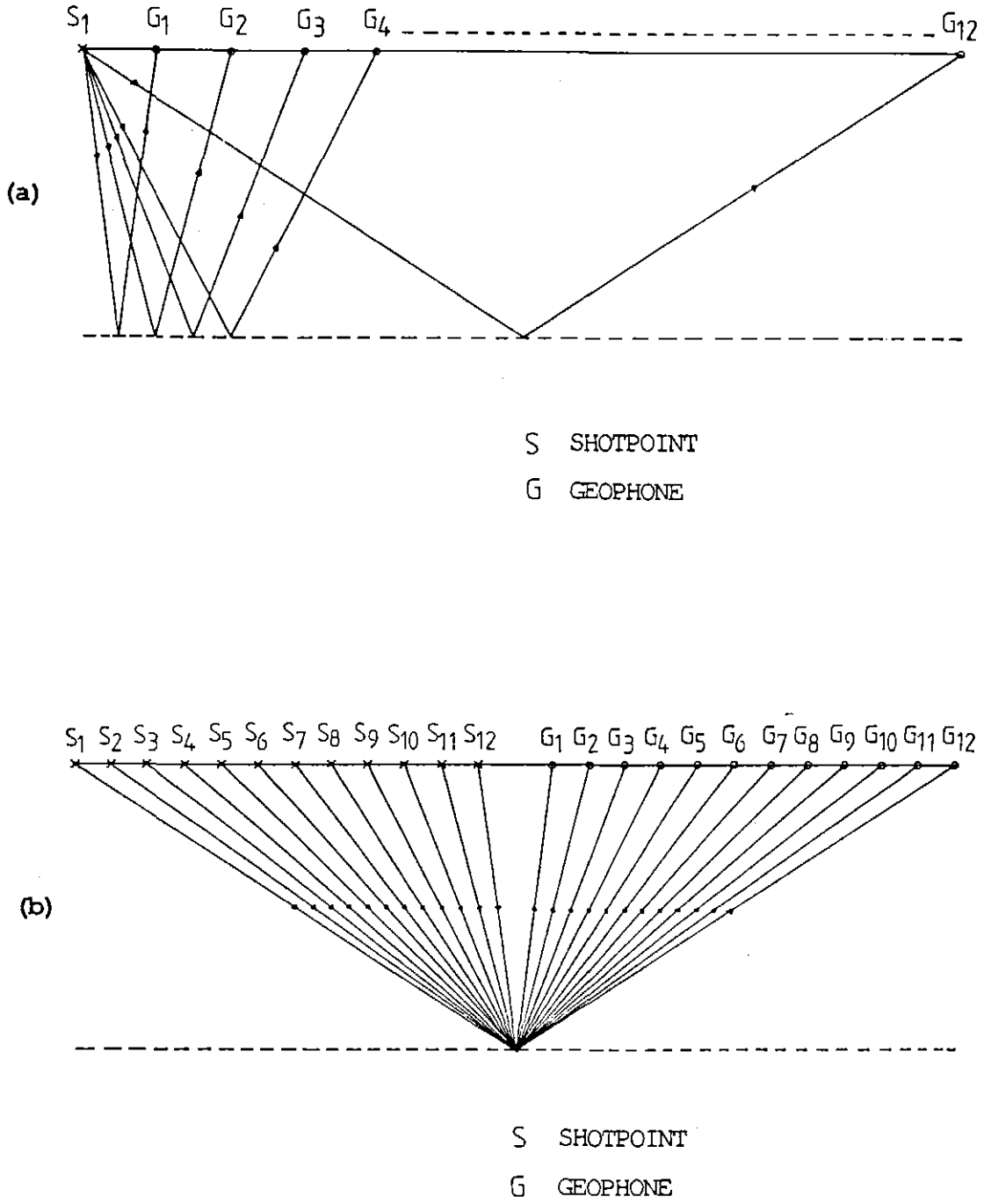

Fig.3.11. Collection of CDP gathers. **(a)** Data as recorded. **(b)** Data as reordered to form a CDP gather.

The fold achieved depends on the number of traces and the ratio of detector spacing (group interval) and shotpoints spacing. If we assume that the number of traces is equal to n and the ratio between group interval and shotpoints spacing is $\Delta d/\Delta s$, the general relation among them can be given as

$$\text{The fold coverage} = (n/2)(\Delta d/\Delta s) \qquad (3\text{-}27)$$

This relation (Sengbush ,1983) holds for any $\Delta d/\Delta s$ ratio for which the fold is an integer value less than or equal to n.

Before horizontal stacking, corrections generally have to be done for the traces which have a common reflection point. These include static and dynamic correction. The static correction is applied to eliminate the effects of changes in elevation at shotpoint and geophone locations, changes in shotpoint and geophone depths, and the variation in velocity and thickness of the near-surface or low velocity layer. The objective is to determine the reflection arrivaltimes that would have been observed if all measurements had been made on a flat plane with no weathering or low-velocity-material present. The dynamic correction or NMO correction is applied to eliminate the effects due to variable shotpoint-to-geophone distance along the reflection paths (Sheriff ,1982). Sengbush (1983) remarks that the static correction is always critical for land data, and static estimation is one of the most significant problems in reducing the data to a meaningful form for interpretation.

3.4.3.2 Filtering

Filtering in seismic data processing may be defined as a technique of improving a S/N ratio by discriminating a desired signal from unwanted signal or noise on the basis of frequency, apparent-velocity, or wavelength. The basic concepts of filtering have been described by Silverman (1967) including frequency filtering, velocity filtering, deconvolution, etc. A detailed description is given by Sheriff and Geldart (1982), Sengbush (1983), and Dobrin (1976).

Frequency filtering is generally designed on the basis of passing or rejecting certain frequency components of the signal within the processed input data. A band-pass filter which attenuates high and low frequencies, low-cut filter, or high-cut filter may be applied. The greater the differences between the components, the better they can be separated by filtering ; and conversely, the more alike the components, the poorer the separation (Silverman ,1967). This method can be used to eliminate the unwanted signal such as ground-roll, wind noise, and also narrow bands of 50/60 HZ frequencies due to power transmission line interference. A good example of frequency filtered data and some criteria for choosing the best bandwith are given by Swift (1984).

Velocity filtering, also known as fan filtering (Fail and Grau , 1963) or pie-slice filtering (Embree et.al. , 1963) can be applied to enhance signal and attenuate noise, and particularly to suppress high-velocity noise without damage to the reflection quality. The system is a wide-band multichannel filtering technique based upon the apparent velocity or dip moveout of a signal. In this case the range of apparent velocities of the seismic events can be analyzed by means of plotting the frequencies versus

wavenumbers of the events. The plot is called a frequency-wavenumber or F-K plot which is illustrated in Figure 3.12., and the range of apparent velocities will be proportional to the slopes of the radial lines. As the reflection events normally have a small moveout (even with a steep dip) compared with most travelling noise such as surface waves, the reflection events will fall within a narrow wedge centered on the vertical axis ; while low-velocity ground roll fallswithin the gentle slopes ; and high-velocity noise falls within the intermediate slopes.

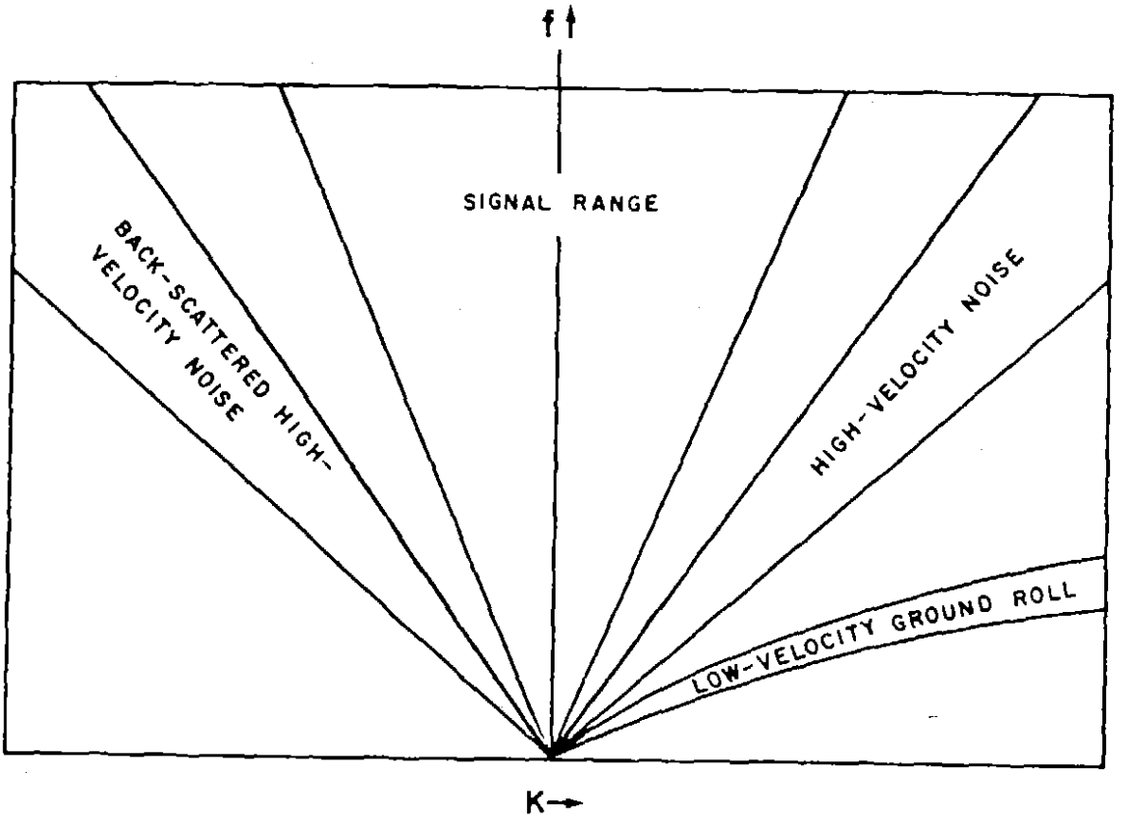

Fig.3.12. Idealized noise analysis-frequency versus wave number (From Embree, 1963).

CHAPTER 4

EQUIPMENT AND DATA ACQUISITION

4.1 SOURCE SEISMIC ENERGY

It is noticeable that characteristics of seismic records are strongly affected by conditions at the shotpoint. This has been demonstrated by many observers. Ziolkowski and Lerwill (1979) suggested that high resolution can be achieved by scaling down the explosive charge size and using single geophones instead of groups, and by reducing sampling interval in space and time. A larger output of higher-frequency components with a smaller-charge size was also observed by Sharpe (1944). Source testing may also be conducted in the field, since the primary objective is to maximize the amplitude and frequency content of the data at the target depth (Walker and Crouse, 1985).

At Eastern Lead, on line B-B', a buried and tamped single seismic electric detonator was used for the reflection work, weathering and noise spread observations. From the seismic records obtained, it appeared that this type of detonator was an adequate source for obtaining shallow seismic reflection. The survey was conducted in the wet season and soil conditions probably were ideal for this source. The northern part of the raw data from the noise spread (the right side of the figure), however, shows a weakening of the seismic wave energy on the way back to the surface. This is shown in Figure 5.19. The writer believed that this was perhaps due to absorption or attenuation of the seismic wave energy in a thicker low velocity layer. It was found that in this zone (even up to the end of the line) the low velocity layer is thick, i.e. ranging from 3 - 6 m with a velocity of about 750 m/s. This is illustrated in Figure 5.23.

Explosive (Gelignite 60) was used during the seismic refraction work along the traverse lines. This type is in the form of 25 mm X 200 mm sticks of 0.13 kg in weight. The shot hole depth ranged from 1 - 1.2 m. The amount of Gelignite 60 for end-shots, middle-shots, and long-shots, ranged from 0.5 - 0.8 kg , 0.3 - 0.4 kg , and 0.9 - 1.3 kg respectively. The size of charges was based on the necessity of obtaining a good first break or first arrivaltime on the refraction records. In some places, however, a problem was encountered due to the occurrence of thick loose sand or gravel wash which made it difficult to abtain a good first arrivaltime. This problem was partly overcome by scaling up the gain during the data processing.

4.2 DETECTORS

Knapp and Steeples (1986) discuss the performance characteristics of a geophone including the natural or resonant frequency, damping, coil impedance, sensitivity, harmonic distortion, and parasitic resonances. A geophone operating as a velocity sensor is the most commonly used detector. For high-resolution work, especially in seismic reflection, high natural frequency geophones are desirable to suppress low frequencies and thereby reduce recorded groundroll and increase the range of high-frequency data.

An experiment investigating geophone-ground coupling was carried out by Krohn (1985). She found that the coupling of vertical geophones depends strongly on the firmness of the soil. In the field, the firmness of the soil increases with depth, and she found that the resonant frequency of the geophone increased with burial or with a longer spike.

In the study at Eastern Lead, GSC-20D 14 HZ production geophones were used during the seismic reflection work, weathered and noise spread observation, while multiple geophones or geophone arrays were used during seismic refraction work. There are some reasons for the use of the multiple geophones. The important reason is to sharpen the first arrival of energy detected by the geophones, since the first break is the only useful data in seismic refraction work. Other reasons are to cancel unwanted energy such as wind noise and ground unrest, and to improve the average coupling between geophone and ground (Lombardi, 1955).

4.3 RECORDING EQUIPMENT

The seismic study at Eastern Lead used the EG & G Geometrics Nimbus ES-1210F multichannel signal enhancement seismograph. This equipment is designed for shallow seismic exploration (refraction, reflection, and borehole surveys). It features signal enhancement by stacking repeated signals in a digital memory, a cathode ray tube for continuous display, and a built-in electric writing oscillograph to provide permanent paper records. It is packaged in a weatherproof, aluminium enclosure, and operates from a nominal 12-volt external supply. The equipment also has a memory size of 10 bits by 1024 words on each of 12 channels, with a selectable sample interval of 50 , 100 , 200 , 500 , 1000 , or 2000 ms with accuracy in time of 0.01 % ; precision delay up to 9.999 seconds in one milisecond increments ; noise monitor ; and independent filtering capabilities on each of the channels. The corner or center frequency is adjustable from 30 to 300 HZ.

A portable digital magnetic tape recorder, the DMT-911, was used to record the data from the Nimbus ES-1210F seismograph. The data were stored on standard half-inch nine-track (1600 bpi) magnetic tapes, recorded in SEG-D standard format, and then transferred to a computer (PRIME 9955) for further processing.

4.4 LINE SURVEYS

The topography of the area is relatively flat except at the northern end of the traverse lines A-A', B-B' and C-C'. The difference in elevation between the lowest and the highest point is about 20 m, and about fifty percent of the total length of the traverse line is situated in thick scrub. Positioning was done along the traverse lines using a tripod-mounted theodolite and a 5 m long graduated staff. The datum point denoted m21 shown in Figure 4.1. was used. Unfortunately, the marker for Lands and Surveys Department, point m21 has been lost, although its horizontal position is well defined. Accordingly all elevations are relative to a local datum. The surveying results are given in Appendix B. As the aim of the seismic study was basically to map the granite basement, to test the hypothesis of an ancient channel, and to compare seismic methods, four parallel traverse lines A-A', B-B', C-C', and D-D' were laid across the inferred channel with an approximate northeast-southwesterly direction.

4.5 Refraction data acquisition

A shotpoint-geophone configuration shown in Figure 4.2. with 17 m geophone spacing was used for seismic refraction data acquisition. Shots

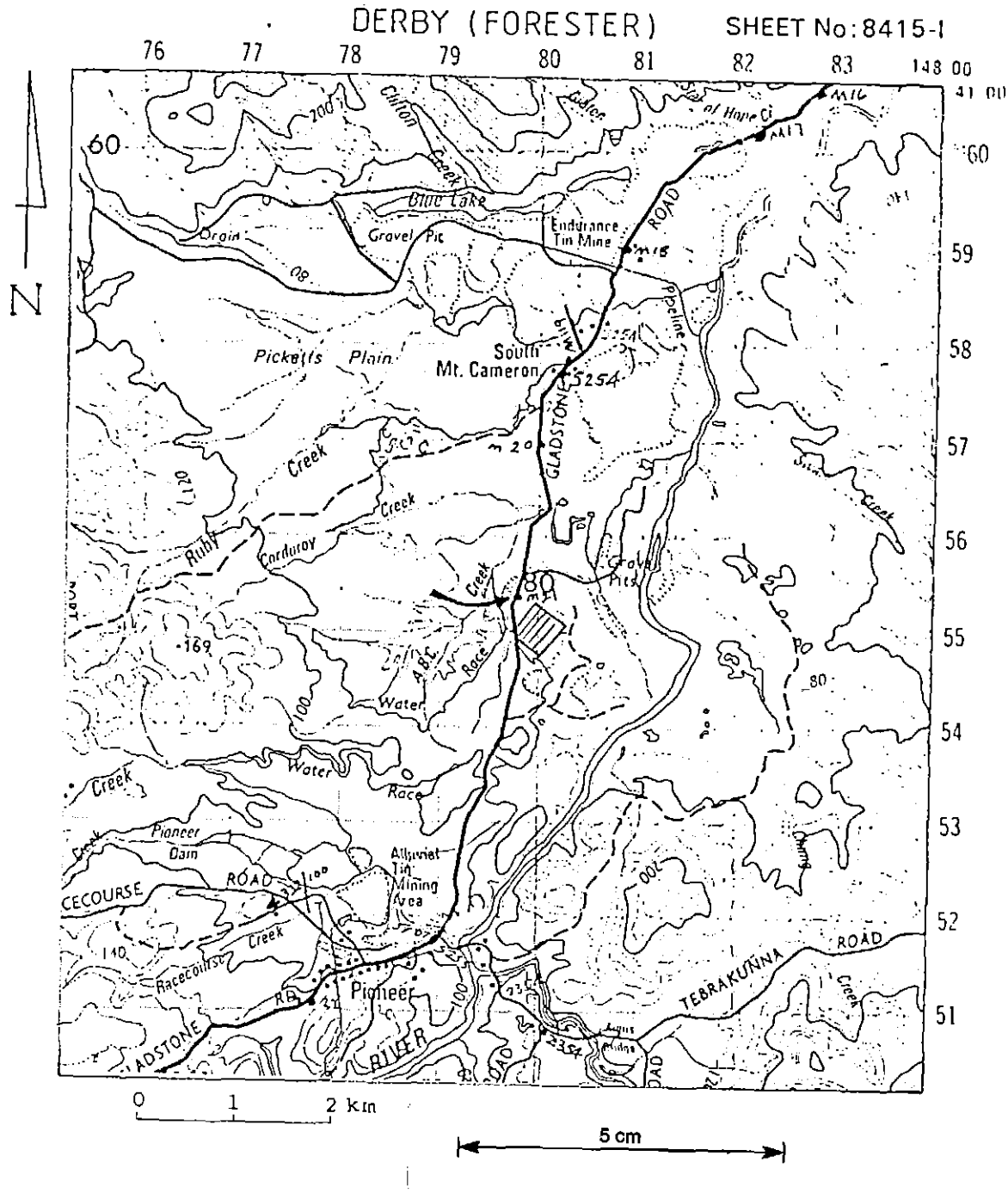

Fig.4.1. Location of the known datum points from which topographical surveying used herein has been taken. The arrow indicates the datum point (m21) used in the survey, and the hatched area indicates the location of the seismic profiles.

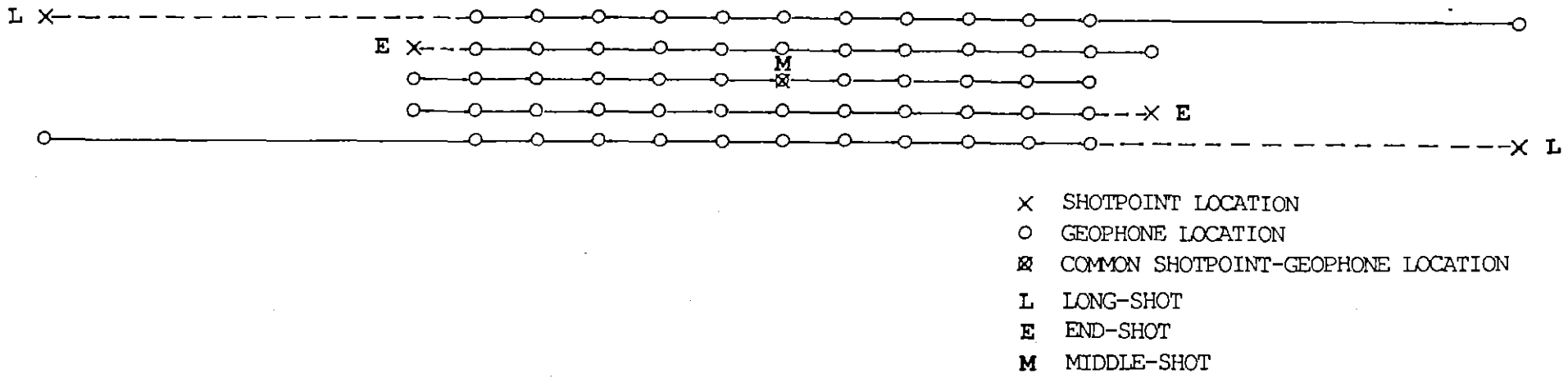

Fig.4.2. Shotpoint-geophone locations of refraction spreads represent long-shot (forward and reverse), end-shot (forward and reverse), and middle-shot.

were fired in the middle , at the ends , and at the far ends of each spread and will be referred to as middle-shots , end-shots , and long-shots respectively. A continuous profile was obtained throughout the traverse lines by shifting the entire configuration a half spread length at a time so that the spreads have a common end-shot points.

Exceptions were for line B-B' at stations 16 and 34 , and for line C-C' at stations 1 and 25. For line B-B' at stations 16 and 34, the long-shots were fired from the offset distance of only 50 m from the end-shots. This was due to the occurrence of thick undergrowth and swampy conditions. For line C-C' , the Pioneer - Gladstone road lay along the western part of the study area, making long-shots impossible to perform.

Another shotpoint-geophone configuration was used along line C-C', i.e. a profile with 8.5 m geophone spacing. The continuous coverage was obtained by shifting the entire configuration one spread length after every second shot. This was intended to obtain arrival times from the near-surface layers, and to examine the depth of the clay as compared with borehole data at the southwestern end of the line. Note for the last northeastern end spread this line was shifted southwesterly by 8.5 m from the station 61 . The aim was to obtain the direct wave velocity of what was thought to be a possible outcrop of weathered basement. From the observed direct velocity, however, it seems likely that the outcrop is made up of boulders.

A reversed profile including end-shots and middle-shot with a geophone spacing of 3.75 m was used for weathering spread observations. A continuous weathering profile along the line B-B' was made by moving the configuration one spread length after every third shot. The objective was

to determine the velocities and thicknesses of near-surface layers which is important in the weathering corrections, especially for the static corrections applied in the seismic reflection data processing. In collecting the refraction data, all-pass filters were set on all channels and the gains were increased successively as the source-geophone offset increased.

4.6 Noise test and reflection data acquisition

A noise spread observation was done on the line B-B' with 3.75 m geophone spacing. The shotpoint-geophone configuration is shown in Figure 4.3. A single buried and tamped detonator placed in a single fixed shotpoint was fired midway between the spreads. Each spread was moved from one side of the shotpoint to the other after each shot in such a way that a continuous noise spread profile was obtained. The results, as shown in Figure 5.19., and 5.20., are very helpful in determining the choice of field parameters. These include the record time length, sample interval, maximum and minimum source-geophone offset, and spread type.

The Common Depth Point technique (CDP) was used in collecting the seismic reflection data. A decision was made to locate the seismic reflection profile along line B-B' as this line has good access being relatively flat and mostly situated on an open area so that the spread could be moved without difficulty. The spread type was an end-on arrangement as shown in Figure 3.10. The shot offset and geophone spacing was the same, that is 7.5 m. To be able to obtain 12-fold coverage, the spread was shifted for half a geophone spacing or 3.75 m after each shot. A single buried and tamped detonator was also used at each shotpoint and was fired at

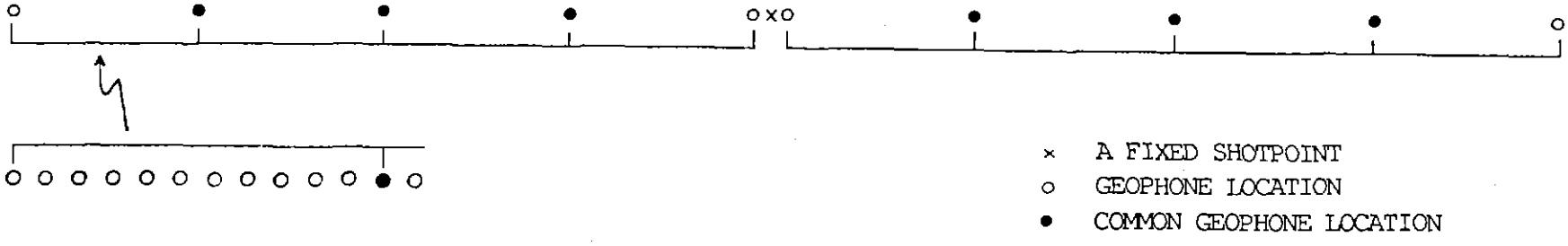

Fig.4.3. Noise spread configuration.

a depth ranging from 0.2 - 0.5 m. The data was collected using all-pass filters on all channels and the gain was adjusted to prevent the occurrence of trace clipping. Some difficulties were encountered during the observation as it was the rainy-season with windy conditions. A record length of 200 ms was applied throughout the data sampling. In fact it was found difficult to observe reflection events from the raw data displayed on the Nimbus.

CHAPTER 5

DATA PROCESSING AND INTERPRETATION

5.1 REFRACTION DATA PROCESSING

Data processing commenced with the conversion of the digitally recorded field data into plotted individual shot records using a seismic processing package written by Dr. R.J.G. Lewis. As the first break or arrival time is the most important thing on a seismic refraction record, a trial was made to enhance the first breaks by means of frequency filtering and setting up the magnification factor to a suitable value. Traces are normally plotted with the peak amplitude set to a constant value ; the magnification factor increases this value. Band-pass filters were used with pass bands of 2-10 HZ, 5-30 HZ, 10-50 HZ, and 30-100 HZ, with a 6 dB per octave attenuation slope. Different band-pass filters were used due to the variable noise frequencies on the seismic traces, especially before the first arrivals of the refracted waves. Most of the records were filtered using a band-pass filter with a pass band of 10-50 HZ. Some were also filtered using a band-pass filter with pass bands of 5-30 HZ and 2-10 HZ , particularly the records obtained from the area where a considerable thickness of loose superficial material occurs. The magnification factor was always 5 except for the weathering spread. For the weathering spread the magnification factor ranged from 3 to 5 and no filtering was done whatsoever.

The second step was picking of the first-arrival times and plotting them in the form of traveltime-distance curve as shown in Figures 5.1., 5.2., 5.3., and 5.4. Measured first-arrival times have been lodged with the curator, Geology Department, and are arranged sequentially, from large

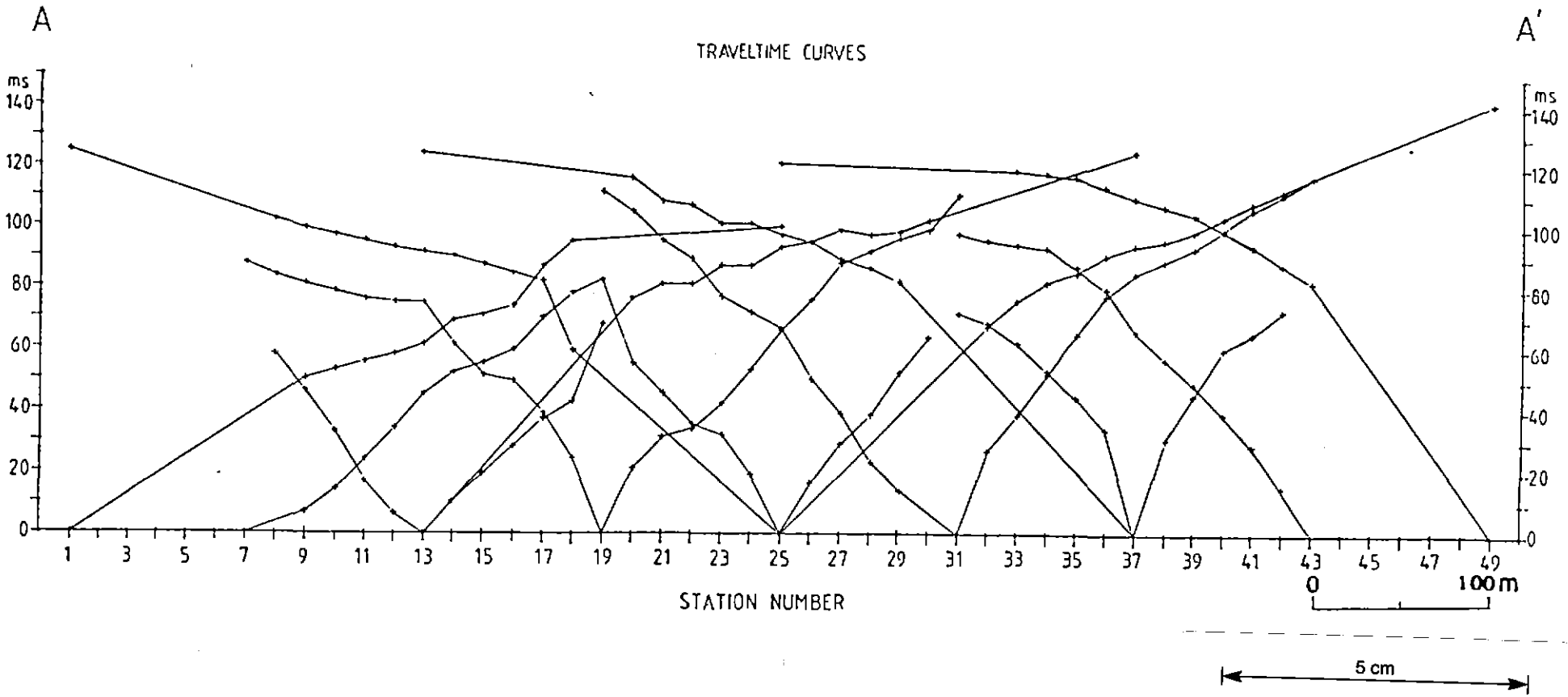

Fig.5.1. Traveltime curves for seismic line A-A', Eastern Lead.

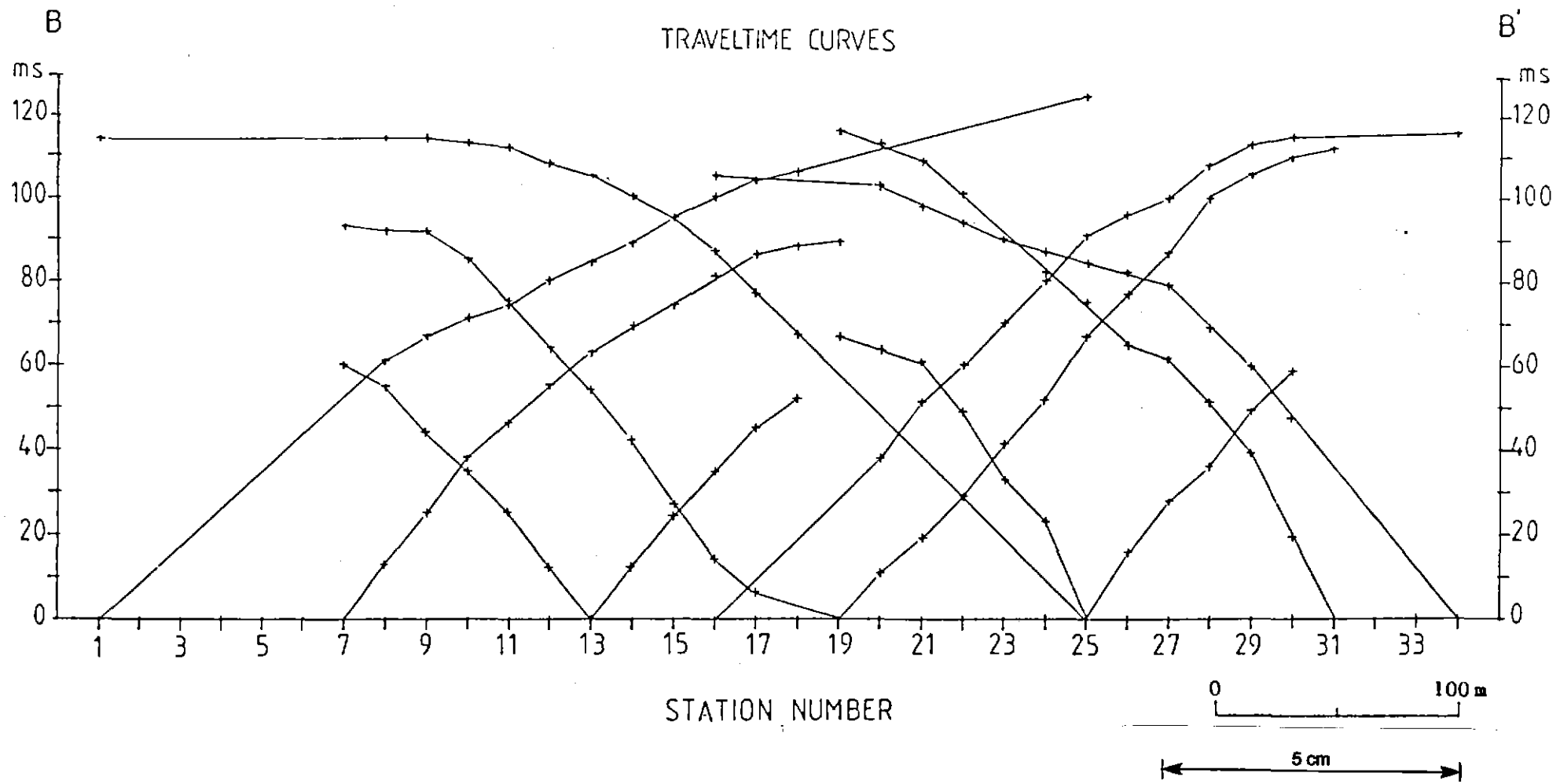

Fig.5.2. Traveltime curves for seismic line B-B', Eastern Lead.

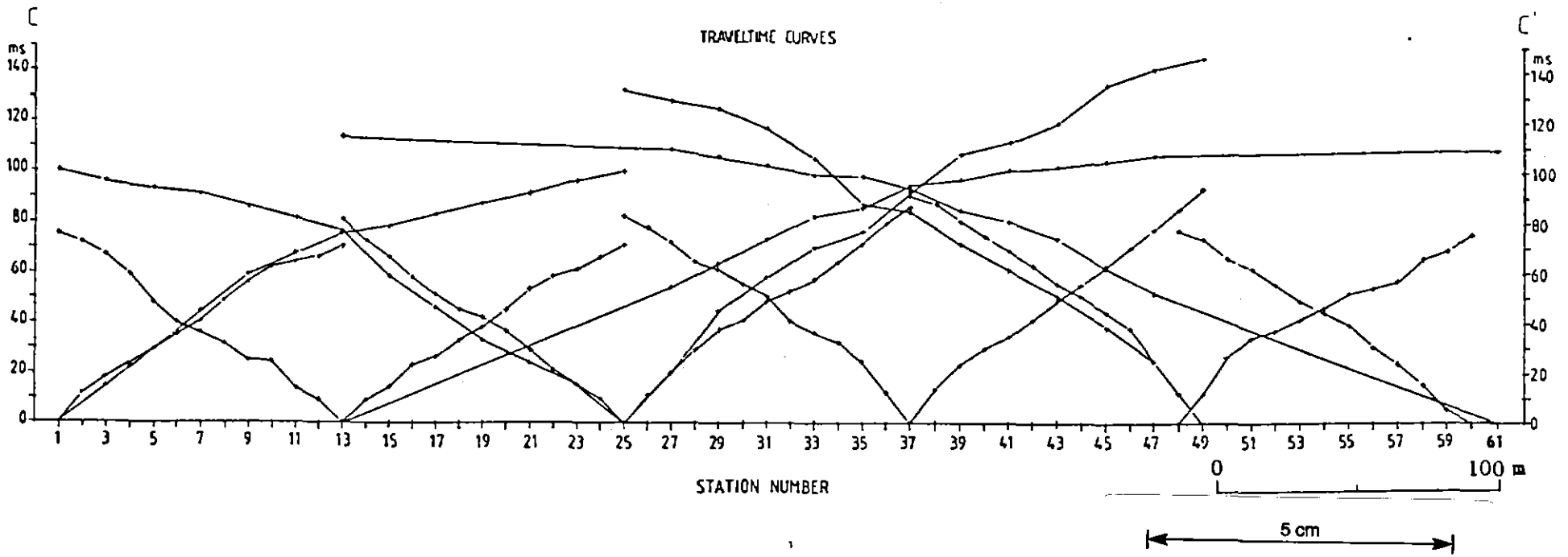

Fig.5.3. Traveltime curves for seismic line C-C', Eastern Lead.

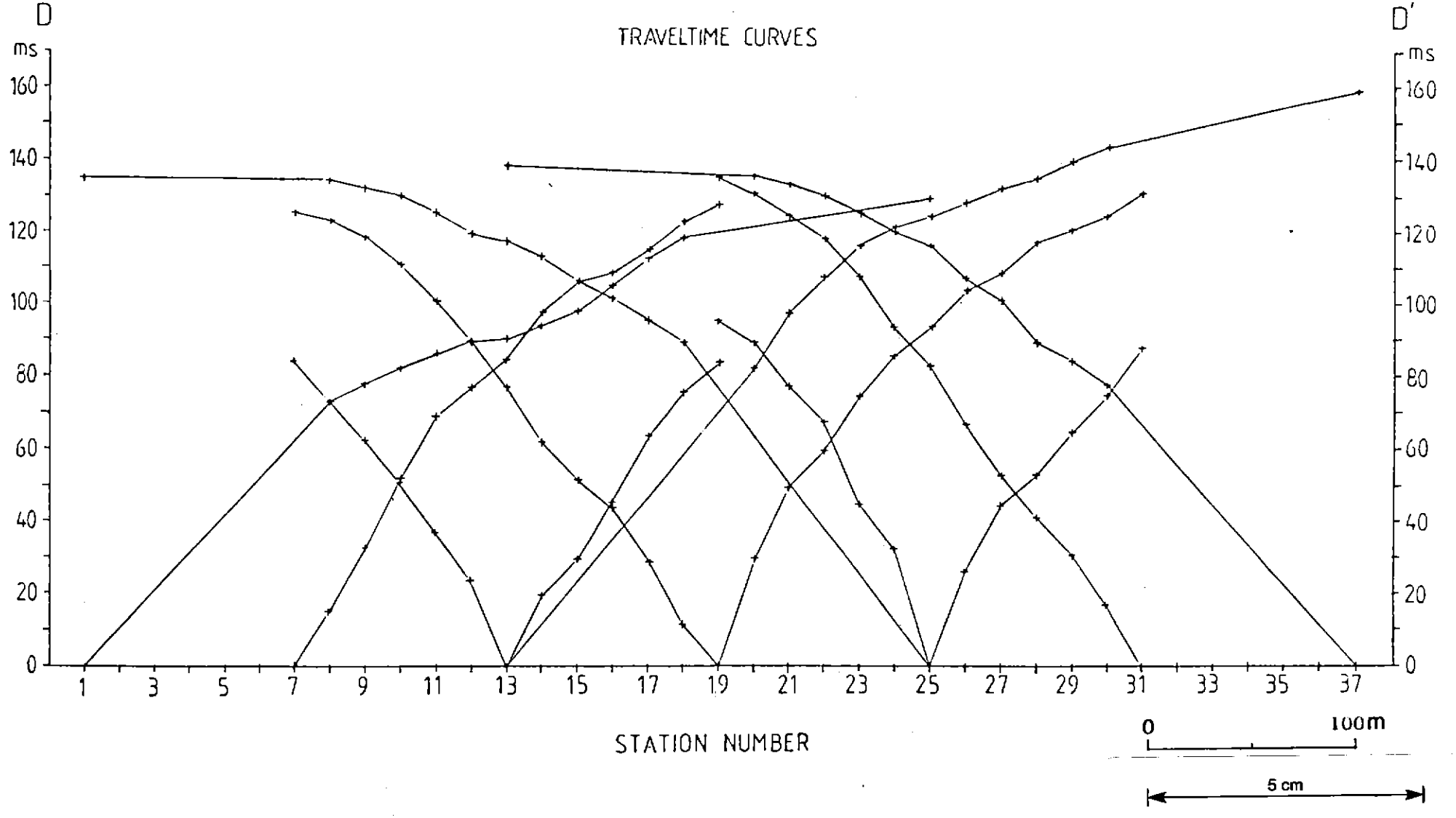

Fig.5.4. Traveltime curves for seismic line D-D', Eastern Lead.

station spacings to smaller spacing. During the data processing, individual traveltime errors due to disturbance of the ground near the shotpoints as a result of previous shots were excluded. An interpolation was made to smooth the curve, i.e. by drawing a line through a shotpoint and the nearest point representing an arrival time.

Third, the reciprocal time correction has to be assigned since this is required in the computation of velocity analysis functions and time-depths. As the number of shots inside the spread was two, i.e. the forward and reverse shots, the average of the reciprocal time was multiplied by minus half (using the formula 3-6) and then added to all of the traveltimes from given shot pairs or reversed traveltime curves.

The fourth step dealt with the calculation of the velocity analysis functions using equation (3-8). In this calculation, different XY values were used for each of the reversed traveltime curves. For the reversed traveltime curves with 17 m geophone interval, the XY values applied were 0 , 17 , 34 , 51 , 68 , 85 , and 102 metres. For the reversed traveltime curves with 8.5 m and 3.75 m geophone intervals, XY values of 0 , 8.5 , 17 , 22.5 , 34 , 42.5 , 51 , and 0 , 3.75 , 7.5 , 11.25 , 15 , 18.75 , 22.5 metres were used respectively. Note that for shorter reversed traveltime curves such as those resulting from a middle shot, the first 3 XY values specified above were used. In the case when XY is equal to zero, the velocity analysis function is obtained using equation (3-9) provided by Hawkins (1961). As the values of the velocity analysis functions for different XY separations were obtained, they were plotted against distance so that a refractor velocity Vn' could be determined, i.e. by measuring the inverse slopes of given optimum XY values. The optimum XY values are indicated by the simplest form of the plots or when the velocity analysis

functions most closely approximate a straight line. Other methods for determination of an optimum XY value are mentioned in section 3.3.5. An example of these plots taken from a synthetic model provided by Palmer (1980) is shown in Figure 5.5., and a schematic representation of the velocity analysis functions for a refractor with a step in depth is illustrated in Figure 5.6. As shown in these figures , at the optimum XY values , the velocity analysis function is a straight line. An example of the variation with XY values of 0-102 m from the study area is also shown in Figure 5.7. In this thesis only the optimum XY values are plotted either on velocity analysis functions or on time sections. This is because all of the plotting of the refraction curves or sections was done manually, and for clarity. Velocity analysis functions for optimum XY values are illustrated in Figures 5.8., 5.9., 5.10., and 5.11.

The fifth step is the calculation of time-depths near the shotpoints and the geophone time-depths. The former can be obtained using equation (3-12), and the latter using the equation (3-11). The time-depths near the shotpoints can also be obtained from the intercept of the line given by the velocity analysis functions. The values taken from the geophone time-depths and from the time depths near shotpoints can then be plotted in the time sections. Theoretically these values have to be agree with the half-intercept times. But when a constant discrepancy occurs among them, it is attributed to reciprocal time errors used in calculating the time-depths. The error can be removed by adjusting all of the time-depths by that discrepancy. This has been described in detail by Hatherly (1986). Palmer (1980) suggested that it is also possible to interpolate between time-depths and half intercept times if necessary. However, the accuracy of interpolation will depend upon the complexity of the geology. The time sections of the study area are illustrated in Figures 5.12, 5.13., 5.14.,

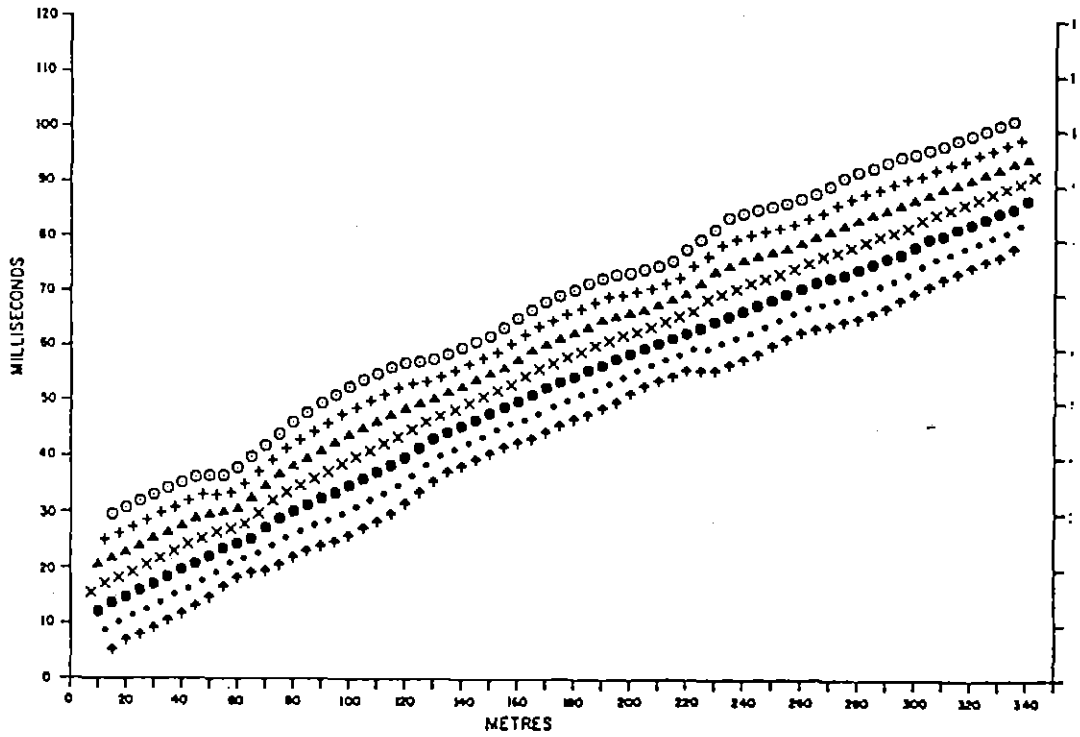

Fig 5.5. Velocity analysis functions for XY-values from 0 to 30 m, derived from the traveltime data in Figure 5 of Palmer (From Palmer, 1980).

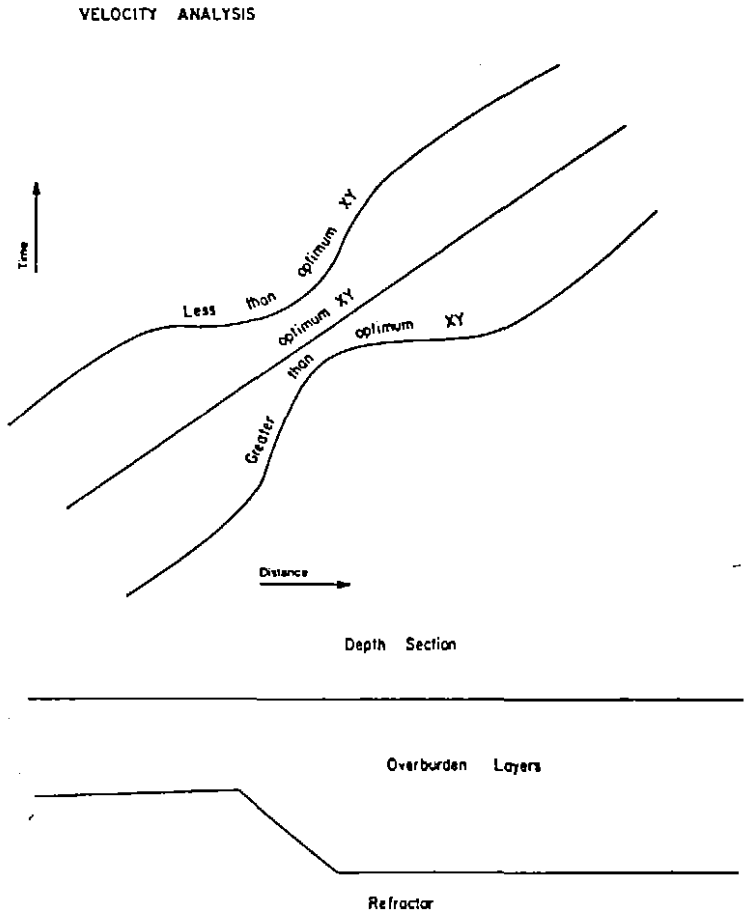

Fig 5.6. Schematic representation of velocity analysis functions for a refractor with a step in the depth (From Palmer, 1980).

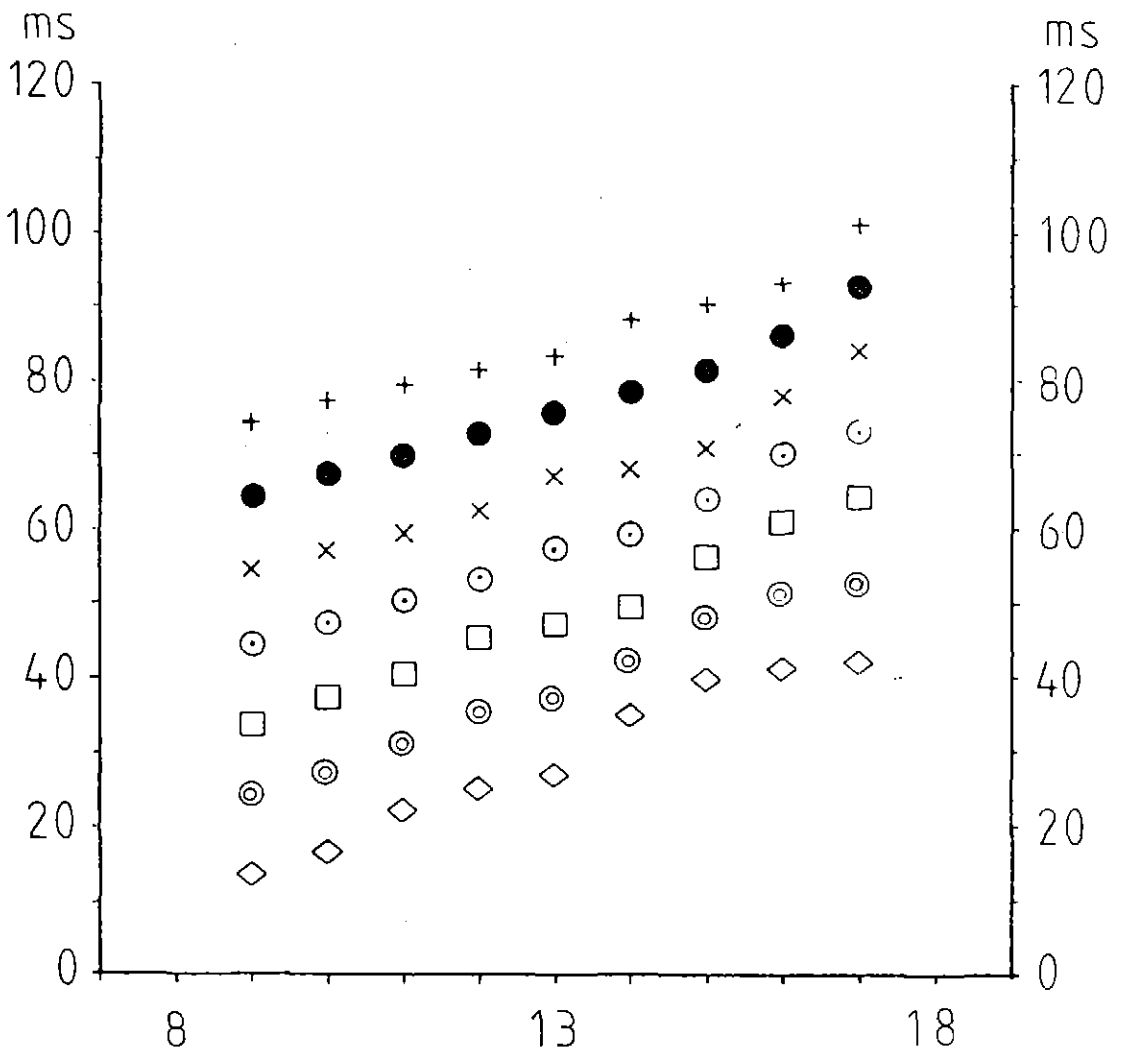

Fig.5.7. Velocity analysis functions with XY-values of 0-102 m from line A-A', Eastern Lead, with shot positions at station numbers 1 and 25.
Symbols : +, ●, ×, ⊙, □, ◎, and ◇, are XY values of 0, 17, 34, 51, 68, 85, and 102 m respectively.

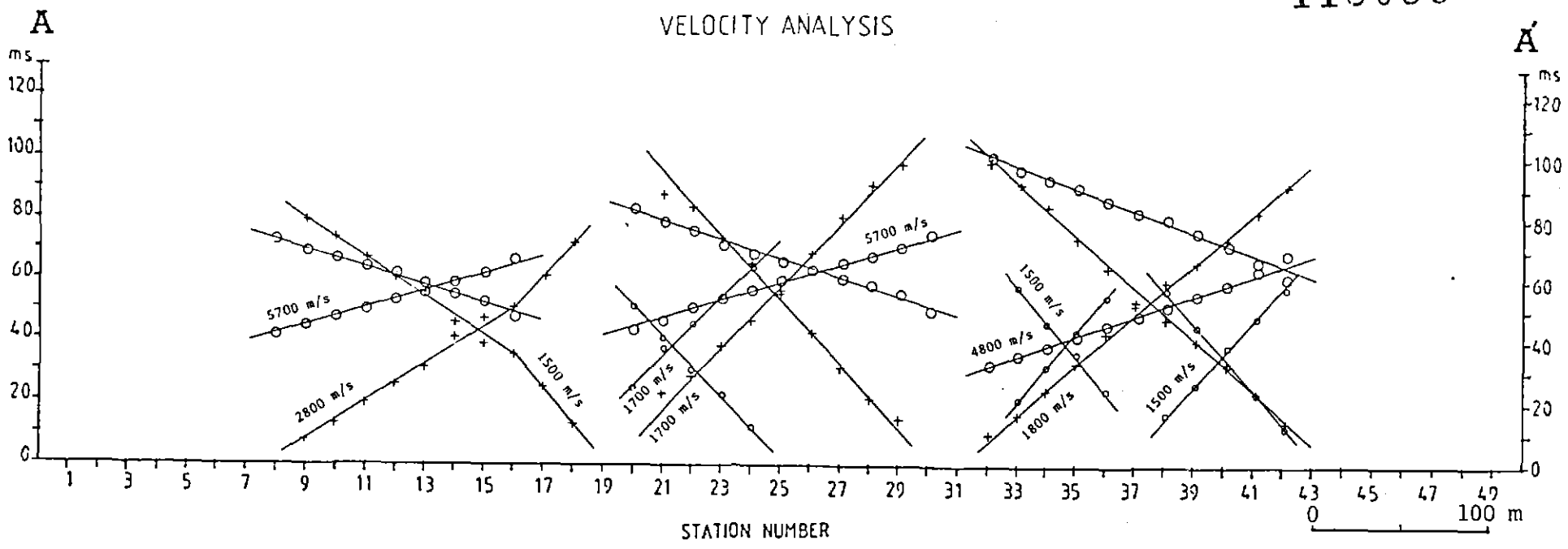

o SHOTS LOCATED AT: 19 ; 25
RECIPROCAL TIME : 74.5 ms
XY = 17 m

o SHOTS LOCATED AT: 31 ; 37
RECIPROCAL TIME : 78.5 ms
XY = 0

o SHOTS LOCATED AT: 37 ; 43
RECIPROCAL TIME : 73.0 ms
XY = 0

\+ SHOTS LOCATED AT: 7 ; 19
RECIPROCAL TIME : 85.5 ms
XY = 0

\+ SHOTS LOCATED AT: 19 ; 31
RECIPROCAL TIME : 111.0 ms
XY = 0

\+ SHOTS LOCATED AT: 31 ; 43
RECIPROCAL TIME : 107.5 ms
XY = 0

O SHOTS LOCATED AT: 1 ; 25
RECIPROCAL TIME : 112.5 ms
XY = 17 m

O SHOTS LOCATED AT: 13 ; 37
RECIPROCAL TIME : 124.5 ms
XY = 17 m

O SHOTS LOCATED AT: 25 ; 49
RECIPROCAL TIME : 131.5 ms
XY = 17 m

5 cm

Fig.5.8. Velocity analysis derived from data shown in Figure 5.1.

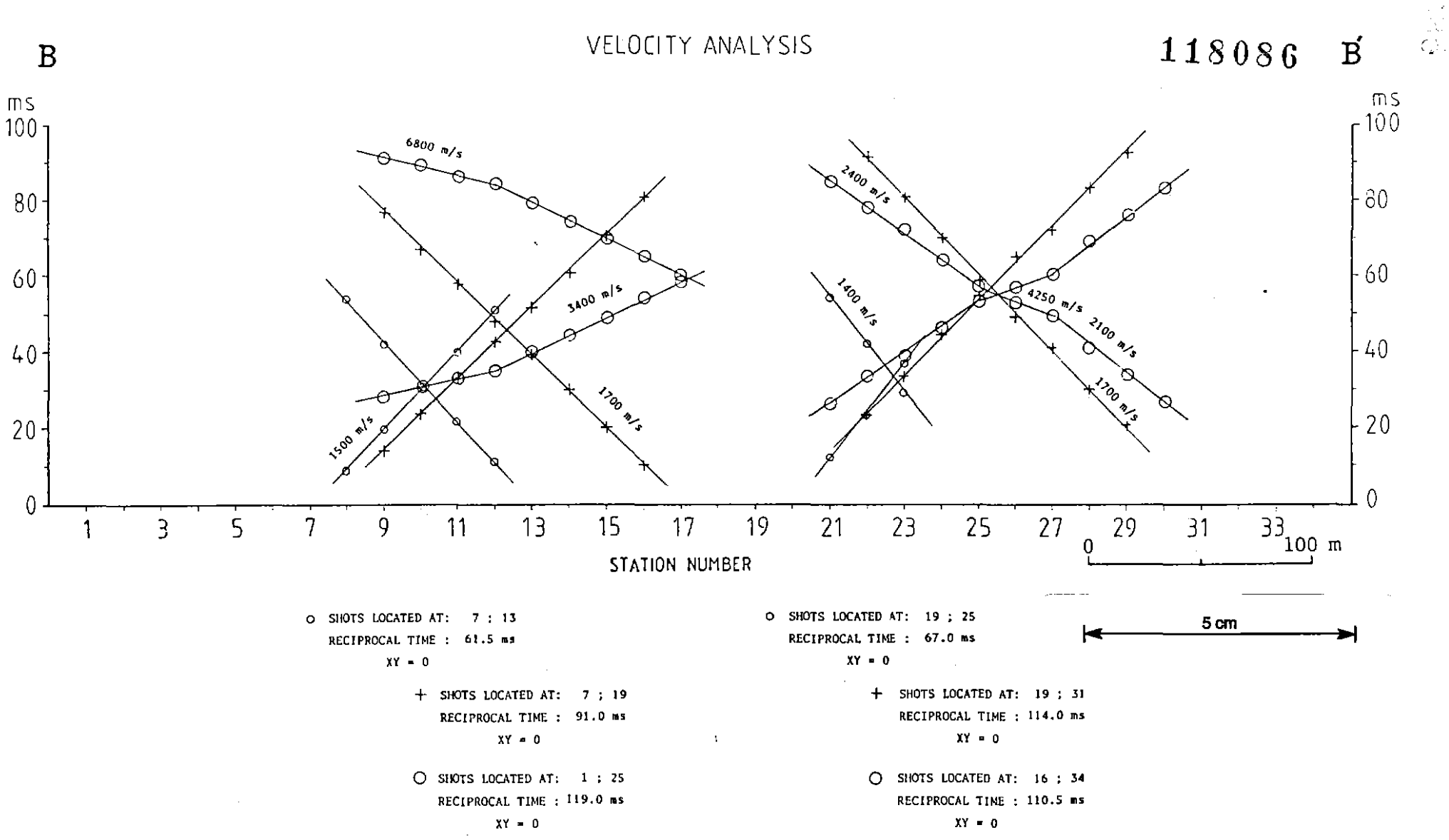

Fig.5.9. Velocity analysis derived from data shown in Figure 5.2.

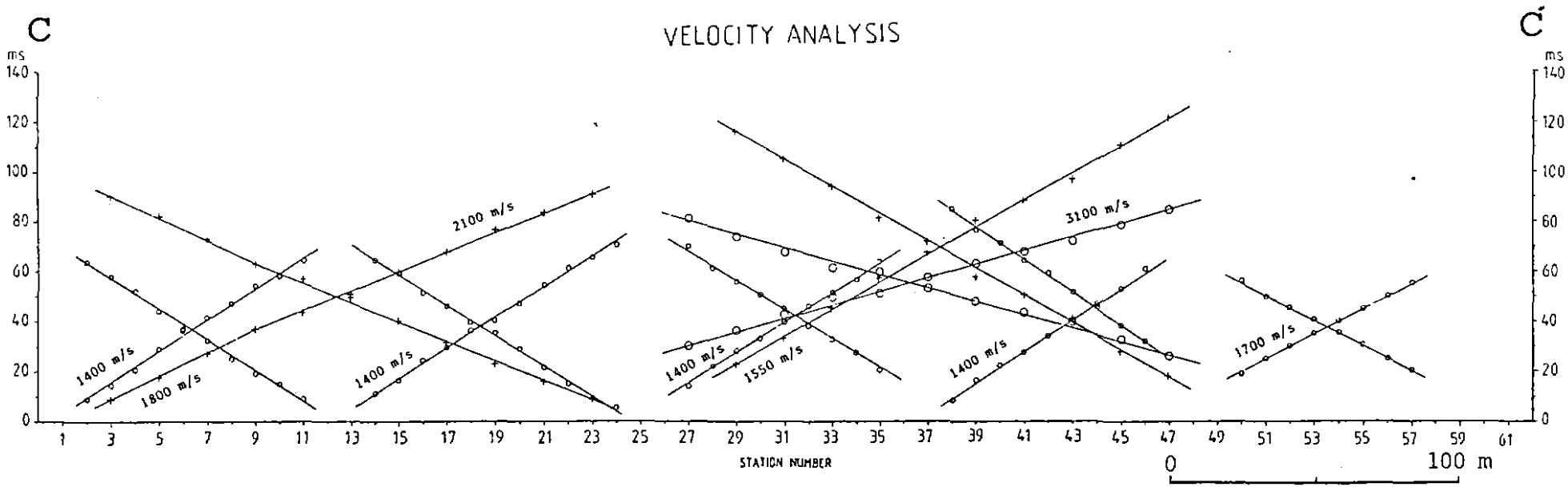

o SHOTS LOCATED AT: 1 ; 13
RECIPROCAL TIME : 72.6 ms
XY = 0

o SHOTS LOCATED AT: 13 ; 25
RECIPROCAL TIME : 75.4 ms
XY = 0

o SHOTS LOCATED AT: 25 ; 37
RECIPROCAL TIME : 84.0 ms
XY = 0

o SHOTS LOCATED AT: 37 ; 49
RECIPROCAL TIME : 91.5 ms
XY = 0

o SHOTS LOCATED AT: 48 ; 60
RECIPROCAL TIME : 76.0 ms
XY = 0

+ SHOTS LOCATED AT: 1 ; 25
RECIPROCAL TIME : 100.0 ms
XY = 0

+ SHOTS LOCATED AT: 25 ; 49
RECIPROCAL TIME : 138.8 ms
XY = 0

o SHOTS LOCATED AT: 13 ; 61
RECIPROCAL TIME : 111.0 ms
XY = 0

5 cm

Fig.5.10. Velocity analysis derived from data shown in Figure 5.3.

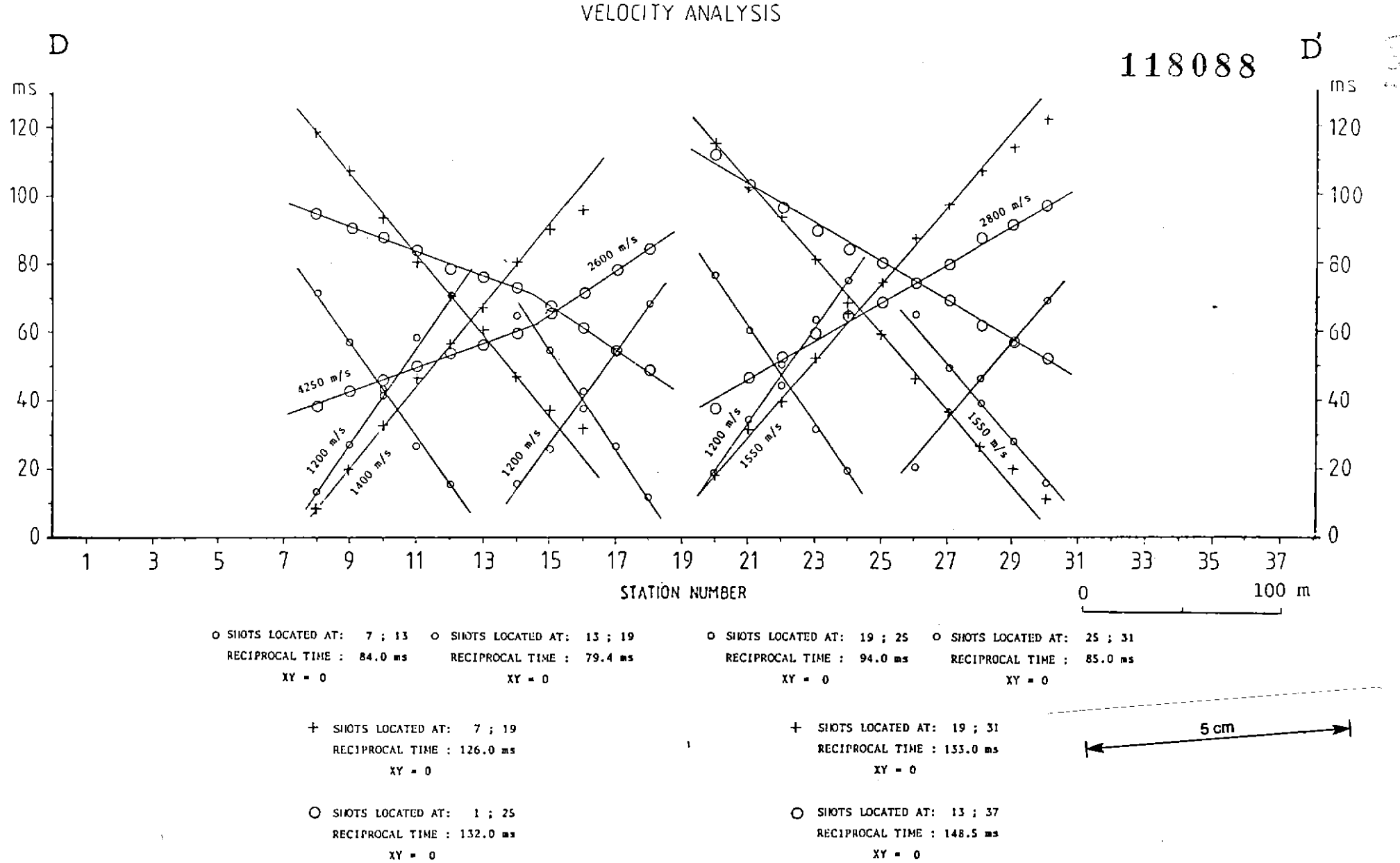

Fig.5.11. Velocity analysis derived from data shown in Figure 5.4.

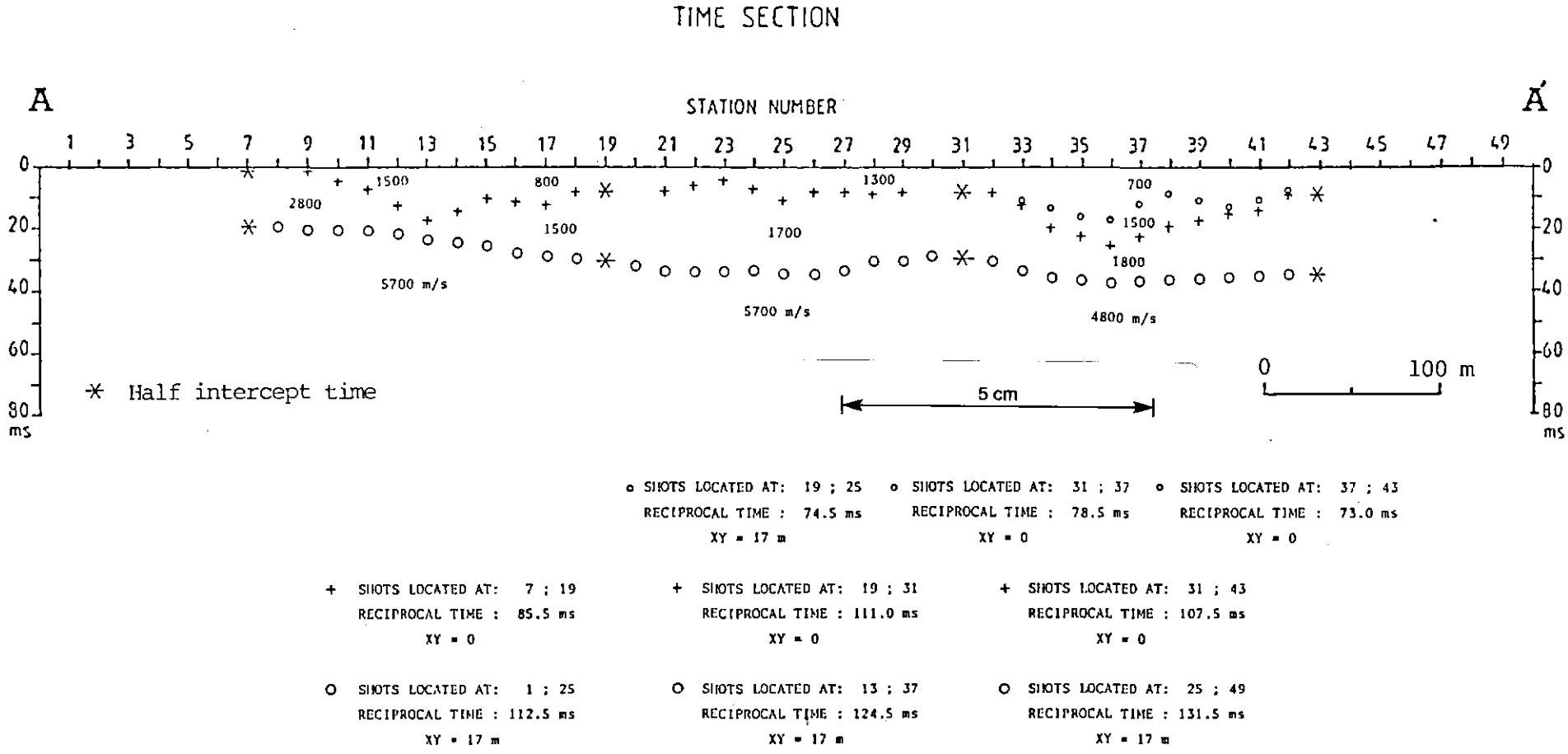

Fig.5.12. Time section derived from data shown in Figure 5.8.

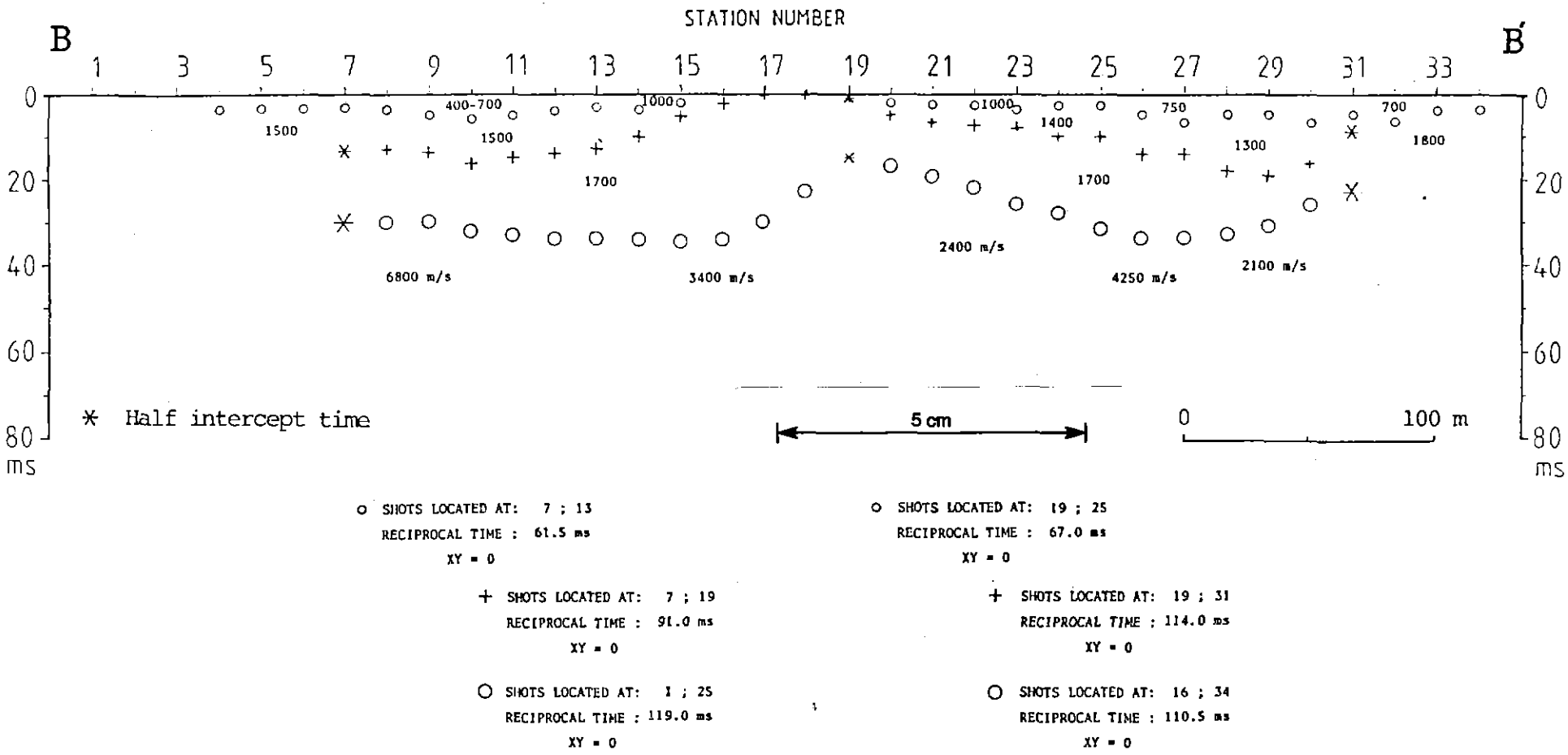

Fig.5.13. Time section derived from data shown in Figure 5.9.

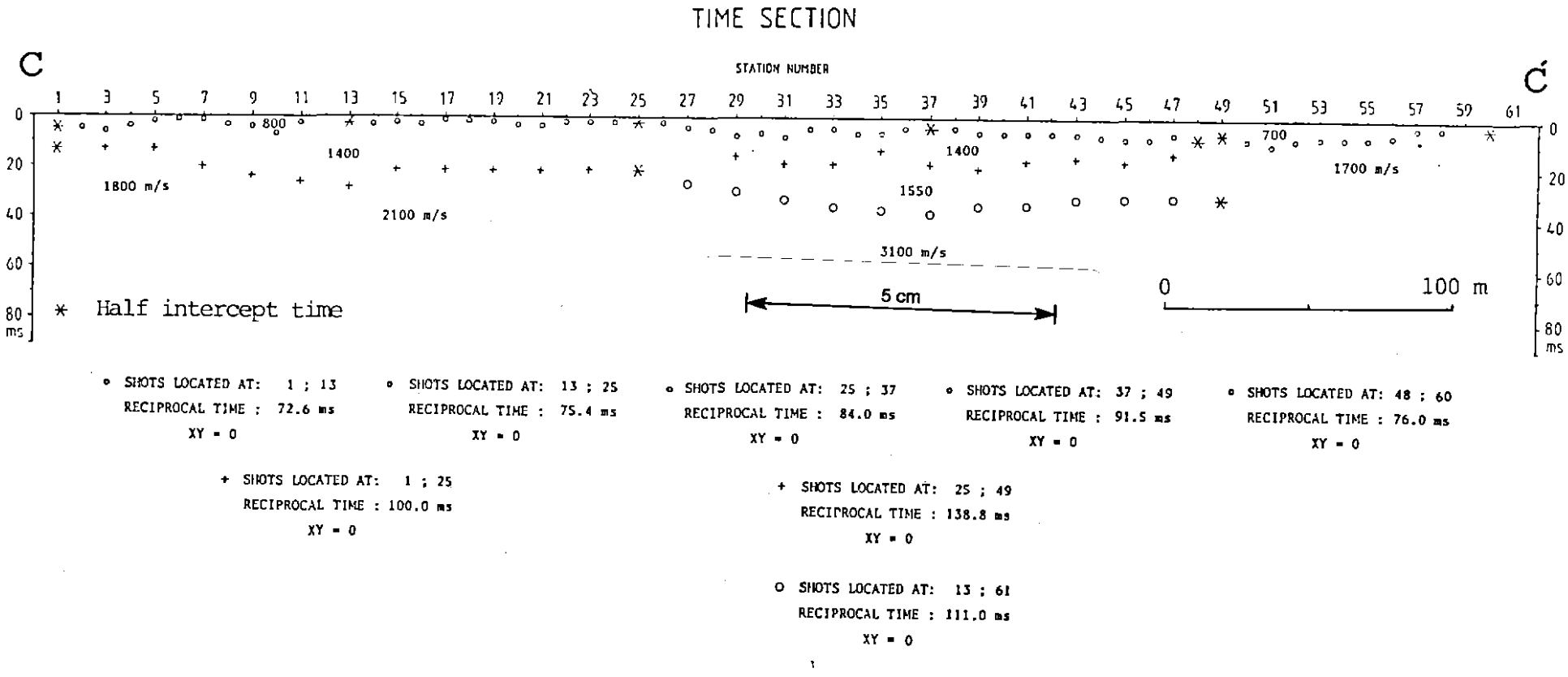

Fig.5.14. Time section derived from data shown in Figure 5.10.

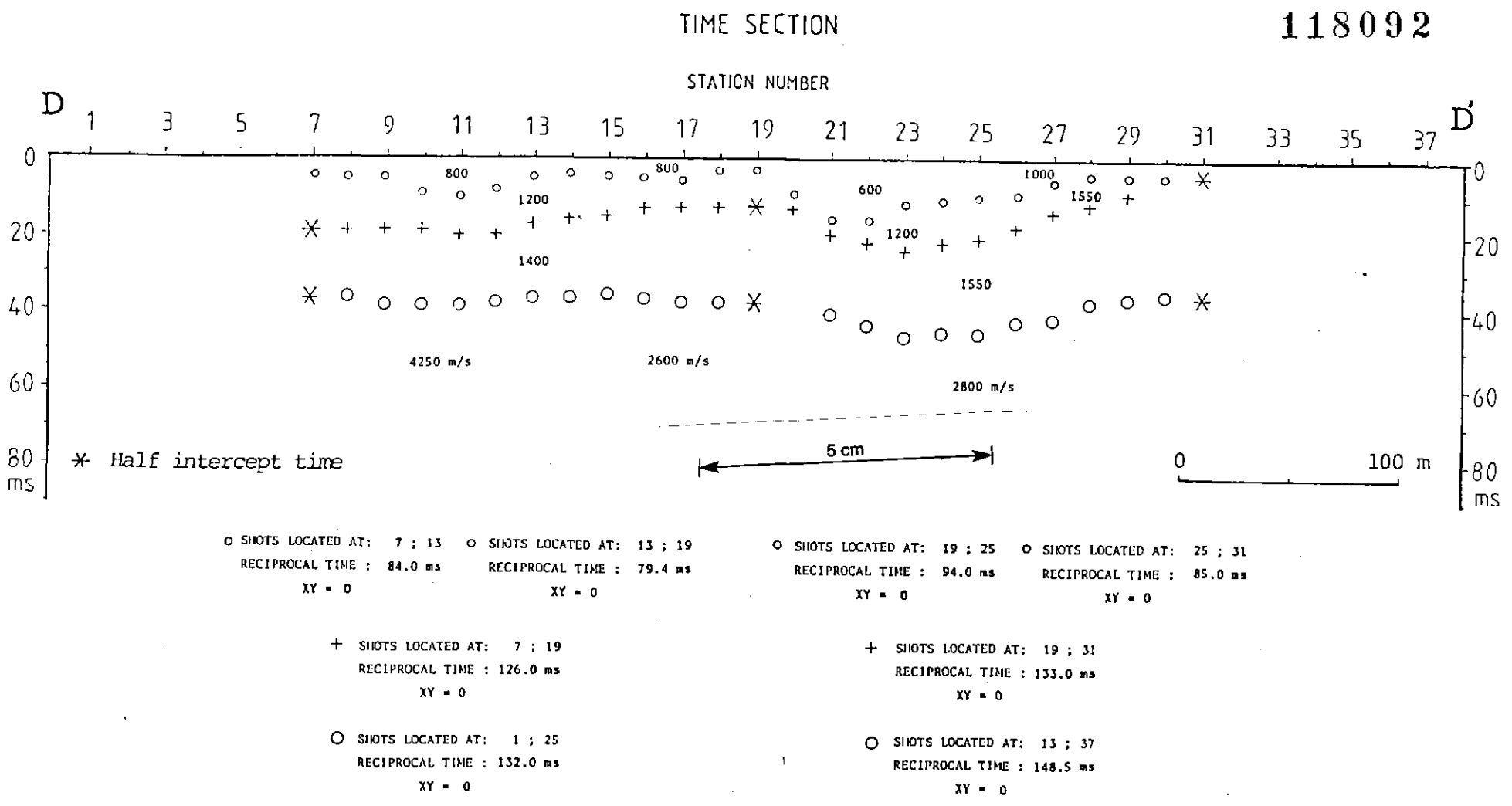

Fig.5.15. Time section derived from data shown in Figure 5.11.

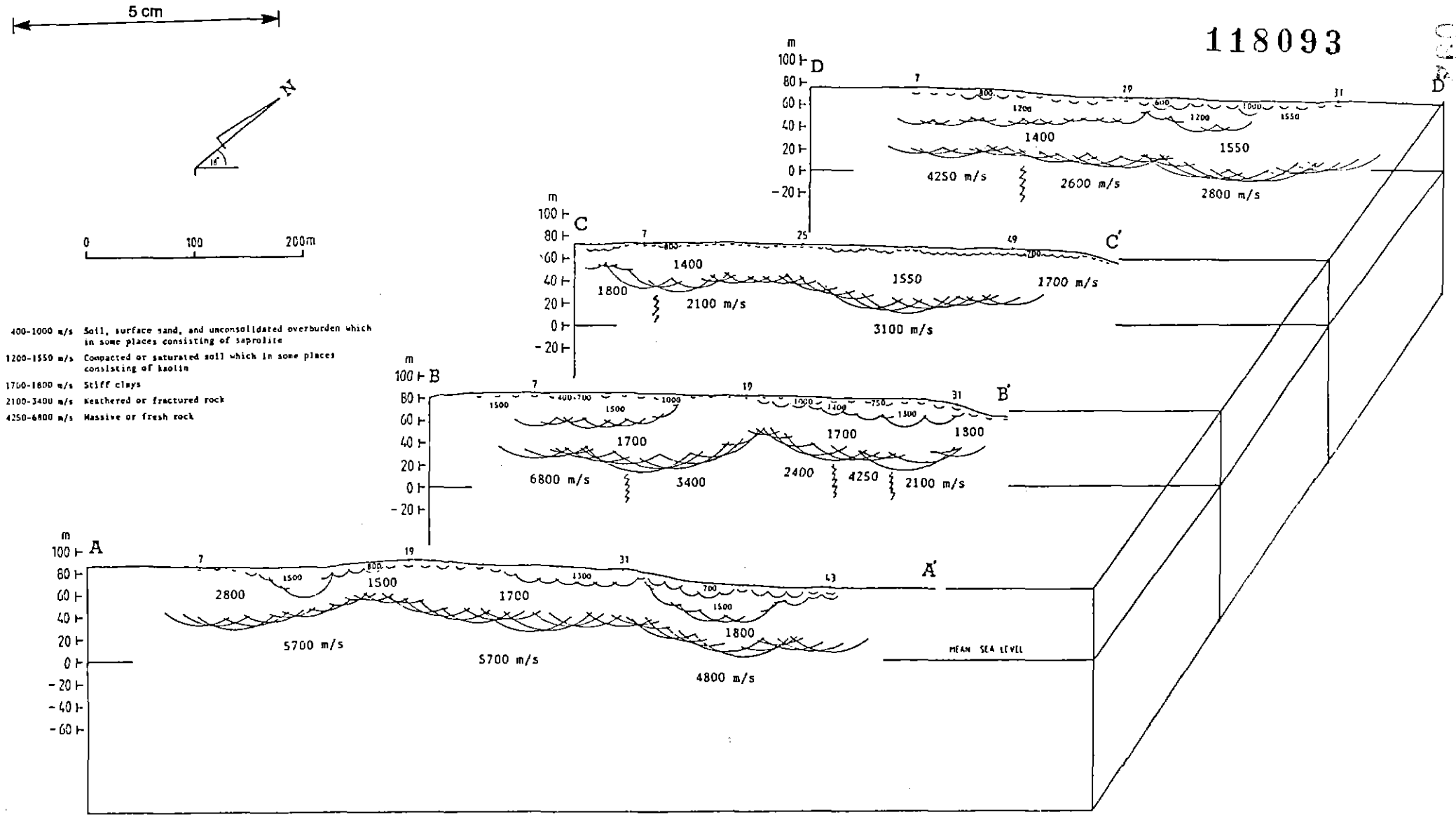

Fig.5.16. A block diagram of depth sections derived from data shown in Figures 5.12. , 5.13. , 5.14. , and 5.15.

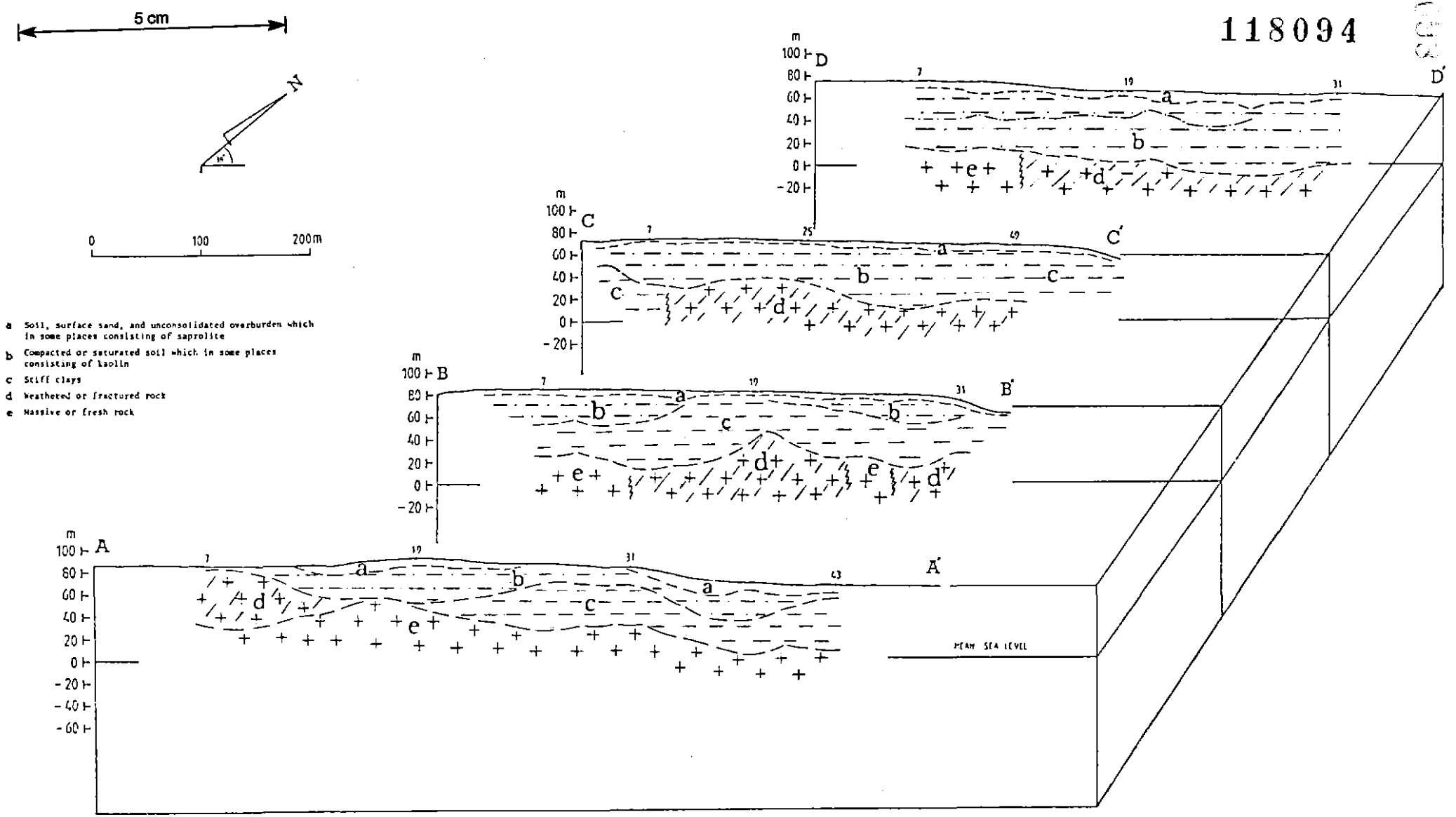

Fig.5.17. A blok diagram of interpreted geologic conditions derived from the depth sections shown in Figure 5.16.

and 5.15., which are derived from the data shown in Figures 5.8., 5.9., 5.10., and 5.11. respectively. The half-intercept times were determined using the concept proposed by Palmer (1980) and discussed in section 3.3.2. When the result is ambiguous, the use of parallelism (Ackermann et.al., 1986) is necessary to ensure that the half-intercept times agree with the time-depths. If the line segments in the traveltime curves are perfect, the intercept times can be obtained by simply projecting the lines back to the shotpoints.

The next step was converting the time sections into depth sections which were then finally transformed into interpreted geological sections. The depth sections were obtained from the multiplication of the time sections and depth conversion factors. The depth conversion factor is a velocity term given in equation (3-14). The value obtained from this multiplication is actually a perpendicular thicknesses which can be regarded as describing a locus of possible refractor positions rather than the actual vertical depth. This is shown in the block diagram (Figure 5.16.). From these sections, the refractor boundaries can be defined by drawing the envelope to the loci of possible refractor positions. The boundaries are specified by continuous dashed lines as illustrated in Figure 5.17. and are interpreted as lithological boundaries.

All of the refraction data including the weathering spread have been processed following the procedure outlined above. As stated by Palmer (1980) the GRM is a powerful method of seismic refraction interpretation which is applicable to irregular refractor configurations and lateral changes in refractor velocity. With this method the depth to the important refractor can be calculated without defining every layer above the

refractor. However, this feature was not used here because of the availability of the velocities above the main refractor.

5.2 REFRACTION RESULTS

In general the field data are of good quality and there was no difficulty in picking up the first arrival times. Traveltime curves are presented in Figures 5.1., 5.2., 5.3., and 5.4. for the lines A-A', B-B', C-C', and D-D' respectively. As seen throughout the curves, clear breaks between the line segments are generally rare except for those at the end of the line segment representing the direct wave arrival. This is likely to be due to variation in the velocity of the near-surface layers and also perhaps due to the refractor undulation or both. In some cases such as that shown in the traveltime curves to the east of the shots at station numbers 19 and 31 on line A-A', for example, the curves depart from the law of parallelism. A similar case is also shown on lines B-B', C-C', and D-D'. This illustrates the irregularity of the refractor and the presence of channels or leads. The traveltime curves shown from Figure 5.1. to 5.4. were plotted without reciprocal time corrections. From examination of the traveltime curves a four layer model seems appropriate.

The velocity analysis curves are illustrated in Figures 5.8., 5.9., 5.10., and 5.11. The shotpoint locations, reciprocal times, and optimum XY separation for each given shot pair or reversed traveltime curve are presented. Each given shot pair can be distinguished by a given symbol which includes small circles, plus signs, and large circles. As mentioned earlier in section 5.1 for Generalized Reciprocal Method interpretations, only the optimum XY value curves are plotted on the sections. The

velocities from the velocity analysis curves were assumed to be the correct velocities and are indicated on the sections.

Based upon the velocity distribution shown in the block diagram of the depth sections in Figure 5.16., the velocities found throughout the seismic profiles can be divided into five groups. The velocities obtained from the weathering spread along line B-B′ (shown in Figure 5.23.) are also included in this discussion.

The first group are velocities from 400-1000 m/s , representing soil, surface sand, and unconsolidated overburden which in some places consists of a brown and white soft clay containing birdseye quartz known as saprolite. The thickness of this layer varies from about 4-11 m in the line A-A′ and it reaches about 14 m in between station numbers 31 and 43. This layer does not seem to appear around station number 7 and between station numbers 25 and 31. In line B-B′ the thickness of the same layer varies from about 2-6 m , and in line C-C′ is about 1-8 m. In line D-D′ the thickness of this layer undulates and varies from 3-8 m, and in some places around station numbers 11 , 21-22 , and 26 , the thicknesses reach up to about 10 m , 11 m , and 12 m respectively.

The second group shows velocities from 1200-1550 m/s with thicknesses ranging from 5-59 m. These are interpreted as saturated and or compacted soil which in some places consists of kaolin. It seems that the kaolin consists mostly of the material with the velocity greater than or about 1300 m/s. This is interpreted from the results in the area where good bore hole control of the geometry of the clay deposit or kaolin is available which is situated on line C-C′ in between station numbers 1 and 22. The thickness

of the second group is variable up to 28 m on line A-A' and 33 m on line B-B', and getting deeper toward line C-C' and D-D'. On line C-C' it was found at about 15 m around station number 3 and 58 m around station number 38. On line D-D' this group is found to have a greater thickness compared to that on the lines A-A', B-B', and C-C', that is in the range of about 47-65 m, the deepest part being found between station numbers 23 and 27. This group dominates the sediments on lines C-C' and D-D'. This may be due to different erosional histories in different parts of the area or to different depositional histories.

The third group shows velocities from 1700-1800 m/s with thickness variable up to 61 m. These are interpreted as stiff clays representing Tertiary sediments. These velocities are in the range of those obtained from the seismic refraction surveys in Boobyalla Road and Picketts Plain conducted by Leaman and Moore in 1973-1974. As illustrated in Figure 1.5., this area is situated about 2 km to the northwest of the study area. The seismic velocity range at Boobyalla Road is 1400-1850 m/s with thickness variable up to 40 m, and at Picketts Plain the velocity range is 1400-1800 m/s with thickness variable up to 57 m. Leaman (1973) stated that these values are near the maxima for Tasmanian Tertiary materials, and much clay is indicated at depth. Leaman's interpretation agreed with the known presence of Tertiary sediment in a bore hole near spread 7 (Figure 1.6.). He concluded that the maximum thickness of the sediment in this region is around 60 m and at Picketts Plain is up to 64 m. It thus appears that the geology at Eastern Lead is similar to that at Boobyalla Road and Picketts Plain. These velocities are not found on line D-D' which may indicate lack of deposition there or subsequent erosion.

The fourth group shows velocities of 2100-3400 m/s and represents weathered or fractured rock. These velocities are also similar to velocities from the weathered or fractured granite found by Leaman (1973) at the Boobyalla Road (2000-3200 m/s).

The fifth group shows velocities of 4250-6800 m/s which by analogy with the seismic velocities obtained from adjacent areas represent the granite basement.

5.3 COMPARISON BETWEEN REFRACTION AND BOREHOLE RESULTS

Bore hole data from work by the Dorset Tin Division is shown in Figure 1.4. and that provided by the Utah Development Company is shown in Figures 2.1. and 2.2. A comparison may be made between a lithological section derived from the bore hole data provided by the Utah Development Company and refraction section between station numbers 7 and 31 , on line A-A' (Figure 5.16.), where it coincides with the lithological section of line 46 (Figure 2.2.). The comparison shows that some of the bore hole data agrees with the seismic refraction results. For example, around station number 7 the thickness of the compacted or saturated soil with velocity of 1500 m/s is about 2-6 m and is underlain by a weathered or fractured rock with velocity of 2800 m/s. A greater part of this comparison, however, shows that the thickness of the sediment derived from the bore hole is much smaller than that derived from the seismic results. The most unreliable thing is what was interpreted as a lithological boundary separating the sediment and the basement, especially around the station number 13 up to 31. According to the seismic results this boundary becomes deeper toward the station number 31 and reaches about 60 m. The bore hole data (Figure 2.2.),

however , shows a depression with the thickness of the sediment ranging from 10 to 14 m in between bore A268 and A270 or station number 14 and 25 on line A-A'. At this spot, the refraction result shows the depth of the basement about 30 m to 60 m. This discrepancy can be due to errors in depth estimation given by the refraction results - it is well known that the depth estimation from refraction may contain significant errors. A more probable reason is that as the lithological sections, given by the Utah Development Company, were derived from the bore hole data rather than drill core, it seems probable that the interpreted depth of the basement was underestimated. This is always a problem when drilling in such materials that a boulder bed may be misinterpreted as basement - so that drilling results tend to underestimate basements depths. Unfortunately none of the drill core has been preserved.

A comparison can also be made between the lithological section on lines 40 and 47 (Figure 2.2.) and the western end of the refraction line B-B', and also with the refraction line C-C' at around station number 13 or midway between station numbers 7 and 25 (Figure 5.16. or 5.17.). The interpreted depth of the basement in bore A220 (Figure 2.2.), the nearest bore hole to the station 13 is about 4 m whereas from the refraction at station number 13 a depth of 3 m was found for the top layer with velocity of 800 m/s. This layer is underlain by a formation with a velocity of 1400 m/s which may be interpreted as saturated or compacted soil or possibly kaolin (according to the bore hole data it is granite) with thickness of about 38 m. From the lithological section on line 40 the interpreted depth of the basement at bores A222, A223, and A224 (Figure 2.2.) is about 10 m , 17 m , and 14 m respectively. As shown in Figure 2.1. these bores are located in between the western end of the lines B-B' and C-C'. At the western end of the line B-B' the depth of the top layer or soil (velocity of

400-700 m/s) plus the depth of compacted soil and or kaolin (velocity of 1500 m/s) ranged from 11 m to 33 m compared to the depth of 10 m and 17 m derived from the bores A222 and A223 (Figure 2.2.). This material is underlain by a layer with a velocity of 1700 m/s representing stiff clays with thickness of 30-40 m. It is thus apparent that there are discrepancies between the two sets of results. The writer believes that what was interpreted as a basement in the bore holes probably represents a very compact material of clayey coarse grained sand or a cemented birdeye quartz wash or gravel. There are some cemented materials exposed at the surface. These are silcretes. Another possibility is that this perhaps corresponds to stiff clays as is shown from the refraction results.

Another result was shown from the comparison between the bore hole data on the line 47 (Figure 2.2.) and the western end of profile B-B' (Figure 5.16.), and between the data from bore A212 of the line 7 (Figure 2.2.) and the western end of the profile C-C' (Figure 5.16.). From line 47 the depth to the basement is about 13 m , and from bore A212 the depth is about 16 m . The depth from bore A212 may correspond to a layer with a velocity of 1400 m/s which around this spot reaches a depth of about 22 m and is underlain by a layer with velocity of 1800 m/s. Based upon the velocity distribution taken from refraction results (along line C-C'), no fresh basement was found by the refraction survey. The velocity of 2100 m/s and 3100 m/s represents weathered or fractured rock.

A good correlation is perhaps between the bore hole data and the western end of the profile C-C'. There is good bore hole control of the geometry of the clay deposit. Subsurface contours of the clay deposit were drawn and the position of the refraction profile was estimated as accurately as possible. This is illustrated in Figure 1.4. The results show that

the undulation of the boundary between overburden and the clay deposit along the line of profile C-C′ derived from the refraction results agrees with the depth of the clay deposit represented by the subsurface contour lines. The depth to the clay or the thickness of the overburden varies from about 6 m at the western end of the line to about 2 m around station number 7 and then increases again to about 7 m at station number 10, with an average of about 3 m in between station numbers 11 and 25. The velocity of the overburden at this spot was about 800 m/s and the velocity of the clay deposit (kaolin) was 1400 m/s. The velocity of the clay deposit is believed to be greater than this at a greater depth. This is deduced by the velocity range belonging to this formation between the traverse lines. The lateral and vertical changes of seismic velocity could be due to the difference in the degree of compaction or of water saturation or both.

5.4 REFLECTION DATA PROCESSING

The objective of data processing is basically to convert the raw data into a form that most greatly facilitates geological interpretation. In seismic reflection work, the processing is intended to eliminate or suppress all noise and to enhance the signal so that final record sections with the greatest possible resolution can be achieved. The techniques employed in the data processing have been described in detail by many authors and some of them are mentioned earlier in the seismic reflection section 3.4. In this thesis, the data processing includes frequency and velocity filtering, velocity analysis and normal moveout corrections, static corrections, and CDP stacking. The data was processed on the Prime 9955 computer using a processing package provided by Dr. R.J.G. Lewis. For static corrections, the programs Fieldstat.Ftn and Autostat.Ftn written by Blaha (1986) were

used in calculating field statics and residual statics on the basis of the optimal trace shifts determined by cross-correlation.

The first step in data processing was the plotting of the raw data and editing. This involves repacking the data in the right order to suit the CDP method. A selective examination was also made throughout the shot records. However, it was found difficult to select "best" shot records as mostly the records have the same appearance. The presence of reflection events was not obvious as there is considerable noise on the traces. In addition, the absence of obvious reflection alignment was thought to be due to irregular reflectors, and also the presence of thicknesses and velocity variation in the low velocity layers at the surface. Accordingly all the data recorded at a trace length of 200 ms was used in the analysis.

The second step was filtering which includes frequency and velocity filtering. The basic ideas of frequency and velocity filtering are given in section 3.4.3.2. Frequency filtering is generally intended to eliminate the unwanted noise on the basis of the frequency content. Based on the noise spread result shown in Figure 5.19. the frequency content of the traces ranged between 30 HZ and 130 HZ, while the frequency of the ground roll ranged between 30 HZ and 40 HZ. On the basis of trial and error using different band-pass filters, it was found that the best improvement was obtained by filtering between 50 HZ and 90 HZ. Direct arrival and ground roll are generally found to have low apparent velocities. As shown in the following section (Figures 5.19. and 5.20), the apparent velocity was about 492 m/s to 677 m/s for the direct arrivals, about 300 m/s and 377 m/s for the groundroll, and in the range of 1765-4533 m/s for the head waves. These events may be eliminated with the use of a velocity filter. A trial

was made using different cut-off velocities in the range between 2000 m/s and 6000 m/s. A cut-off velocity of 4000 m/s was found suitable.

The third step was arranging the data in the form of common-depth-point gathers. Each CDP gather contains traces for shot-receiver pairs in the configuration illustrated in Figure 3.11.b. To be able to do this, all the traces from the shot records have to be arranged and merged , and then collected as CDP gathers. As the data was collected by shifting the spread for half a geophone spacing, a twelve-fold gather was obtained.

The fourth step was field static corrections. Such corrections are used to eliminate the effects of changes in elevation at shotpoint and geophone locations, changes in shotpoint and geophone depths, and the variations of the thickness and velocity of the near-surface layer. In this case, a datum line is generally selected below the base of weathering and the reflection arrival times are those that would have been observed if all measurements had been made on the datum line. The principle of static computations is illustrated in Figure 5.18., and was adopted from Brescianini (1986). If E is the elevation above the datum line, T is the weathered layer thickness, S is the shot depth, and VWL and VONE are the velocity in weathering layer and in the underlying layer respectively ; a shot static (SST) and receiver static (RST) can be defined as

$$SST = \frac{(T - S)}{VWL} + \frac{(E - T)}{VONE}$$

$$RST = \frac{E}{VWL} + \frac{(E - T)}{VONE}$$

so that the total static (TST) for each shot-receiver pair will be given as

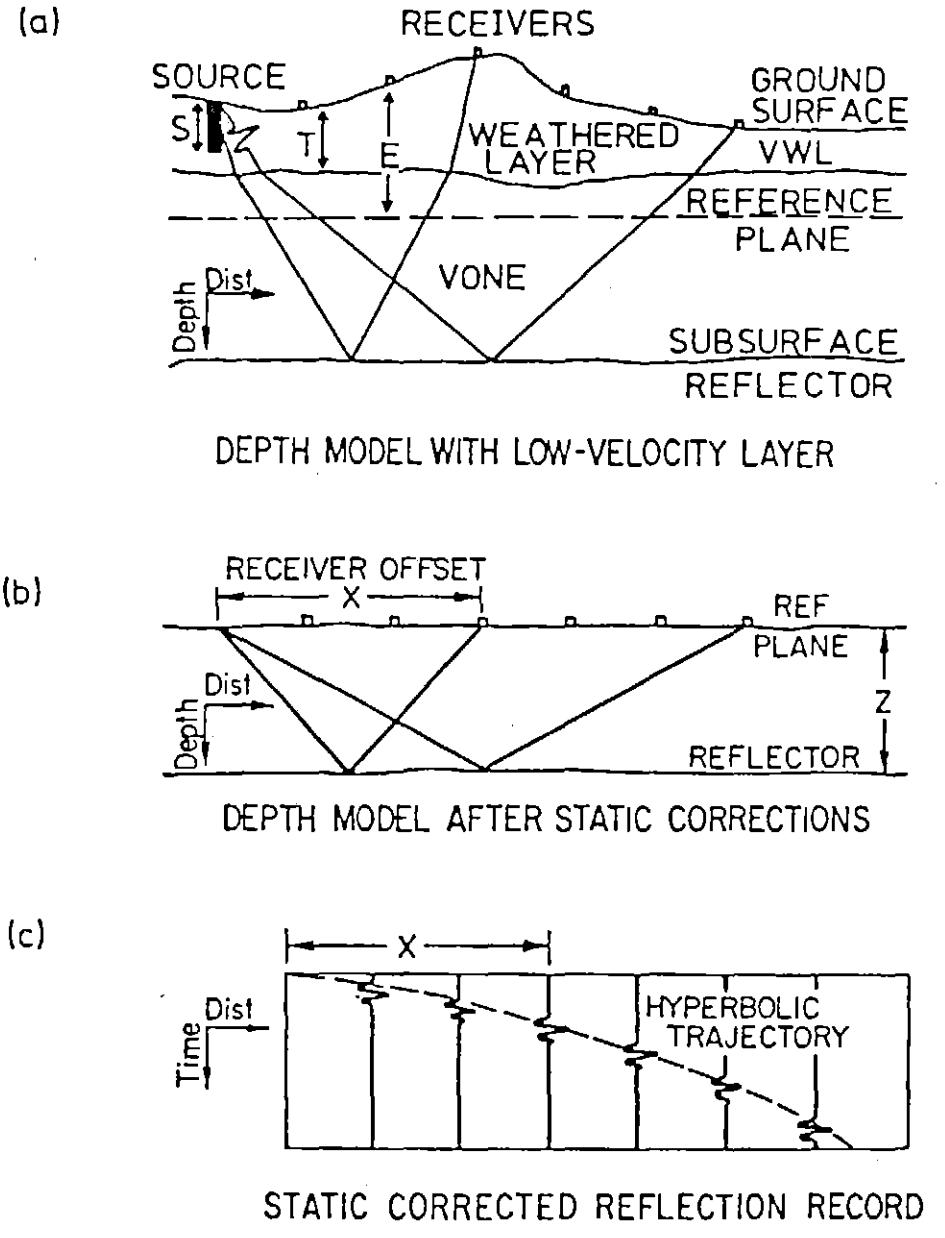

Fig.5.18. Static correction model. (a) Depth model with low-velocity layer ; (b) depth model after static corrections ; (c) static corrected reflection record. (From Brescianini, 1986).

$$TST = SST + RST$$

This total static is generally known as the "field static" and was applied to the gathered CDP data before undertaking velocity analysis. This was intended to give a better estimate of the velocities. The program Fieldstat.Ftn was used for the static corrections. This program was written by Blaha (1986) and listed in his thesis. The input file contains the information for each shot record and geophone position along the survey line, starting with the shot of the first spread position and ending with the largest offset geophone of the last spread position. The output file of Fieldstat.Ftn includes the static inputs Field, Gather, Relative, and Average . The static input Field is basically a file which contains the result of calculating shot and receiver statics (total statics) using the formulae mentioned above. Each line of this file contains the values of field static corrections corresponding to the traces of the shot record. The static input Gather is a file where the results of this calculation are gathered into a CDP gather form. Similarly, this file also contains the values of field static corrections corresponding to the traces of the CDP gather. The static input Relative is a file which contains a relative difference calculated between the static correction for a given trace and the average static for the corresponding gather. The static input Average is a file which contains on each line a number of identical average values of the field static corrections obtained by averaging the corrections in each gather. This program is applicable for the end-on spread type where the number of geophones is equal to the number of fold-coverage, and the number of traces per record is assumed to be 12.

The fifth step was velocity analysis and NMO corrections. The most important part of velocity analysis is the choice of a stacking velocity

which is approximately equal to the NMO velocity. As mentioned in section 3.4.2, velocity distribution can be obtained by analysis of the time-distance relationships on the reflection records themselves or by determining the velocity from non-reflection travel paths. The former is generally based upon the NMO measurements. This can be obtained using the $X^2 - T^2$ method, i.e. by plotting the squared reflection arrival times against the squared offset distance. However, this method probably is not suitable for data without good hyperbolic alignments because the plot will be scattered rather than showing a good alignment. Another procedure is based on examining reflected events across the gathers. In this case, a suitable velocity will be specified by a horizontal alignment of reflected events across the gathers. If the alignment is convex upward, it indicates too high a velocity, and conversely if the alignment is concave it indicates too low a velocity. Since the NMO is large throughout the section (especially for the top and intermediate layers), it was found difficult to identify the reflected events across the gathers. A trial velocity model using the known velocity derived from the refraction did not result in horizontal alignment of events. Another trial and error approach using different velocity-depth structure models and inspection was made for all the stacked sections. A good result was obtained using a stacking velocity in the range of 2200-2800 m/s, but the best value was about 2800 m/s which is somewhat above the usual sediment velocity but well below the basement velocity. From the refraction data the velocity of the fresh basement was found to be 4250 m/s and 6800 m/s, while for the sediment the velocity was found to be about 1700 m/s. While the stacking velocity is not closely comparable to the refraction velocity, this result may indicate that the velocities estimated by refraction are low. This could be due to the complex layering seen on the reflection data which is averaged in the refraction results. The stacking velocity is more comparable to the

sediment velocities found by Sedmik (1964) at Winnaleah. The velocity of the unconsolidated and saturated overburden in this area, for example, was found to be about 1500-2400 m/s. This means that the stacking velocity seems quite reasonable.

The sixth step was residual static corrections using the program Autostat.Ftn written by Blaha (1968). This method has been described by Hileman et.al. (1968). Basically, this correction was applied to eliminate the effects of lateral changes in the thickness and velocity of the low-velocity layer. This concept derives from the fact that there still remain plus and minus errors which can not be solved or eliminated by the field static corrections. This problem may be solved with the use of a correction known as the automatic statics correction. In this case cross-correlation functions are used to determine the optimum relative time shifts of each of the traces within a CDP gather (Hileman, 1968). As an input, the program requires the NMO and field static corrected gather file and its stacked equivalent. The cross-correlation window has to be specified and should be chosen so that it covers a time interval where primary events are dominant (Taner et.al., 1974).

The final step was CDP stacking. The use of CDP stacking is well known and is the most important aspect of data processing in improving data quality. The CDP stacking involves a process of summing the NMO corrected traces of a CDP gather. As the process is applied to the CDP gathers along a seismic reflection profile, this produces a seismic section. Generally, a good alignment of the primary reflection events will stand out and be distinguishable throughout the section, especially in the case where good contrasts in velocity with horizontal layering is present. But in the case where the reflector undulates, and the thickness of the low velocity

layer is not negligible, which is typical of deep leads or buried channels, the problem generally becomes complex.

Automatic gain control may be applied just before the display, and is the last processing option. The effect is generally shown by changes in amplitudes throughout the section which facilitates easy interpretation. A pruning option was used to tidy up spikes at the end of traces resulting from either electronic noise in the field or some processing operations.

Peak normalization is an option usually applied before the stacking process. Basically, peak normalization takes the largest amplitude and adjusts all other amplitudes accordingly. The effect is to override the gain settings used on the field recorder and put the gains to the same level (Swift, 1984). The output or stacked section can be obtained using a dot matrix printer. The stacked sections from the study area are displayed in section 5.6.

5.5 NOISE AND WEATHERING SPREAD RESULTS

Noise test results are shown from Figure 5.19. to 5.22. A seismogram of the raw data is shown in Figure 5.19. The frequencies in this section ranged between 30 HZ and 130 HZ and the apparent velocity ranged between 300 m/s and 4533 m/s. At around station number 25 , the seismogram does not show any distinct seismic events. This is probably due to the absorption of seismic energy in the low velocity top layer which in this region is about 4-6 m in thickness. This can be seen from the weathering spread shown in Figure 5.23. Another possibility might be a depression in the

basement (shown in Figure 5.28) so that the geometry of reflection raypaths might be such that the energy will not be detected by the receivers.

On the basis of the apparent frequency and apparent velocity, ground roll or surface waves are characterised by low frequencies of 33-43 HZ and low apparent velocities of 300-377 m/s. However, as shown in Figures 5.21. and 5.22., the ground roll still survives frequency filtering using 50-90 HZ and 70-120 HZ band-pass filters.

Apparent direct wave velocities were about 492 m/s and 677 m/s. These of course were not the typical direct wave velocities within the area, because the velocity of the top most layers generally varies from place to place and is very dependent on the surface or near-surface conditions such as loose material, cemented gravels, etc. Head waves or refracted waves were found to be about 1765 m/s and 4533 m/s which represent the velocity of the sediments (stiff clays) and the granite basement respectively.

As shown in Figure 5.20. the reflection event from a shallow horizon is at times of about 25 ms and from a deeper horizon is at times below 114 ms. The presumed reflections shown in the lower part of the noise spread section are possibly contaminated by coherent noise. The deeper reflection events become clearer after frequency filtering (Figure 5.21.). From trial and error, a band-pass filter of 50-90 HZ with 6 dB per octave attenuation slope was found to be the most suitable. For comparison, the same raw data has also been frequency filtered using a 70-120 HZ band-pass filter with a 6 dB per octave attenuation slope which is shown in Figure 5.22. The figure indicates that the signal to noise ratio was poor, so that the expected signal was indistinguishable without processing.

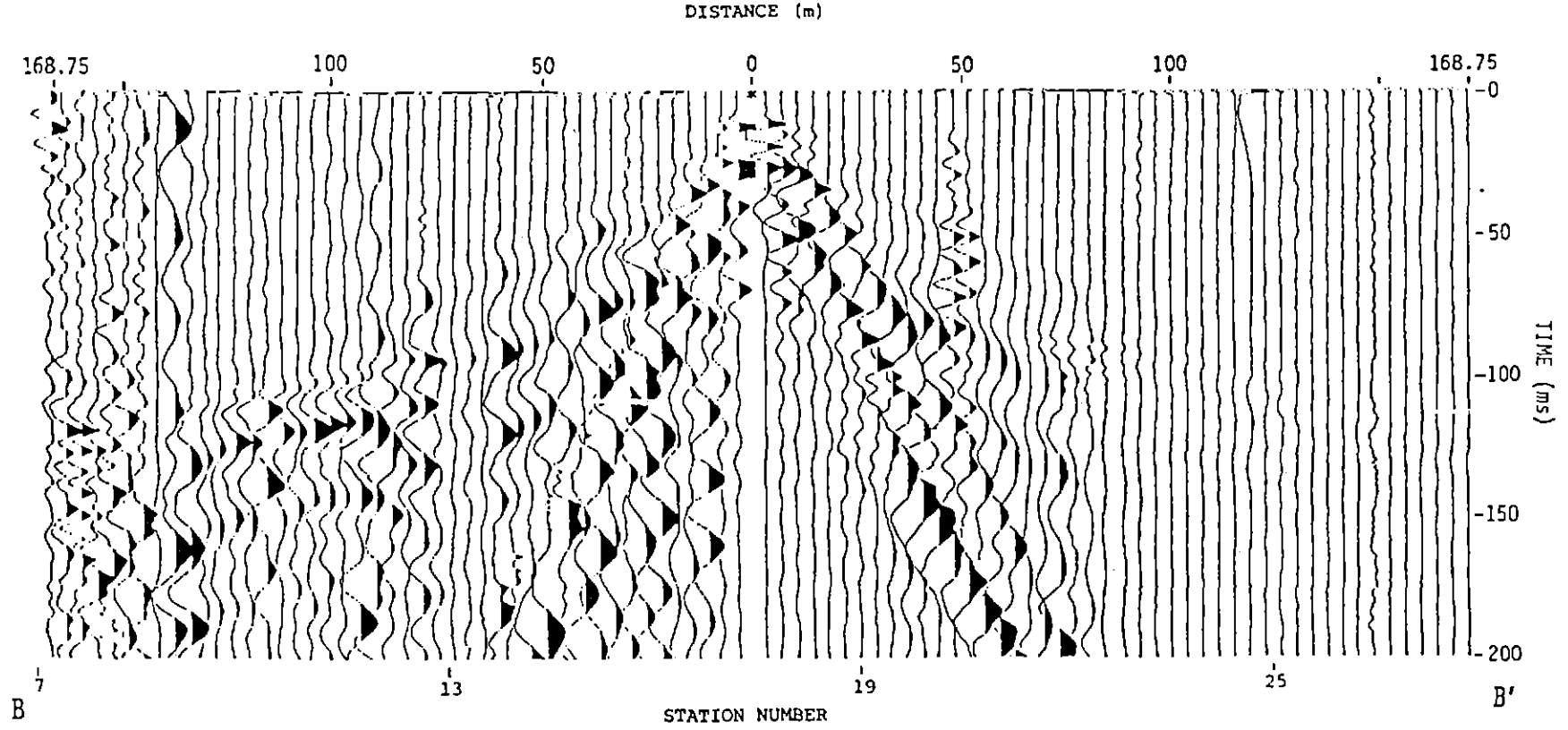

Fig.5.19. A seismogram of a noise spread for line B-B'. The star indicates the position of a fixed shotpoint.

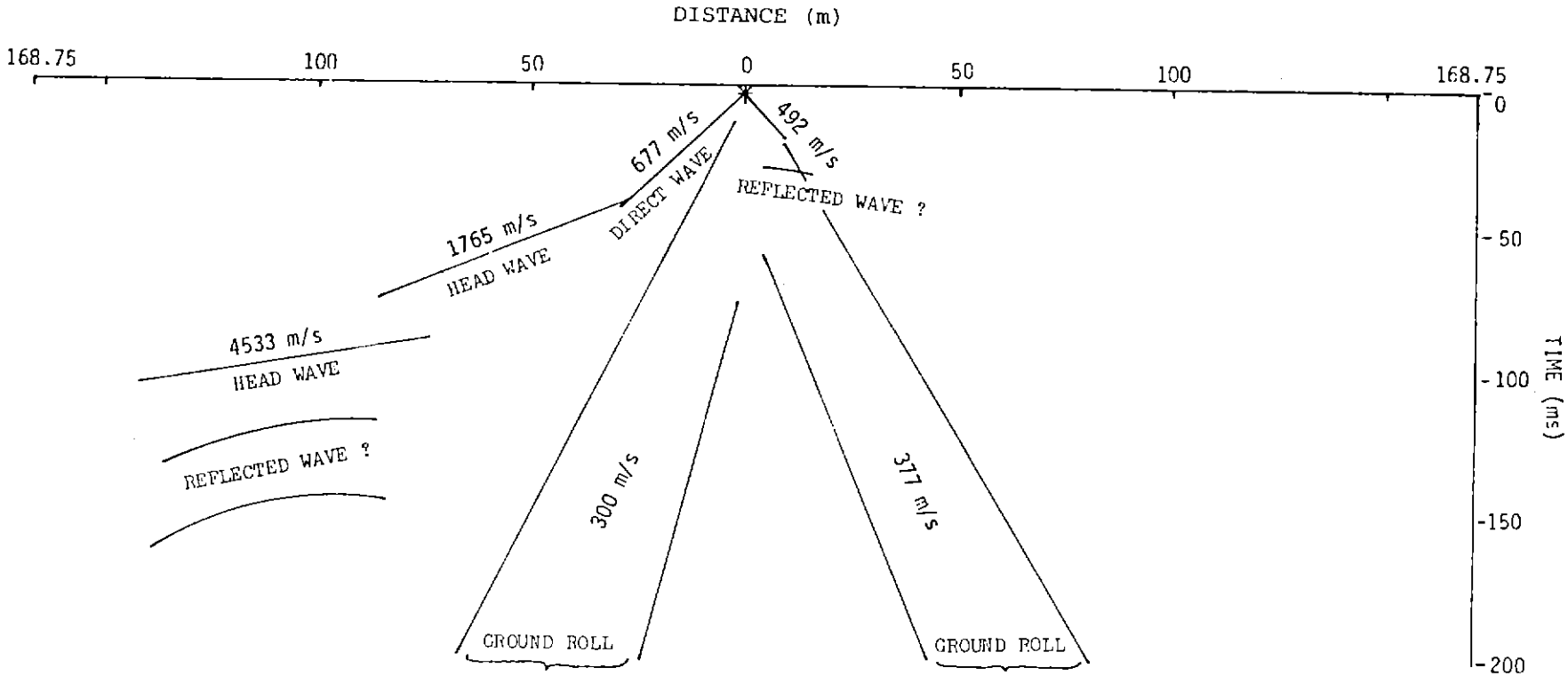

Fig.5.20. Line drawing interpretation of the noise spread shown in Figure 5.19. Expected reflectors are not clearly seen on this diagram.

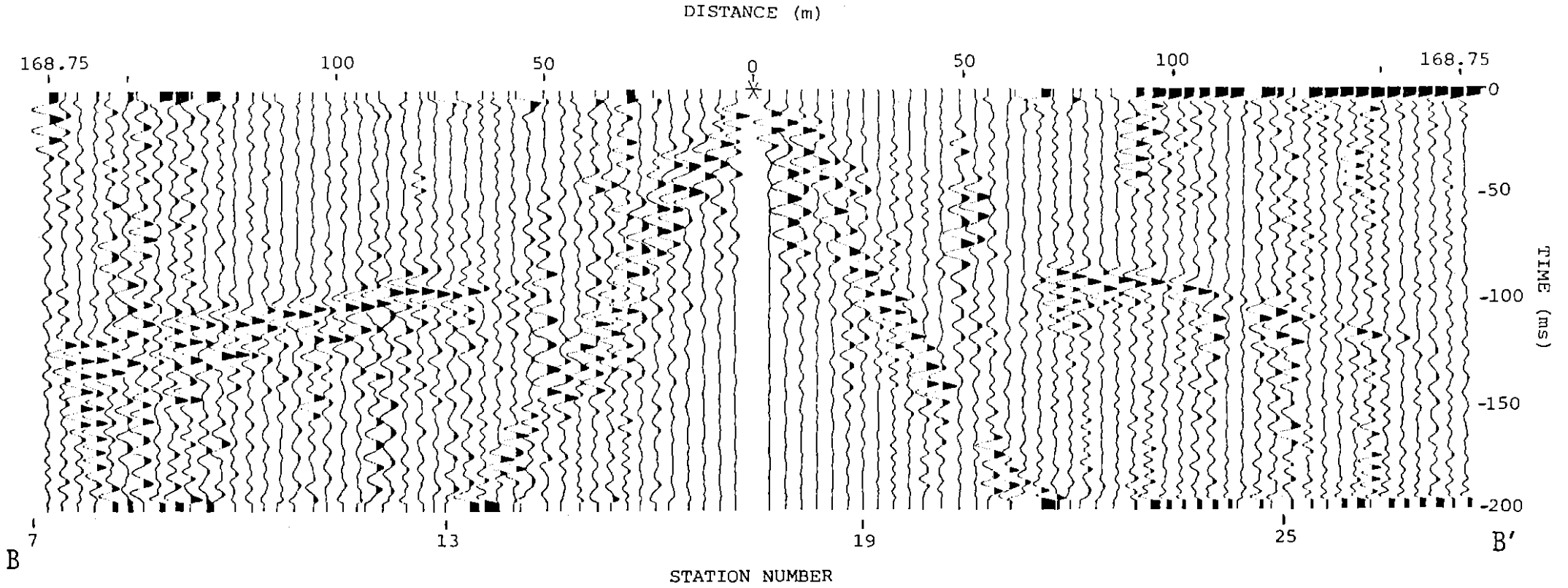

Fig.5.21. The noise spread from Figure 5.19. which has been frequency filtered using a 50-90 HZ band-pass filter with a 6 dB per octave attenuation slope, normalized peak amplitude, and pruned.

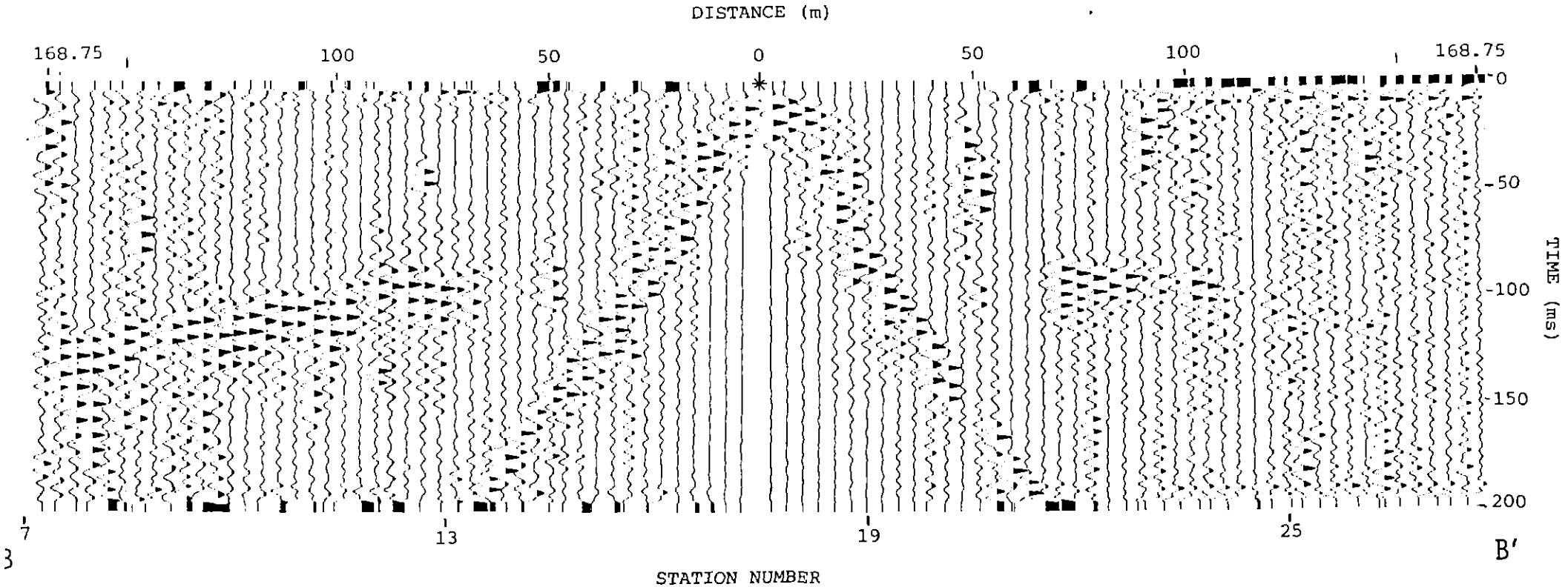

Fig.5.22. The noise spread from Figure 5.19. which has been frequency filtered using a 70-120 HZ band-pass filter with a 6 dB per octave attenuation slope, normalized peak amplitude, and pruned.

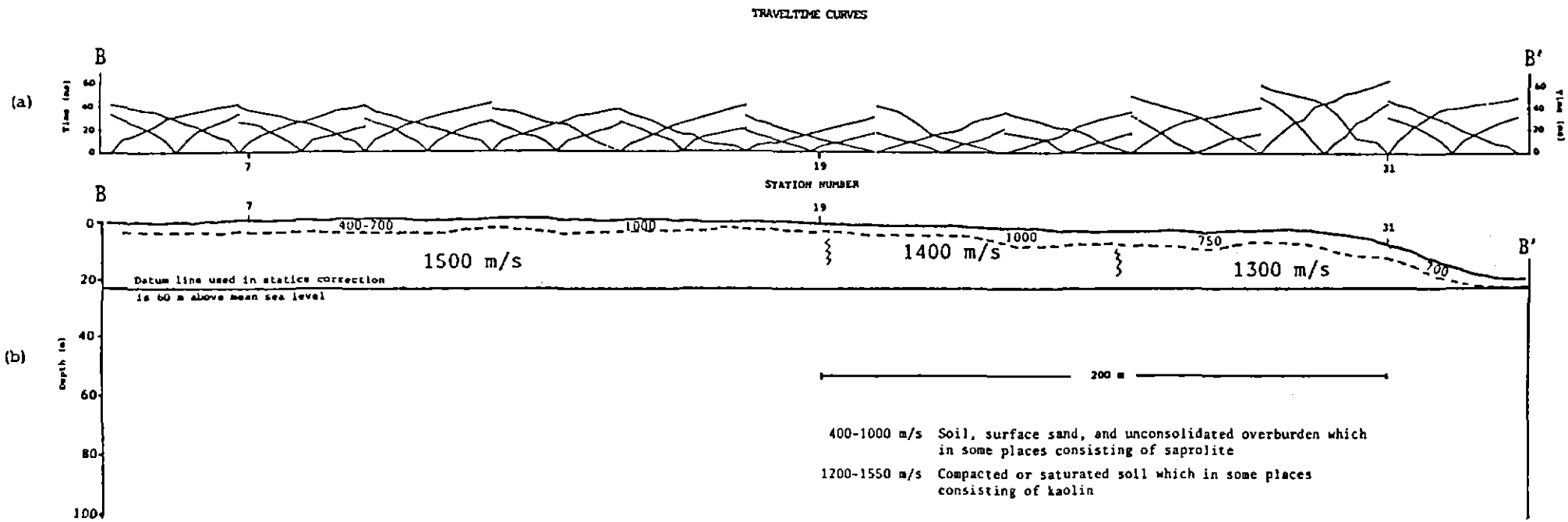

Fig.5.23. (a) Traveltime curves of the weathering spread in seismic line B-B', Eastern Lead, and (b) the cross section of interpreted geologic condition.

5 cm

The result of the weathering spread is illustrated in Figure 5.23. The cross section shows that there was a variation within the near-surface layer which was indicated by the lateral changes ranged between 400 m/s and 1000 m/s. The velocity range of 400-750 m/s was found to be associated with the presence of soil, loose sand, and unconsolidated overburden. In the middle of the section around station number 19 or between station numbers 13 and 25, the velocity was about 1000 m/s. Based on the appearance at the surface and the result of augering, the changes in velocity of the top most layer are generally associated with the presence of clay or a cemented gravel of birdseye quartz wash. These layers are underlain by a layer with a velocity ranging between 1300 m/s and 1500 m/s which is believed to represent the saturated and or compacted soil with patchy kaolin. These results were used in the static correction calculation.

5.6 REFLECTION RESULTS

Seismic reflection final sections are displayed in Figures 5.24. to 5.27. As shown in Figure 5.24. where field statics only were applied to the data, it seems likely that there are problems due to the presence of shallow, low velocity layers obscuring any deeper structures. The effect of a large NMO seems to dominate almost one fourth of the whole section so that event alignment on the CDP gather is in general difficult to obtain, especially for reflections from layers below the shallow, low velocity zone.

The data were processed using the residual statics calculated over cross-correlation windows from 19-33 ms, 30-60 ms, 15-75 ms, and 10-150 ms, and the results are shown in Figures 5.26.a. to 5.26.d. These sections

indicate reflections with good alignment of events. Some of the improvements shown are a result of the residual static program and a further improvement is obtained by prunning 260 points from the trace shown in Figure 5.27. This last operation removes large amplitude points from the trace which is then automatically re-scaled as the display is generated.

Interpretation of the results can be inferred from the analysis of the reflection patterns, and some useful parameters can be used to identify their nature. These include amplitude, frequency, continuity, and parallelism of the reflections, which have been discussed by Sangree and Widmier (1979). They suggest that reflection amplitude contains information on the velocity and density contrasts at individual interfaces and on the extent of interbedding, and that the frequency is primarily a characteristic of the nature of the seismic pulse, but it is also related to geological factors such as the spacing of reflectors or lateral changes in interval velocity. The continuity of the events is closely associated with continuity of bedding such as widespread, layered deposits.

Based upon these classifications, the structures shown on the reflection section from the study area, in general, may be divided into two main groups. These are : (1) a reflection zone with stratified patterns in which parallel reflections are present and have a reasonable degree of continuity ; and (2) a reflection zone where reflections are discontinuous, and or reflection-free zones where few reflecting surfaces exist.

The first group is indicated by reflections with dominant frequencies of about 90 Hz with a variation of the amplitudes from moderate to high, and good alignments. A strong amplitude event in this group is thought to represent a boundary separating a sediment and possibly boulder beds. The

depth of this boundary is indicated by crosses in Figure 5.28., and is found to deepen towards the B side. In addition, this boundary might also represent a subsequent period of erosion throughout the area as there are indications of pinching out of the underlying layers which is shown around station numbers 13 and 23 (see Figure 5.29.). The parallelism on the section may indicate layering. Apparent layering is also found below about 50 ms, which is below the depth of sediments indicated by the refraction data, and indicates that possibly "basement" as seen on refraction data is really boulder beds, fresh basement being at greater depths. Some of the very deep events are probably greatly amplified multiples and noise.

The second group is characterised by discontinuity of the reflections together with broadening of the wavelets which are bounded by the events with good alignments. This group may represent lenses within the section. The small lenses are thought to be patches of small channel-fills perhaps associated with small tributaries through the area. The largest one may reveal the main channel which is filled with slump materials or other channel-fill. This is in between station numbers 7 and 19 in Figure 5.29. This feature is shown by oblique or complex stratified reflection configurations with relatively low amplitudes which are bounded by good reflection alignments.

Continuous reflections with relatively uniform amplitude and frequency in the upper part of the section seem to be associated with layering of the sediments, which are uniform in thickness and lithology, and were deposited during the period of stable conditions. In contrast the lack of high amplitude reflections in the deep part of the channel is pressumed to be associated with different materials deposited during an earlier period of

deposition in a more unstable environment with no good stratification. Such structures would be expected and are typical of the geological features in surrounding areas, and are exposed , for example, by the Pioneer open cut mine near the study area. The sedimentology of the Pioneer placer deposits has been discussed by Morrison (1980). Based upon all this evidence, it seems very likely that there may be two cycles of deposition closely related to a period of rise and fall of the sea level throughout the region.

Confirmation of the interpretation can be made by comparing the reflection and refraction results, by overlapping them as shown on Figures 5.28. and 5.29. Based upon the refraction results on line B-B', it seems likely that the zone of interest lies between depths of about 20 m up to 50 m from the datum line or about 40 m up to 70 m from the surface. On the reflection section this zone appears to be within the reflection events from 20-70 ms. As can be seen around station numbers 13 and 25, for example, where the reflectors show discontinuity, there are changes in boulder bed (basement ?) velocity as measured by the refraction survey. This suggests that the refractions may not be originating from a single interface, but from different layers within sediment/basement in different areas. An exact coincidence between the refraction and reflection results would be surprising in view of the complex lensing and layering shown by the reflection section and the difficulties in velocity estimation that it might well produce, but there is broad overall agreement between the results from the two methods. Since the section is most probably close to minimum phase, this would result in an overestimation of the depth. However, it must be remembered that the seismic trace is a composite of reflections from closely spaced beds, and the event corresponding to a particular interface may not lag by very much.

The dashed line shows the geological boundaries derived from the refraction survey. The thickness of the top most layer varies from 2-6 m with velocity of 400-1000 m/s and becomes deeper in the B' direction. This layer is underlain by the layer with velocity of 1300-1500 m/s representing compacted or wet soil which in some places might be related to a soft clay formation or kaolin. Below these layers a possible formation of stiff clays of the Tertiary sediments occurs. The top and the bottom boundaries of this layer have roughly sinusoidal forms which parallel one another with the velocity being fairly uniform (1700 m/s). From the reflection results, however, it is clear that this formation is much more complex containing lenses and layers probably indicating different material and velocities. This is what would be expected in the deep lead depositional environment. The reflections are indicated in orange.

Around station number 20, an unusual event occurs at a depth of about 40-60 m below the surface and appears to be a lense of different seismic character within a formation. This is indicated by the discontinuity of an horizon on the lens boundary together with a broadening of the peaks with traces providing a different character on the section. If we had refraction results only, there would be no indication of this structure. However, this lens coincides with the ridge shown by refraction results, the depth position is comparable with that from the refraction results and it may well be that this lens is providing the observed refraction at this point in the section. This structure and the reflection results, in general, illustrate the superior structural information that can be obtained from the reflection survey. However, it is likely that the best velocity estimations are from the refraction data.

Another example of the advantages of the seismic reflection method is depicted in the interval between 25-50 ms where the refraction result shows the boundary between the sediment and the presumed basement. In this case, especially at the position between station numbers 1-19 or 1-24 the reflection results show a number of layers below the boundary indicated by the refraction. It is clearly seen that below this zone there are many multiples and possibly even deeper layering of some sort. This is indicated by the piece-wise continuity of the seismic events along the section. The broken alignments may indicate normal depositional structures.

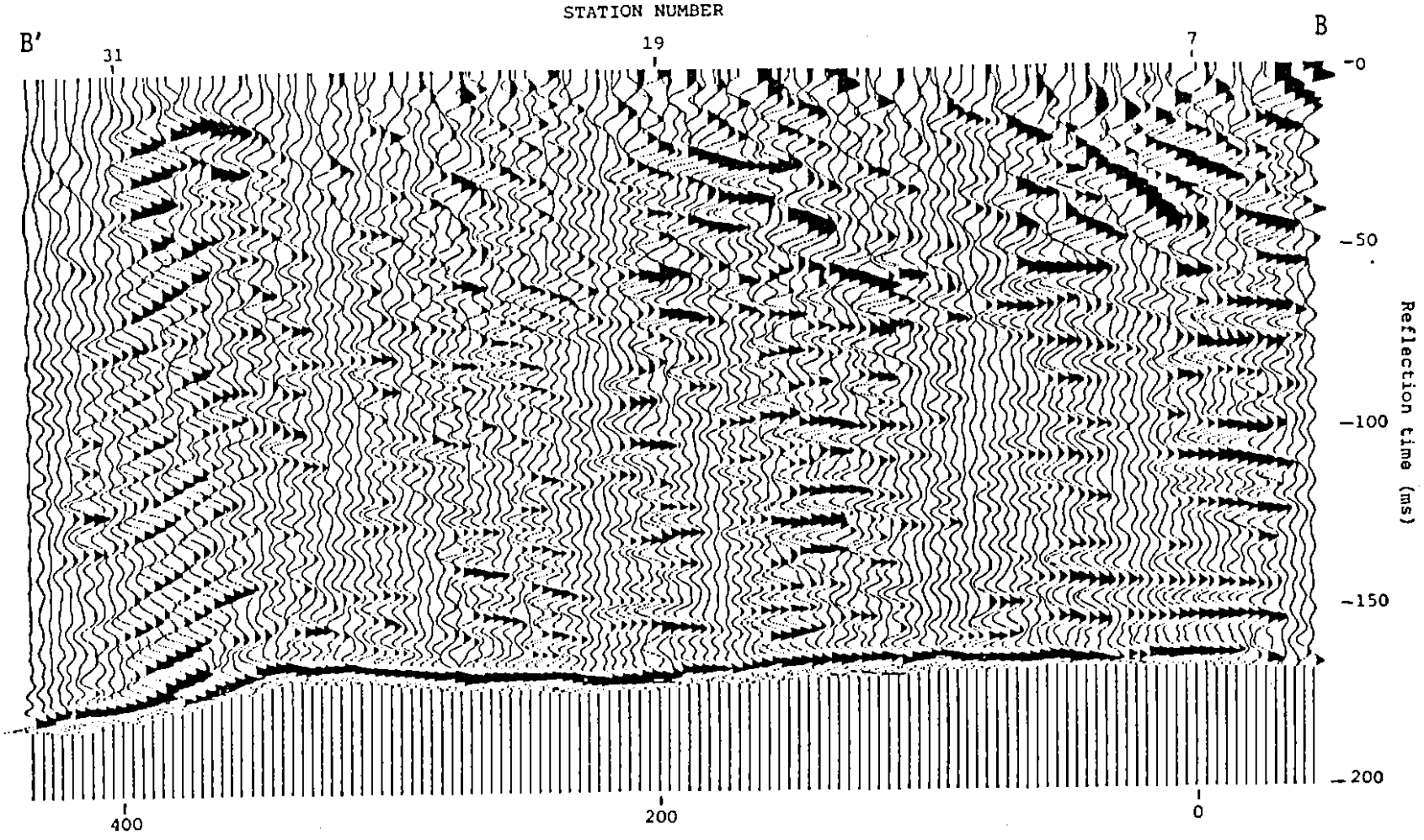

PROCESSING SEQUENCE

(1) Velocity Filter (4000 m/s)
(2) Frequency Filter (50-90 HZ, 6 dB)
(3) CDP Gather
(4) Field Static Corr's (STATICSINPUT-GATHER)
(5) NMO Corr's (Velocity model VEL-2800)
(6) Stack and Peak Amplitude Normalization

Fig.5.24. The final reflection section from Eastern Lead which has been corrected using field statics only.

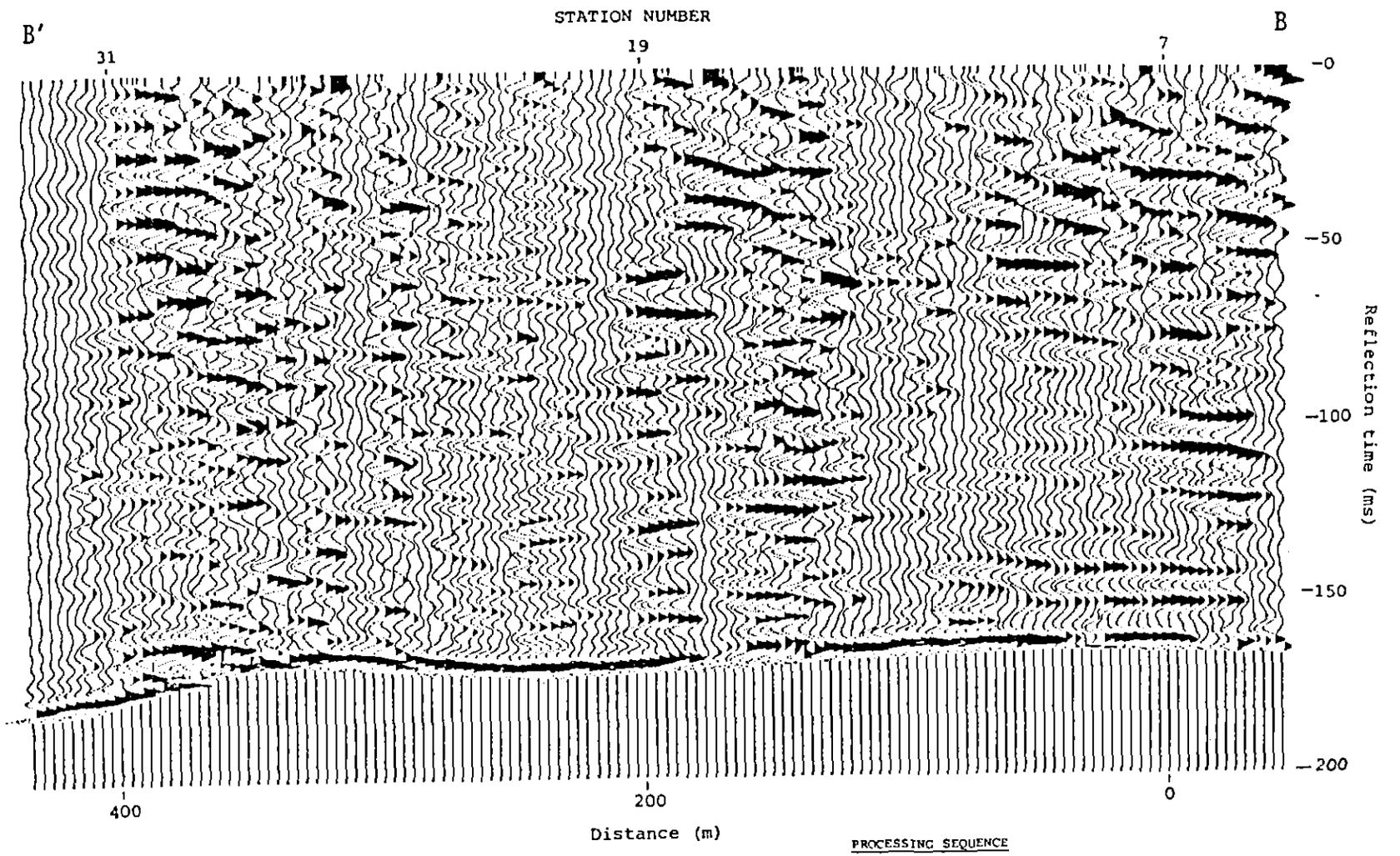

PROCESSING SEQUENCE

(1) Velocity Filter (4000 m/s)
(2) Frequency Filter (50-90 HZ, 6 dB)
(3) CDP Gather
(4) Relative Static Corr's (STATICSINPUT-RELATIVE)
(5) NMO Corr's (Velocity model VEL-2800)
(6) Average Static Corr's (STATICSINPUT-AVERAGE)
(7) Stack and Peak Amplitude Normalization

Fig.5.25. The final reflection section from Eastern Lead which has been corrected using the concept of relative statics.

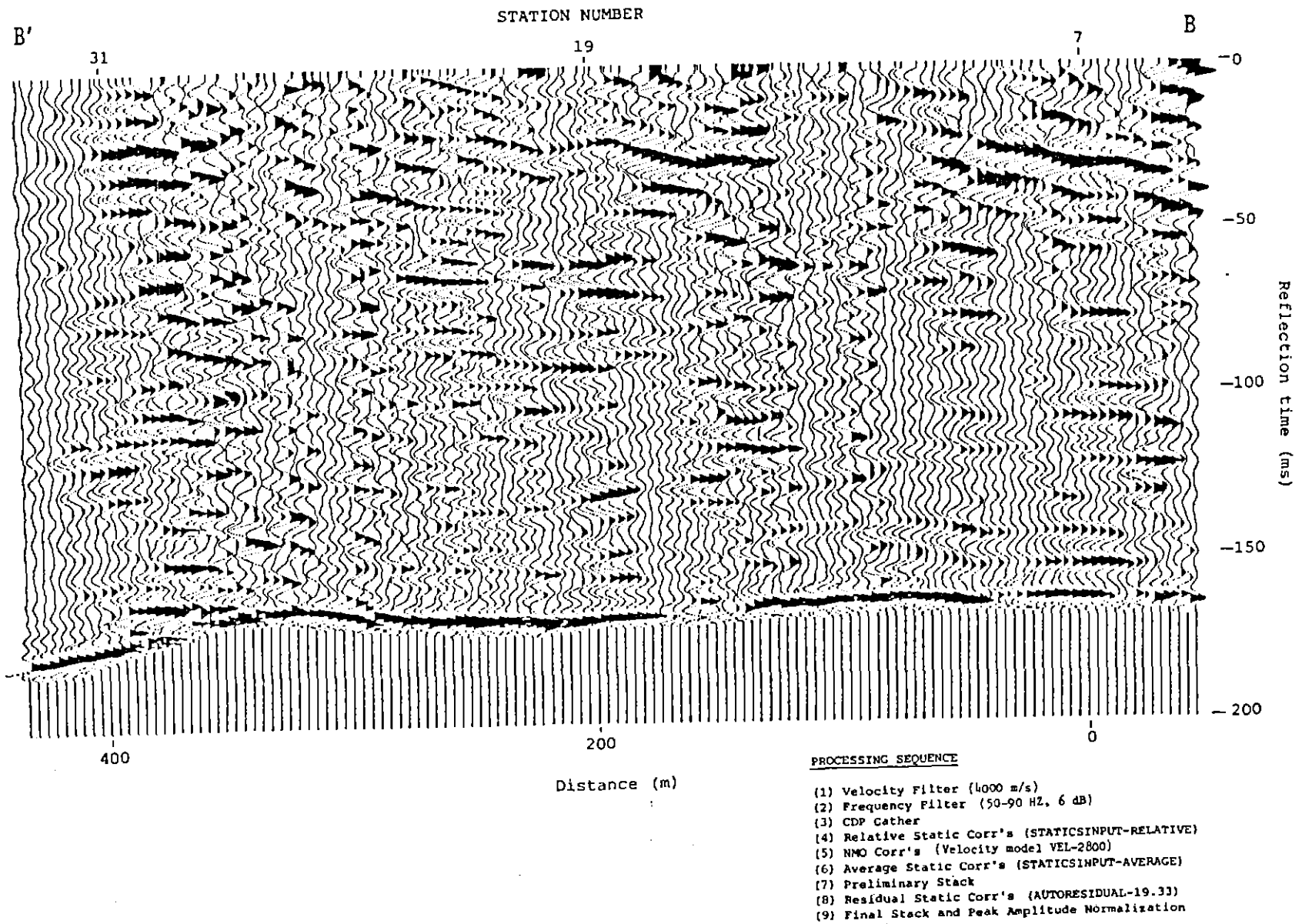

Fig.5.26.a. The final reflection section from Eastern Lead which has been corrected using field and residual statics, with cross-correlation window of 19-33 ms.

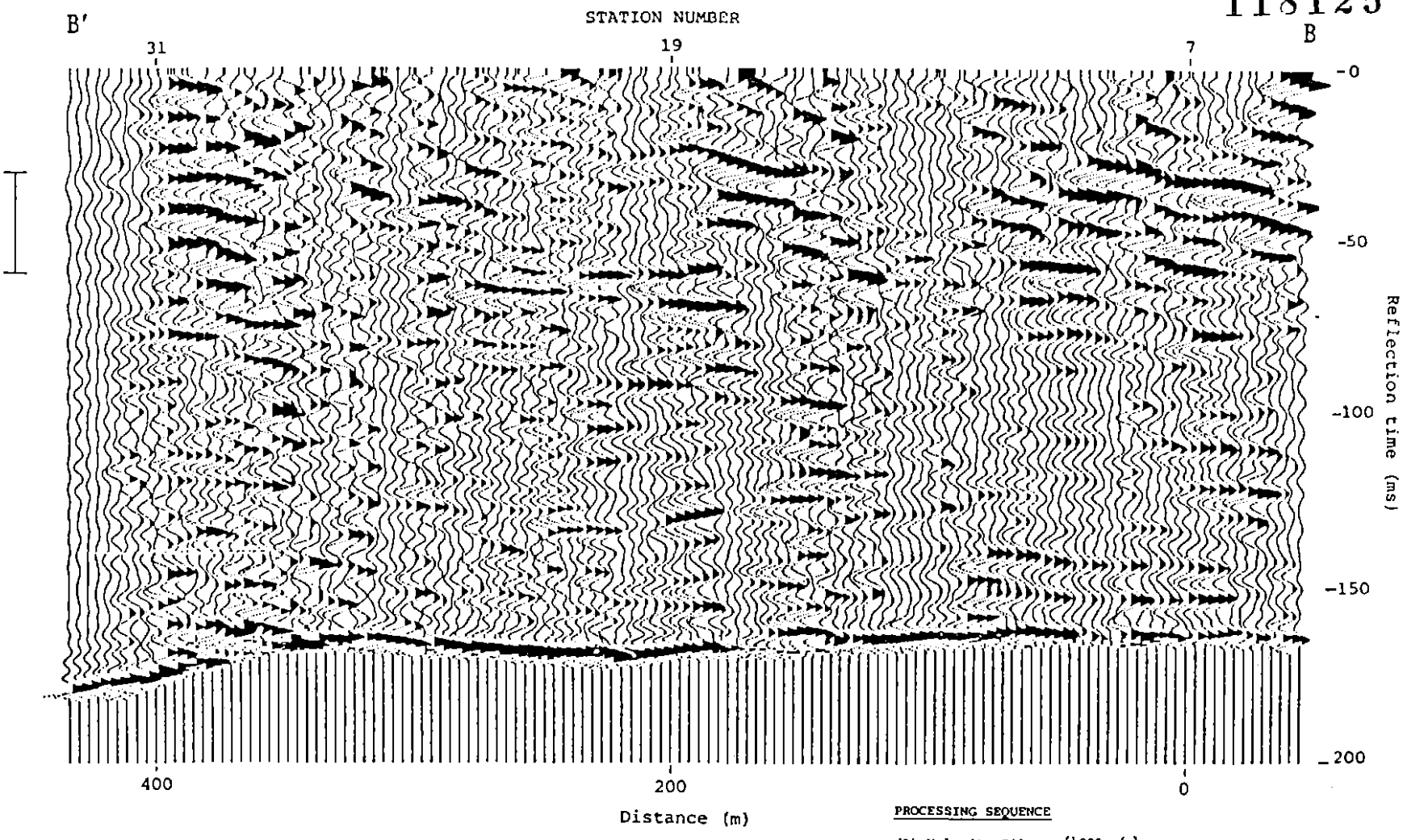

PROCESSING SEQUENCE

(1) Velocity Filter (4000 m/s)
(2) Frequency Filter (50-90 HZ, 6 dB)
(3) CDP Gather
(4) Relative Static Corr's (STATICSINPUT-RELATIVE)
(5) NMO Corr's (Velocity model VEL-2800)
(6) Average Static Corr's (STATICSINPUT-AVERAGE)
(7) Preliminary Stack
(8) Residual Static Corr's (AUTORESIDUAL-30,60)
(9) Final Stack and Peak Amplitude Normalization

Fig.5.26.b. The final reflection section from Eastern Lead which has been corrected using field and residual statics, with cross-correlation window of 30-60 ms.

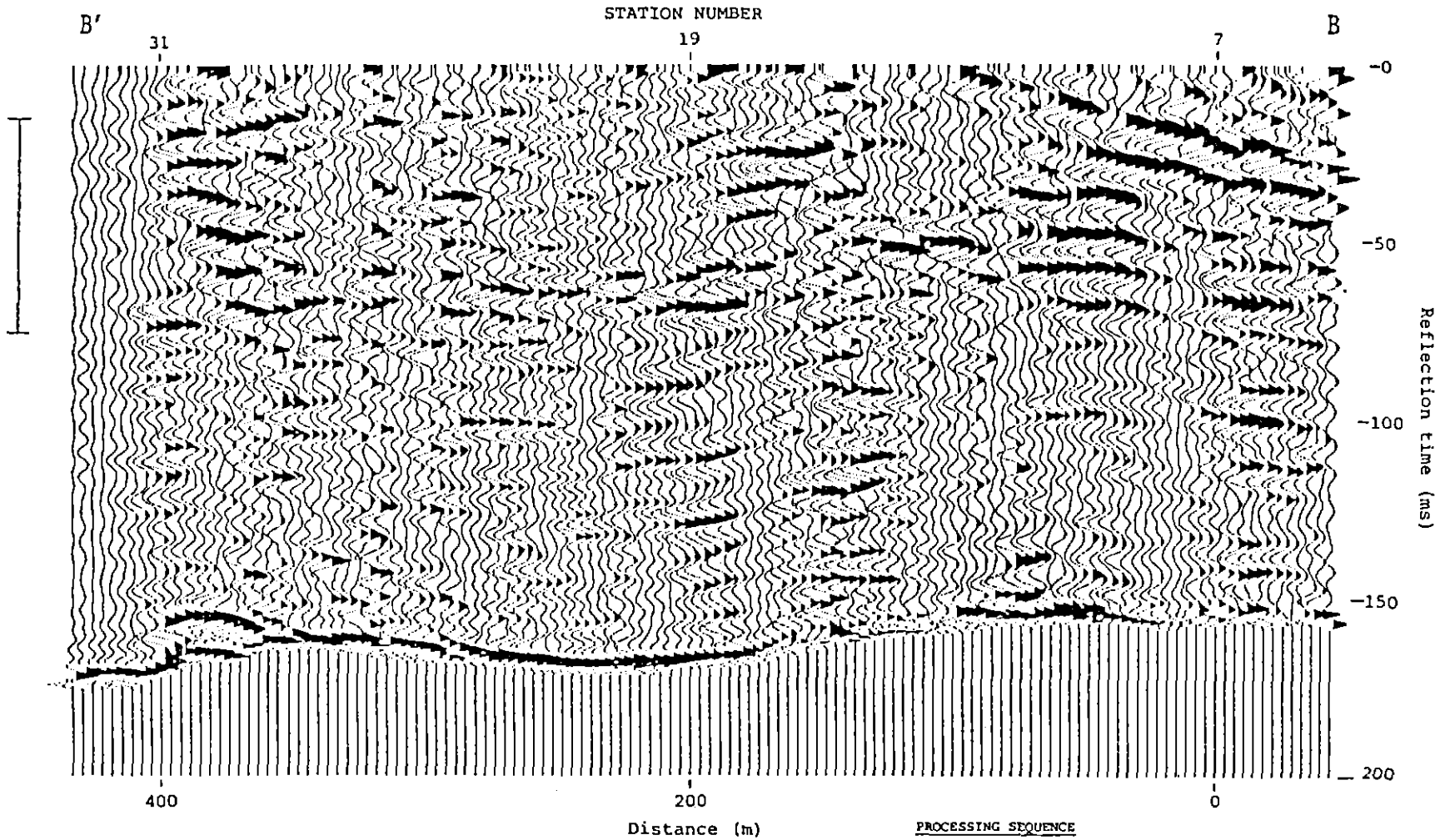

PROCESSING SEQUENCE

(1) Velocity Filter (4000 m/s)
(2) Frequency Filter (50-90 HZ, 6 dB)
(3) CDP Gather
(4) Relative Static Corr's (STATICSINPUT-RELATIVE)
(5) NMO Corr's (Velocity model VEL-2800)
(6) Average Static Corr's (STATICSINPUT-AVERAGE)
(7) Preliminary Stack
(8) Residual Static Corr's (AUTORESIDUAL-15.75)
(9) Final Stack and Peak Amplitude Normalization

Fig.5.26.c. The final reflection section from Eastern Lead which has been corrected using field and residual statics, with cross-correlation window of 15-75 ms.

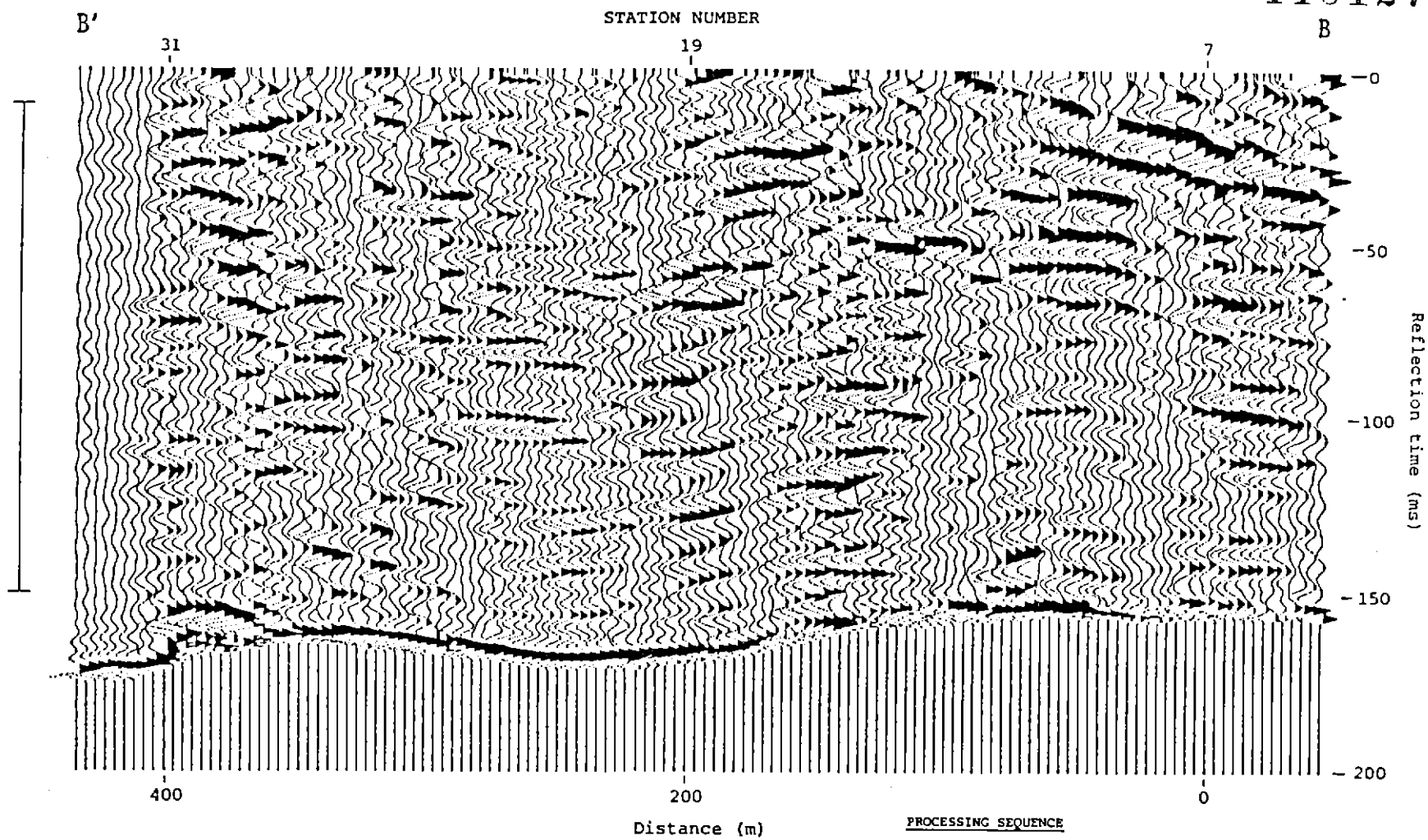

PROCESSING SEQUENCE

(1) Velocity Filter (4000 m/s)
(2) Frequency Filter (50-90 HZ, 6 dB)
(3) CDP Gather
(4) Relative Static Corr's (STATICSINPUT-RELATIVE)
(5) NMO Corr's (Velocity model VEL-2800)
(6) Average Static Corr's (STATICSINPUT-AVERAGE)
(7) Preliminary Stack
(8) Residual Static Corr's (AUTORESIDUAL-10.150)
(9) Final Stack and Peak Amplitude Normalization

Fig.5.26.d. The final reflection section from Eastern Lead which has been corrected using field and residual statics, with cross-correlation window of 10-150 ms.

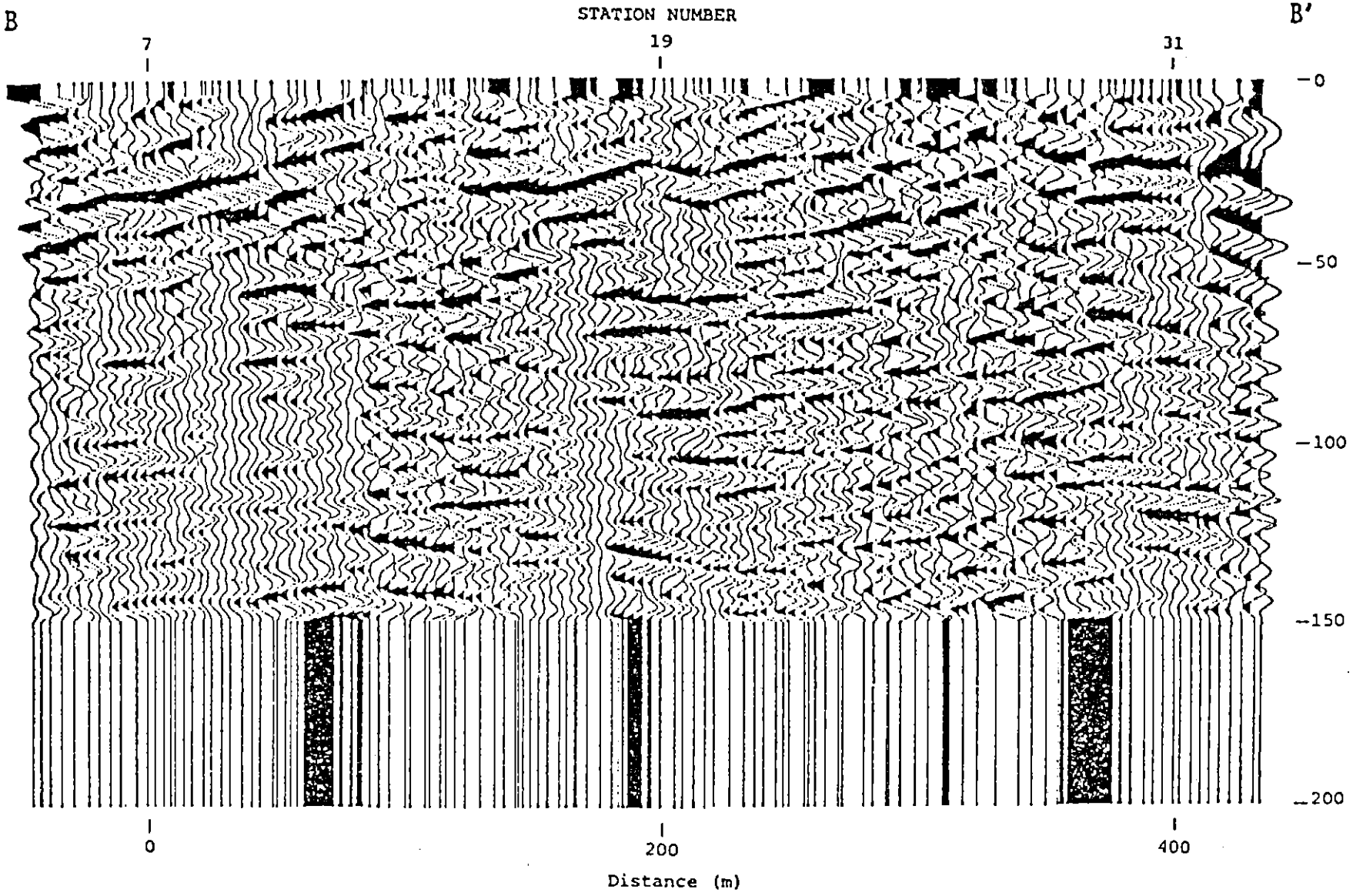

Fig.5.27. Further improvement obtained by pruning 260 points from the trace shown in Fig.5.26.a.

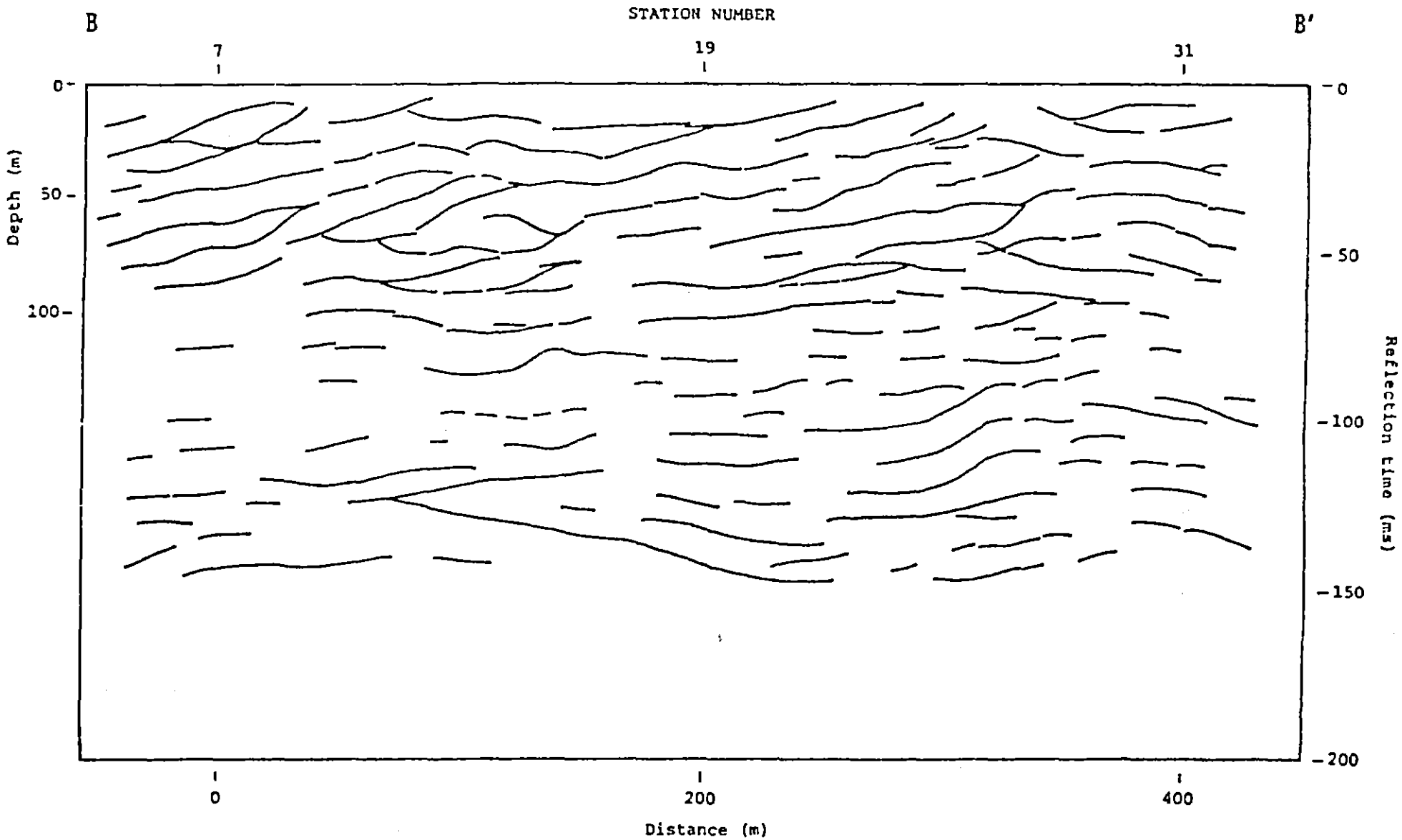

Fig.5.29. Cross section based on the reflection results shown in Fig.5.27.

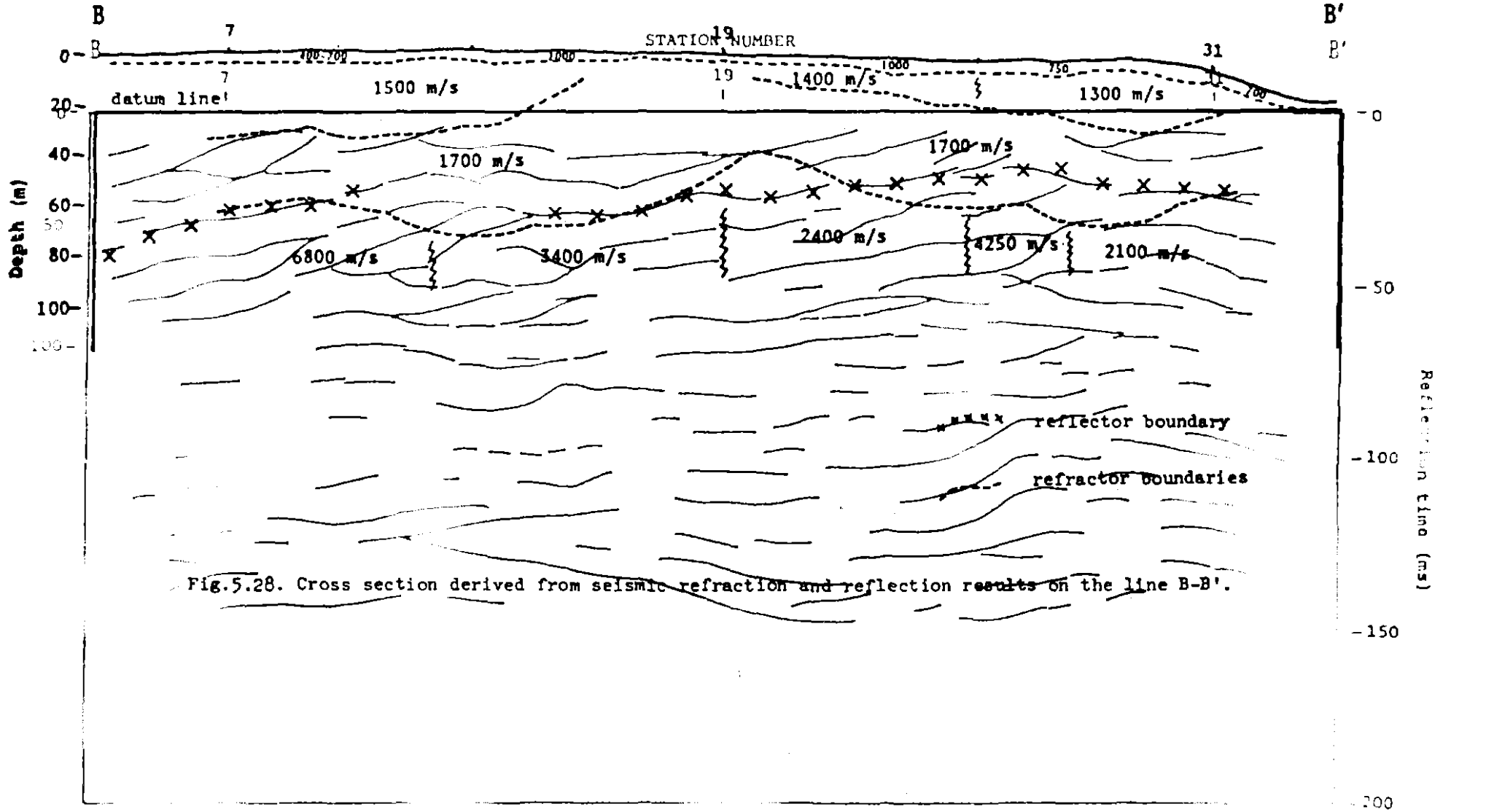

Fig.5.28. Cross section derived from seismic refraction and reflection results on the line B-B'.

Distance (m)

...section based ... reflection results shown in Fig.5.27.

CONCLUSION

Refraction results show the irregularity of the refractors along the lines, especially for the lines A-A′ and B-B′, which are believed to be an indication of a typical granite terrain. Based upon the velocity distribution obtained from the refraction results, the layers have velocities in the range of 1200-1550 m/s and 1700-1800 m/s, which are presumably compacted or saturated soil with patches of kaolin, and stiff clays. These layers may be regarded as recent alluvium and Tertiary sediment respectively. Generally the layers become deeper towards line D-D′ in a northwesterly direction, with the deepest part between station numbers 23 and 27 at a thickness of about 65 m. The absence of the group of velocities from 1700-1800 m/s on most of line C-C′ and along line D-D′ might be as a result of an erosion event. The decreasing of the velocity of the main refractors towards line D-D′ (an exception is that at the western end of line D-D′) probably indicates that there is a considerable variation in the nature of the materials throughout the area.

The depth estimation of the main refractors seems to be too shallow from a comparison between the refraction and reflection results. Part of the discrepancy is almost certainly due to the problem of identifying events corresponding to particular interfaces without the benefit of synthetic traces. Reflection data suggests that the main refractor is probably a series of boulder beds. Good agreement was found between the depth of a boulder bed or weathered basement derived from refraction results and the depth of the granite basement indicated by auger hole data. This is shown at around station number 7 on line A-A′, where the velocity of the material which can be related to that formation is about 2800 m/s. Another good correlation is also indicated from the comparison between the bore hole

data of the clay deposit, and refraction results in between station numbers 1 and 25 on line C-C'. The velocity of the corresponding material seems to be about 1400 m/s. From this, it seems reasonable to expect that the occurrence of kaolin will be in areas where this velocity is found. Based upon the observed velocity distribution of the sections, it seems likely that kaolin will be found as patches or lenses throughout the area. The remaining comparisons between bore hole data and refraction results show a discrepancy which may be either due to errors in depth estimation given by the refraction results or from the interpreted geology in the bore holes.

Complex structures are shown by the reflection section with the occurrence of structures such as layering, lensing, and even an indication of the distinctive nature of the main channel fill was obtained. A combination of these two methods clearly provides more sophisticated interpretation. It has been shown that there is a channel-cut around station number 13 on line B-B' which is likely to be the main channel. The complex structure within this channel indicates that the deposition of the channel-fill occurred under unstable conditions. This suggests that the area was situated near the source of origin of the deposits. The "basement" refractor in part follows the reflection layering and is close to a number of cut outs of reflection horizons. It seems likely to indicate an unconformity in the section rather than true basement. Parallelism and large lateral extent of the upper reflection events indicate that the deposition occurred under more stable conditions.

More precise interpretation requires better velocity determination and the detailed examination of bore hole samples. This would require further drilling as none of the material from earlier holes has been preserved. The best hole location would be in the center of the main channel at station

number 13 and would test the most favourable location for a cassiterite deposit.

REFERENCES

Ackermann, H.D., Pankratz, L.W., and Dansereau, D., 1986: Resolution of ambiguities of seismic refraction traveltime curves. Geophysics, 51: 223-235.

Appleby, W.R., and McEwan, I.R., 1966: Progress report on the exploration for alluvial tin deposits in N.E. Tasmania and the Furneaux Group. Unpubl. Rep. Utah Devel. Co. 139.

Attewell, P.B., and Ramana, Y.V., 1966: Wave attenuation and interval friction as functions of frequency in rocks. Geophysics, 31: 1049-1056.

Barry, K.M., 1967: Delay time and its application to refraction profile interpretation, in Seismic Refraction Prospecting. A.W. Musgrave, Ed., SEG, Tulsa: 348-361.

Bates, R.L., and Jackson, J.A., 1980: Glossary of geology, 2nd ed., Americal Geological Institute, Falls Church, Virginia.

Bendall, M., 1983: Report on South Mount Cameron kaolin deposit. Unpubl. Rep. Dep. Mines Tasmania.

Blackburn, G.J., 1982: Some problems with seismic reflection techniques. Unpubl. Ph.D. thesis, University of Tasmania.

Blaha, A., 1986: Improvement in static corrections for shallow seismic reflection. Unpubl. Hons. thesis, University of Tasmania.

Brescianini, R.F., 1986: Seismic reflection mapping of the Langloh coal mine workings. Unpubl. Hons. thesis, University of Tasmania.

Chesnut, W.S., 1965: Report on Ringarooma deep lead tin prospecting, North-east Tasmania, 1964/65. Unpubl. Rep. Broken Hill Pty Co. Ltd.

Dix, C.H., 1955: Seismic velocities from surface measurements. Geophysics, 20: 68-86.

Dobrin, M.B., 1976: Introduction to geophysical prospecting, 3rd ed., New York, McGraw-Hill Book Co., Inc.

Ellsworth, T.P., 1948: Multiple reflections. Geophysics, 13: 1-18.

Embree, P., Burg, J.B., and Backus, M.M., 1963: Wide band velocity filtering - The pie-slice process. Geophysics, 28: 948-974.

Fail, J.P., and Grau, G., 1963: Les filtres en eventail. Geophys. Prosp., 11: 131-163.

Gardner, L.W., 1967: Refraction seismograph profile interpretation, in Seismic Refraction Prospecting. A.W. Musgrave, Ed., SEG, Tulsa: 338-347.

Grant, F.S., and West, G.F., 1965: Interpretation theory in applied geophysics. New York, McGraw-Hill Book Co., Inc.

Green, R., 1962: The hidden layer problem. Geophys. Prosp., 10: 166-170.

Gurvich, I., 1972: Seismic prospecting. MIR Publishers, Moscow.

Hansen, R.F., 1948: Multiple reflections of seismic energy. Geophysics, 13: 58-85.

Hare, R., 1961: Estimate of reserves of kaolinitic clay in the South Mount Cameron area, Tasmania. Unpubl. Rep. Dep. Mines Tasmania.
TCR 63-355 EL 2/60

Hatherly, P.J., 1980: Computer processing of seismic refraction data. Bull. Aust. Soc. Explor. Geophys., 11: 69-74.

Hatherly, P.J., 1986: Attenuation measurements on shallow seismic refraction data. Geophysics, 51: 250-254.

Hatherly, P.J., and Neville, M.J., 1986: Experience with the generalized reciprocal method of seismic refraction interpretation for shallow engineering site investigation. Geophysics, 51: 255-265.

Hawkins, L.V., 1961: The reciprocal method of routine shallow seismic refraction investigations. Geophysics, 26: 806-819.

Heiland, C.A., 1940: Geophysical Exploration. Prentice Hall, New York.

Hileman, J.A., Embree, P., and Pflueger, J.C., 1968: Automated static corrections. Geophys. Prosp., 16: 326-358.

Jack, R., 1960: Areas selected for geophysical work North-eastern tin fields. Tech. Rep. Dep. Mines Tasmania, 5.

Jakosky, J.J., 1950: Exploration Geophysics, 2nd ed., Trija, Los Angeles.

Jennings, I.B., Williams, E., 1967: Geology and mineral resources of Tasmania. Geological Survey Bulletin, 50.

Johnson, C.H., 1948: Remarks regarding multiple reflections. Geophysics, 13: 19-26.

Junger, A., 1951: Deep basement reflections in Big Horn County, Montana. Geophysics, 16: 499-505.

Kilty, K.T., Norris, R.A., McLamore, W.R., Hennon, K.P., and Euge, K., 1986: Seismic refraction at Horse Mesa Dam: An application of the generalized reciprocal method. Geophysics, 51: 266-275.

Kleyn, A.H., 1983: Seismic Reflection Interpretation , 269 pp. Applied Science Publishers, London.

Knapp, R.W., and Steeples, D.W., 1986: High-resolution common-depth-point seismic reflection profiling: Instrumentation. Geophysics, 51: 276-282.

Knapp, R.W., and Steeples, D.W., 1986: High-resolution common-depth-point reflection profiling: Field acquisition parameter design. Geophysics, 51: 283-294.

Krohn, C.E., 1984: Geophone ground coupling. Geophysics, 49: 722-731.

Krohn, C.E., 1985: Geophone ground coupling. The leading edge of exploration, 4, 4: 56-60.

Lombardi, L.V., 1955: Notes on the use of multiple geophones. Geophysics, 20: 215-226.

Leaman, D.E., 1973: Summary of geophysical work, Gladstone area. Tech. Rep. Dep. Mines Tasmania, 16: 89-96.

Leaman, D.E., and Moore, W.R., 1973: Seismic survey, South Mount Cameron. Unpubl. Rep. Dep. Mines Tasmania, 1973/72.

Mayne, W.H., 1962: Common-reflection-point horizontal data stacking techniques. Geophysics, 27: 927-938.

Miller, R.D., Pullan, S.E., Waldner, J.S., and Haeni, F.P., 1986: Field comparison of shallow seismic sources. Geophysics, 51, 11: 2067-2092.

Moore, J.F., 1970: Data processing in shallow seismic refraction. Unpubl. Hons. thesis, University of Tasmania.

Moore, W.R., and Leaman, D.E., 1974: Further geophysical work, Gladstone. Tech. Rep. Dep. Mines Tasmania, 17: 88-98.

Morrison, K.C., 1980: Sedimentology of the Pioneer placer deposit. Unpubl. Hons. thesis, University. of Tasmania.

Musgrave, A.W., Ed., 1967: Seismic Refraction Prospecting, SEG, Tulsa.

Muskat, M., and Meres, M.W., 1940: The seismic wave energy reflected from various types of stratified horizons. Geophysics, 5: 149-155.

Nye, P.B., 1925: The sub-basaltic tin deposits of the Ringarooma Valley. Bull. Geol. Surv. Tasmania, 35.

Nye, P.B., 1930: Report on the age and mineral characteristics of the granites of Tasmania. Unpubl. Rep. Dep. Mines Tasmania, 24.

Olhovich, V.A., 1964: The causes of noise in seismic reflection and refraction work. Geophysics, 29: 1015-1030.

Pakiser, L.C., and Black, R.A., 1957: Exploration for ancient channels with the exploration seismograph. Geophysics, 22: 32-47.

Palmer, D., 1980: The generalized reciprocal method of seismic refraction interpretation, ed. Kenneth B.S. Burke, SEG, Tulsa.

Parasnis, D.S., 1982: Principles of Applied Geophysics, 3rd ed., 275 pp., Chapman and Hall, London.

Richter, C.F., 1958: Elementary Seismology, 768 pp., Freeman, San Francisco.

Rigdon, H., and Hoover, G., 1987: Quantitative selection of seismic acquisition parameters. The leading edge of exploration, 6, 1: 18-25.

Robinson, E.A., 1983: Seismic velocity analysis and convolutional model, D. Reidl Publishing Company, Boston, USA.

Rothman, D.H., 1986: Automatic estimation of large residual statics corrections. Geophysics, 51: 332-346.

Rowston, D.L., 1961: Ringarooma deep leads seismic refraction survey, Tasmania 1957. Unpubl. Bur. Min. Resour. Aust. Rec. 1961/151.

Sangree, J.B., and Widmier, J.M., 1979: Interpretation of depositional facies from seismic data. Geophysics, 44: 131-160.

Sedmik, E.C.E, 1964: Winnaleah area geophysical surveys, Tasmania 1961-1962. Rec. Bur. Miner. Resour. Geol. Geophys. Aust. 1964/54.

Sengbush, R.L., 1983: Seismic Exploration Methods, 296 pp., IHRDC, Boston.

Sharpe, J.A, 1942: The production of elastic waves by explosion pressures.I. Theory and empirical field observations. Geophysics, 7: 144-154.

Sharpe, J.A., 1944: The effect of charge size on reflection records. Geophysics, 9: 131-142.

Sheriff, R.E., 1982: Encyclopedic Dictionary of Exploration Geophysics, SEG, Tulsa.

Sheriff, R.E., and Geldart, R.L., 1982: Exploration Seismology Vol.1; History, theory, and data acquisition, 253 pp., Cambridge University Press, Cambridge.

Sheriff, R.E., and Geldart, R.L., 1983: Exploration Seismology Vol.2; Data-processing and interpretation, 221 pp., Cambridge University Press, Cambridge.

Shugart, T.R., 1944: Frequency discrimination in the low velocity zone. Geophysics, 9: 19-28.

Silverman, D., 1967: The digital processing of seismic data. Geophysics, 32: 988-1002.

Singh, S.,1983: A study of shallow reflection seismics for placer-tin-reserve evaluation and mining. Geoexploration, 21: 105-135.

Sjogren, B., 1984: Shallow Refraction Seismic, Chapman and Hall Ltd., London.

Sloat, J., 1948: Identification of echo reflections. Geophysics, 13: 27-35.

Soske, J.L., 1959: The blind zone problem in engineering geophysics. Geophysics, 24: 359-365.

Swift, M.G., 1984: Shallow seismic reflection techniques. Unpubl. Hons. thesis, University of Tasmania.

Taner, M.T., Koehler, F., and Alhilali, K.A., 1974: Estimation and correction of near-surface time anomalies. Geophysics, 39: 441-463.

Telford, W.M., Geldart, L.P., Sheriff, R.E., and Keys, D.A., 1976: Applied Geophysics, Cambridge University Press, New York.

Twelvetrees, W.H., 1900: Preliminary report on the deep lead or infrabasaltic stanniferous gravels of the Ringarooma Valley near Derby. Mines Department, Tasmania.

Urquhart, D.F., 1956: The investigation of deep leads by the seismic refraction method. Bull. Bureau Min. Res., Australia, 35.

Walker, C., and Crouse, B.J., 1985: Field processing in the '80s. The leading edge of exploration, 4, 3: 41.

Warin, O.N., Appleby, W.R., 1965: Report on the progress investigations for tin in North-east Tasmania. Unpubl. Rep. Utah Devel. Co. 135.

Waterman, J.C., 1948: Multiple-reflection evidence. Geophysics, 13: 41-44.

West, S.S., 1941: The effect of density on seismic reflections. Geophysics, 6: 45-51.

Ziolkowski, A., and Lerwill, W.E., 1979: A simple approach to high resolution seismic profiling for coal. Geophys. Prosp., 27: 360-393.

APPENDIX A

Catalogue of Data Files Used for Processing

Refraction and reflection data listed below were collected from the Eastern Lead, Pioneer, North Eastern Tasmania. The complete set of repacked files, currently stored on GEOL pack in the University of Tasmania's Prime 9955 computer. Each file corresponds to a single shot, and is labelled in the following fashion, e.g.:

PIONEER.HHHHHHHHHHH

where HHHHHHHHHHH are the constants of the thumbwheel switch on the DMT-911 RECORDER at the time the particular shot was recorded. The refraction data is listed sequentially. The position of weathering spread, noise spread, and reflection profile together with the refraction profile of 17 m station spacing along the line B-B' is shown at the end of this appendix. Other data files and intermediate results used in this thesis have been lodged with the curator, Geology Department.

Refraction with Station Spacing = 17 m.

Line A - A'	Line B - B'	Line D - D'
PIONEER.261185000020	PIONEER.271185000027	SCOTTS.190286000024
PIONEER.261185000019	PIONEER.271185000026	SCOTTS.190286000025
PIONEER.261185000018	PIONEER.271185000023	SCOTTS.190286000026
PIONEER.251185000010	PIONEER.281185000032	SCOTTS.190286000029
PIONEER.261185000021	PIONEER.271185000024	SCOTTS.180286000023
PIONEER.251185000009	PIONEER.281185000031	SCOTTS.190286000030
PIONEER.011185000002	PIONEER.271185000025	SCOTTS.180286000022
PIONEER.261185000022	PIONEER.281185000028	SCOTTS.190286000031
PIONEER.251185000017	PIONEER.281185000029	SCOTTS.190286000028
PIONEER.011185000003	PIONEER.281185000030	SCOTTS.190286000027
PIONEER.251185000016		
PIONEER.241185000008		
PIONEER.251185000011		
PIONEER.251185000012		
PIONEER.251185000014		

APPENDIX A (cont)

Catalogue of Data Files Used for Processing

Refraction with Station Spacing = 8.5 m.

Line C - C'

SCOTTS.140286000002
SCOTTS.140286000005
SCOTTS.150286000008
SCOTTS.140286000004
SCOTTS.160286000015
SCOTTS.140286000003
SCOTTS.150286000006
SCOTTS.150286000010
SCOTTS.160286000014
SCOTTS.150286000009
SCOTTS.160286000012
SCOTTS.170286000020
SCOTTS.160286000011
SCOTTS.160286000016
SCOTTS.170286000019
SCOTTS.160286000017

APPENDIX A (cont)

Catalogue of Data Files Used for Processing

Weathering Spread with Station Spacing = 3.75 m.

Line B - B'

PIONEER1.040986000001
PIONEER1.040986000002
PIONEER1.040986000003
PIONEER1.040986000004
PIONEER1.040986000005
PIONEER1.040986000006
PIONEER1.040986000007
PIONEER1.040986000008
PIONEER1.040986000009
PIONEER1.040986000010
PIONEER1.040986000011
PIONEER1.040986000012
PIONEER1.040986000013
PIONEER1.040986000014
PIONEER1.040986000015
PIONEER1.050986000016
PIONEER1.050986000017
PIONEER1.050986000018
PIONEER1.050986000019
PIONEER1.050986000020
PIONEER1.050986000021
PIONEER1.050986000022
PIONEER1.050986000023
PIONEER1.050986000024
PIONEER1.050986000025
PIONEER1.050986000026
PIONEER1.050986000027
PIONEER1.050986000028
PIONEER1.050986000029
PIONEER1.050986000030
PIONEER1.060986000031
PIONEER1.060986000032
PIONEER1.060986000033
PIONEER1.060986000034

APPENDIX A (cont)

Catalogue of Data Files Used for Processing

Noise Spread with Station Spacing = 3.75 m.

Line B - B'

PIONEER1.040986111111
PIONEER1.040986222222
PIONEER1.040986333333
PIONEER1.040986444444
PIONEER1.040986555555
PIONEER1.040986666666
PIONEER1.040986777777
PIONEER1.040986888888

APPENDIX A (cont)

Catalogue of Data Files Used for Processing

Reflection with Station Spacing = 7.5 m.

Line B - B'

PIONEER3.030986000001
PIONEER3.030986000002
PIONEER3.030986000003
PIONEER3.030986000004
PIONEER3.030986000005
PIONEER3.030986000006
PIONEER3.030986000007
PIONEER3.030986000008
PIONEER3.030986000009
PIONEER3.030986000010
PIONEER3.030986000011
PIONEER3.030986000012
PIONEER3.030986000013
PIONEER2.280886300001
PIONEER2.280886000002
PIONEER2.280886000003
PIONEER2.280886000004
PIONEER2.280886000005
PIONEER2.280886000006
PIONEER2.280886000007
PIONEER2.280886000008
PIONEER2.280886000009
PIONEER2.280886000010
PIONEER2.280886000011
PIONEER2.280886000012
PIONEER2.290886000013
PIONEER2.290886000014
PIONEER2.290886000015
PIONEER2.290886000016
PIONEER2.290886000017
PIONEER2.290886000018
PIONEER2.290886000019
PIONEER2.290886000020
PIONEER2.290886000021
PIONEER2.290886000022
PIONEER2.290886000023
PIONEER2.290886000024
PIONEER2.290886000025
PIONEER2.290886000026
PIONEER2.290886000027
PIONEER2.290886000028
PIONEER2.290886000029
PIONEER2.290886000030
PIONEER2.290886000031
PIONEER2.290886000032
PIONEER2.290886000033
PIONEER2.290886000034
PIONEER2.290886000035

APPENDIX A (cont)

Catalogue of Data Files Used for Processing

Reflection with Station Spacing = 7.5 m.

Line B - B'

PIONEER2.290886000036
PIONEER2.290886000037
PIONEER2.290886000038
PIONEER2.290886000039
PIONEER2.290886000040
PIONEER2.290886000041
PIONEER2.300886000042
PIONEER2.300886000043
PIONEER2.300886000044
PIONEER2.300886000045
PIONEER2.300886000046
PIONEER2.300886000047
PIONEER2.300886000048
PIONEER2.300886000049
PIONEER2.300886000050
PIONEER2.300886000051
PIONEER2.300886000052
PIONEER2.300886000053
PIONEER2.300886000054
PIONEER2.300886000055
PIONEER2.300886000056
PIONEER2.300886000057
PIONEER2.300886000058
PIONEER2.300886000059
PIONEER2.300886000060
PIONEER2.300886000061
PIONEER2.300886000062
PIONEER2.300886000063
PIONEER2.300886000064
PIONEER2.300886000065
PIONEER2.300886000066
PIONEER2.300886000067
PIONEER2.300886000068
PIONEER2.300886000069
PIONEER2.300886000070
PIONEER2.300886000071
PIONEER2.300886000072
PIONEER2.300886000073
PIONEER2.300886000074
PIONEER2.300886000075
PIONEER2.300886000076
PIONEER2.300886000077
PIONEER2.310886200078
PIONEER2.310886200079
PIONEER2.310886200080
PIONEER2.310886200081
PIONEER2.310886200082
PIONEER2.310886200083

APPENDIX A (cont)

Catalogue of Data Files Used for Processing

Reflection with Station Spacing = 7.5 m.

Line B - B'

PIONEER2.310886200084
PIONEER2.310886200085
PIONEER2.310886200086
PIONEER2.310886200087
PIONEER2.310886200088
PIONEER2.310886200089
PIONEER2.310886200090
PIONEER2.310886200091
PIONEER2.310886200092
PIONEER2.310886200093
PIONEER2.310886200094
PIONEER2.010986200095
PIONEER2.010986200096
PIONEER2.010986200097
PIONEER2.010986200098
PIONEER2.010986200099
PIONEER2.010986200100
PIONEER2.010986200101
PIONEER2.010986200102
PIONEER2.010986200103
PIONEER2.010986200104
PIONEER2.010986200105
PIONEER2.010986200106

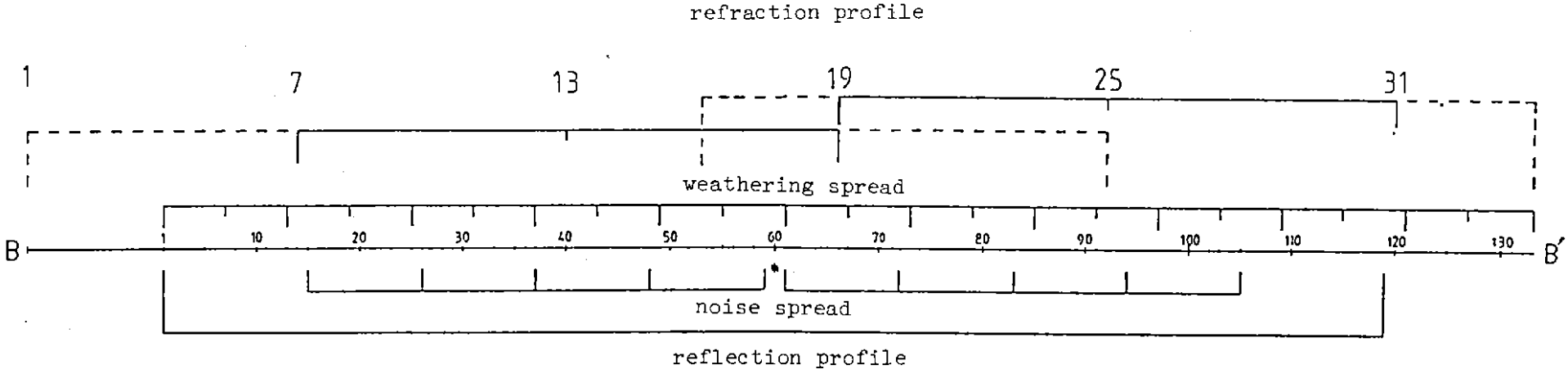

The position of weathering spread ; noise spread ; refraction and reflection profiles along the line B-B'.

APPENDIX B

Surveying results listed below consists of horisontal distances together with their elevation above mean sea level, were obtained from the surveying carried out at Eastern Lead, Pioneer in North Eastern Tasmania.

X is an increment of the horizontal distance with respect to a given point along the corresponding line. The elevation (h) was derived from the base point at m 21 shown in Figure 4.1. The position of the points listed in this appendix shown at the following diagram.

LINE A' - A

X (m):	h (m):	
0	63.5	
100	64.5	
115	65.0	
132	65.4	
149	65.9	
166	66.7	
183	67.3	
200	67.8	
216	68.7	
232	69.7	
248	72.8	
264	75.9	
280	79.0	
296	81.3	
313	80.9	
330	82.2	
347	83.1	
363	85.2	
380	84.1	
396	85.4	
411	85.7	
428	86.6	
445	87.5	
462	89.0	
478	89.9	
495	90.8	at a
512	89.9	
528	89.0	
544	87.6	
560	85.2	
576	83.7	
592	84.7	
609	83.9	
625	83.8	
642	83.8	
658	83.8	
674	83.9	
691	83.9	
741	86.0	
798	85.4	at A

LINE a - b

X (m):	h (m):	
0	90.8	
50	89.1	
114	88.0	
166	85.2	
216	83.4	at b

LINE b - B'

X (m):	h (m):
0	83.4
16	83.8
66	83.9
134	82.5
202	81.3
252	80.9
303	79.9
337	79.1
353	78.9
369	78.9
385	78.2
401	76.7
412	74.2
422	71.3
434	61.3
448	59.8

LINE b - B

X (m):	h (m):
0	83.4
24	83.6
50	83.3
60	81.6
80	80.4
90	79.1
120	76.8

APPENDIX B (cont)

LINE b - c

X (m):	h (m):
0	83.4
10	82.1
50	80.7
100	79.7
148	78.8
170	78.8

LINE C - C'

X (m):	h (m):
0	76.8
50	78.8 at c
100	78.8
150	77.9
200	76.6 at d
250	76.5
300	75.1
400	73.1
450	71.2
500	59.4

LINE d - e

X (m):	h (m):
0	76.6
100	73.7
150	75.1
180	74.2 at e

LINE D - D'

X (m):	h (m):
0	74.6
50	74.3
100	74.2 at e
150	74.0
200	71.2
250	66.2
300	65.6
350	65.7
400	63.4
450	62.2
500	62.3
550	61.4
600	60.8

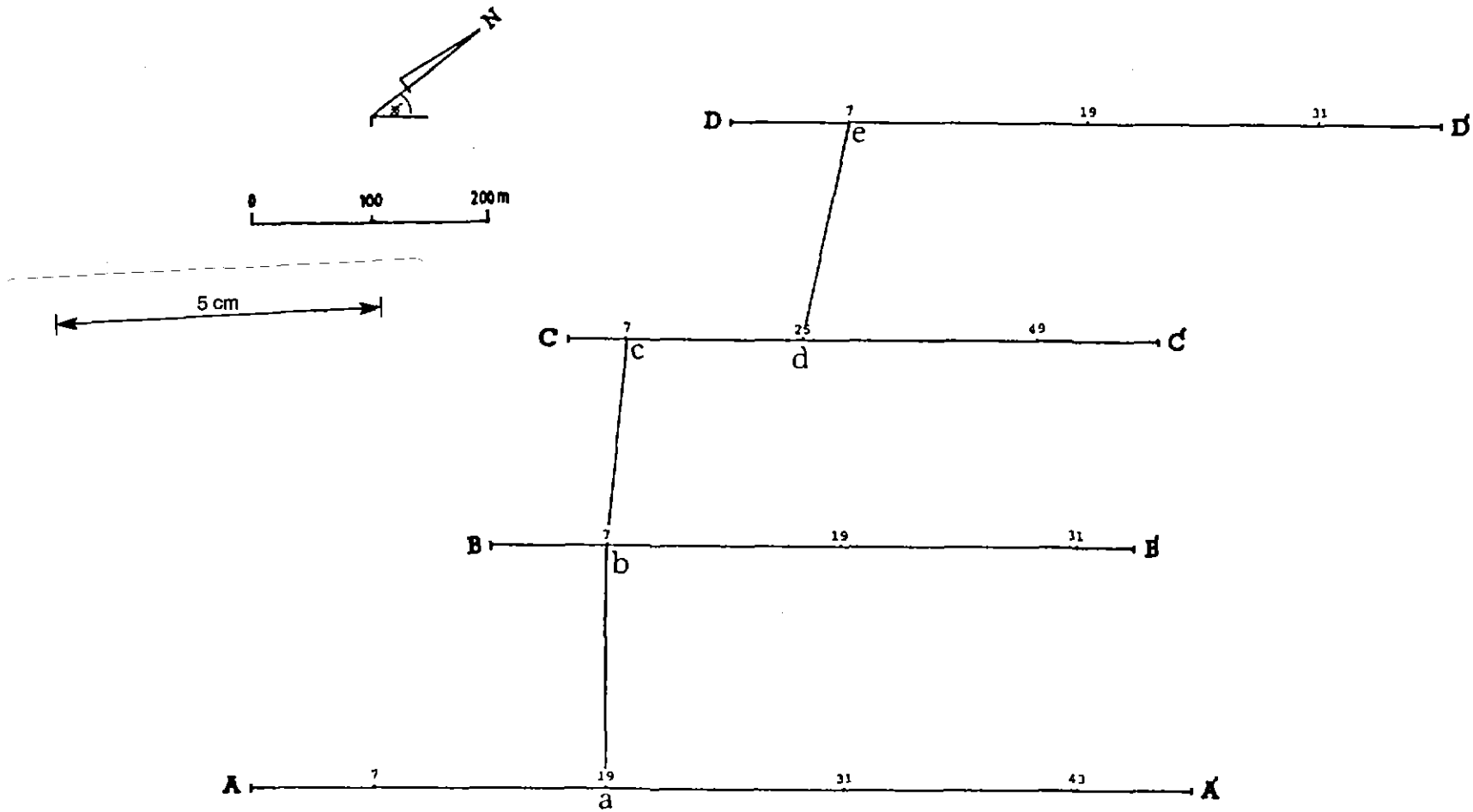

Diagram of the traverse lines in the study area.